JIMMA UNIVERSITY

JIMMA INSTITUTE OF TECHNOLOGY

SCHOOL OF POSTGRADUATE STUDIES

FACULTY OF MATERIAL SCIENCE AND ENGINEERING

Polyaniline nanosphere as electrode material for supercapacitor application

A thesis submitted to the school of graduate studies of Jimma University in partial fulfillment of the requirements for the degree of Master of Science in Material Science and Engineering.

BY

MELESE YALEW AYALEW

December, 2021

Jimma, Ethiopia

JIMMA UNIVERSITY

JIMMA INSTITUTE OF TECHNOLOGY

SCHOOL OF POSTGRADUATE STUDIES

FACULTY OF MATERIAL SCIENCE AND ENGINEERING

MATERIAL SCIENCE AND ENGINEERING

Polyaniline nanosphere as electrode material for supercapacitor applications

A thesis submitted to the school of graduate studies of Jimma University in partial fulfillment of the requirements for the degree of Master of Science in Material Science and Engineering.

BY

Melese Yalew Ayalew

Supervisors

1. **Dr.Fekadu Melak (Assistant Professor), Jimma University, College of Natural Sciences**
2. **Dr.Olu Emmanuel Femi (Associate Professor), Jimma University, JIT**

December, 2021

Jimma, Ethiopia

JIMMA UNIVERSITY

SCHOOL OF GRADUATE STUDIES

FACULTY OF MATERIAL SCIENCE AND ENGINEERING

ADVISORS' THESIS SUBMISSION APPROVAL SHEET

This is to certify that the thesis entitled **"Polyaniline nanospheres as electrode materials for supercapacitor applications''** has been carried out by Melese Yalew in our supervision. Therefore, we recommend that the student has fulfilled the requirements and hence here by can submit the thesis to the department for defense.

_____	_____	_____
Name of the main advisor	Signature	Date

_____	_____	_____
Name of the co-advisor	Signature	Date

JIMMA UNIVERSITY

SCHOOL OF GRADUATE STUDIES

FACULTY OF MATERIAL SCIENCE AND ENGINEERING

EXAMINERS' THESIS APPROVAL SHEET

We, the undersigned, members of the Examiners of the final open defense by **"Melese Yalew Ayalew''**, and examined the candidate's oral presentation. This is, therefore, to certify that the thesis has been accepted.

_____	_____	_____
Name of the Chairperson	Signature	Date
_____	_____	_____
Name of the advisor	Signature	Date
_____	_____	_____
Name of internal examiner	Signature	Date
_____	_____	_____
Name of external examiner	Signature	Date
_____	_____	_____
Approval of the dean	Signature	Date

DECLARATION

I, the undersigned, declare that this MSc thesis is my original work and has not been presented for any degree in any other universities and that all of materials used for this thesis are duly acknowledged.

_____	_____	_____
Name of the Student	Signature	Date

Place of submission: Jimma University, Jimma Institute of Technology, Jimma

Faculty of Material Science and Engineering

December, 2021

ACKNOWLEDGMENT

First and above all, I praise God, the almighty for providing me strength, courage and granting me the capacity to proceed successfully this work. Secondly, I want to express my deep gratitude and sincere thanks to my advisor Dr.Fekadu Melak, for his invaluable suggestion, encouragement, support and supervision on my research work. I would like to express my sincere gratitude to my co-advisor Dr. Olu Emmanuel Femi for his continuous support, guidance and encouragement. They are very responsible and helpful.Without their support and help, this work will not be achieved. I would also like to express my sincerest gratitude to Dr.Mulualem Abebe for the help in XRD result analysis. Also, I wish to thank Mr.Demelash Jado (MSc) for his assistance in experimental works during UV-Vis analysis.

My special thanks goes to Dr. Lodrick Wangatia for his encouragement and endless support.

I am also grateful for Jimma University, Jimma Institute of Technology (JIT) for offering a Scholarship and financial support. And also my appreciation goes to the faculty of material science and engineering, Jimma University department of chemistry and Adama Science and Technology University for their help during this research work by providing the characterization facilities.

I would particularly like to express my gratitude to my elder brother and sisters for their patience, encouragement and unconditional support in my Master of Science study and life. Here also, I would like to acknowledge people who helped me reach my goals, supported me through difficulties, and with whom I shared my good times and bad times.

Most importantly, I wish to thank my friend Mr. Endrias Adane for his assistance with the experimental work, love and encouragement throughout my research work. He is unforgettable man. May God give you a long age.

Finally, this work is dedicated to my parents (Yalew Ayalew and Tehun Andarge) for giving me life and early education and to my sisters and brothers for giving me love and stays with me through the difficult years. I am deeply indebted to my great brother (Fikeremariyam Andarge) and his wife (Tigest Derese) for their continued support and encouragement. This work would not have been possible without them. All in all, dedicated with much love and affection to my beloved family, my mentors and all of my friends.

ABSTRACT

The development of efficient electrode material is essential to promote the performance of energy storage devices. Nowadays, polyaniline materials have been widely used as electrodes for supercapacitors due to their outstanding property, however, the poor electrochemical performance of polyaniline-based materials and low stability limit their large-scale application. In this work, polyaniline (PANI) nanospheres have been successfully synthesized at room temperature by the chemical oxidative polymerization of aniline with ammonium persulfate (APS) in aqueous salicylic acid. Chemically synthesized PANI nanospheres were characterized using Ultraviolet-Visible spectroscopy (UV-Vis), Thermogravimetric analyzer (TGA), Scanning electron microscopy (SEM), X-ray diffraction analysis (XRD) and Fourier transform of infrared spectroscopy (FTIR). The electrical conductivity of the prepared samples were also studied. The electrochemical performance of PANI nanospheres were tested using cyclic voltammetry (CV) technique in H_2SO_4 electrolyte. Polyaniline nanospheres were found to exhibit better specific capacitance when compared to bulk polyanilines. Furthermore, the polyaniline nanospheres, with [salicylic acid]/[aniline] molar ratio of 0.8 or 0.16:0.2, showed highest specific capacitance of 137.7 Fg^{-1} at a scan rate of 250 mVs^{-1}. Electrical conductivity of polyaniline nanosphere is also better when compared to the bulk polyaniline. Thus, PANI nanosphere is found to be promising material for supercapacitors that can deserve intensive study for further enhancements.

Keywords: Electrochemical performance, Polyaniline, Polyaniline nanosphere, Supercapacitors

DEFINITION OF TERMS AND UNITS

Symbol	Definition and Units
A	Surface area of each electrode (m^2 g^{-1})
C	Capacitance (F)
CL	Specific capacitance per unit length (mF cm^{-1})
D	Distance between the two electrodes (mm)
E	Energy (J)
L	Length of the fiber supercapacitors (cm)
P	Power (W)
Q	Stored charge (C)
R	Resistance (ohm)
V	Voltage (V)
ΔV	Voltage of the discharge (V)
ε_o	Dielectric constant of free space (Fm^{-1})
ε_r	Dielecric constant
Cp	Specific capacitance of the electrode (Fg^{-1})
P_{max}	Maximum Power

LIST OF ABBREVIATIONS

3D	Three Dimensional
ACs	Activated Carbon
CNTs	Carbon Nanotubes
CPs	Conducting Polymers
An	Aniline
APS	Ammonium persulfate
BSE	Backscattered electron
DMSO	Dimethyl Sulfoxide
SA	Salicylic acid
SE	Secondary electron
ECs	Electrochemical Capacitors
EDLC	Electric Double Layer Capacitor
ESs	Electrochemical supercapacitors
ESR	Equivalent Series Resistance
HOMO	Highest Occupied Molecular orbital
LUMO	Lowest Unoccupied Molecular Orbital
CV	Cyclic Voltammetry
EIS	Electrochemical Impedance Spectroscopy
GCD	Galvanostatic charge/discharge
PANI	Polyaniline

PPy	Polypyrrole
SOHIO	Standard Oil Company, Cleveland, Ohio
SCs	Supercapacitors
SEM	Scanning electron microscopy
TGA	Thermal Gravimetric Analysis
FT-IR	Fourier Transform Infrared Spectroscopy
UV-Vis	Ultraviolet-Visible Spectroscopy
XRD	X-ray Diffraction

TABLE OF CONTENTS

ACKNOWLEDGMENTS ii

ABSTRACT iii

DEFINITION OF TERMS AND UNITS iv

LIST OF ABBREVIATIONS v

TABLE OF CONTENTS vii

LIST OF FIGURES xi

LIST OF TABLES xiv

CHAPTER ONE 1

INTRODUCTION 1

1.1 Statement of the problem 5

1.2 Objectives of the study 6

1.2.1 General objective 6

1.2.2 Specific objectives 6

1.3 Scope of thesis 7

1.4 Significance of the Study 8

CHAPTER TWO 9

LITERATURE REVIEW 9

2.1 Historical background 9

2.2 Energy storage principles of conventional capacitor and electrochemical supercapacitors 11

2.2.1. Principle of conventional capacitors 11

2.2.2. Principle of supercapacitors 12

2.3. Types of supercapacitors 14

2.3.1. Electrical double-layer capacitors (EDLC) 15

2.3.2. Pseudocapacitors 16
2.3.3. Hybrid supercapacitors 19
2.4 Electrode Materials for Supercapacitors 21
2.4.1 Activated Carbon 22
2.4.2 Carbon Aerogels 23
2.4.3 Carbon Nanotubes (CNTs) 23
2.4.4 Metal oxides 24
2.4.5 Conducting polymer 25
2.5 Literature Survey 30
2.6. Research gaps and literature review summary 34
CHAPTER THREE 36
EXPERIMENTAL: MATERIALS AND METHODS 36
3.1. Reagents and apparatus 36
3.1.1. Chemicals and reagents 36
3.1.2. Instruments and Apparatus 36
3.2 Characterization of the material 37
3.2.1 Physical and Structural characterization 37
3.2.1.1 Ultraviolet-Visible Spectroscopy (UV-VIS) 37
3.2.1.2 Fourier Transform Infrared Spectroscopy (FT-IR) 38
3.2.1.3 Thermogravimetric Analyzer (TGA) 38
3.2.1.4 Scanning Electron Microscopy (SEM) 39
3.2.1.5 X-ray Diffraction (XRD) 41
3.3 Conductivity Measurements 43
3.4 Electrochemical method 43
3.4.1 Cyclic Voltammetry 43
3.5 Experimental procedures 45

3.5.1 Synthesis of Polyaniline 45
3.5.2 Synthesis of polyaniline nanospheres 47
3.5.3 Synthesis of polyaniline solution 49
3.5.4 Synthesis of polyaniline nanosphere solution 49
3.5.5 Synthesis of thick films 49
3.6 Electrical Conductivity Measurement 50
3.7 Electrode Preparation 51
3.7.1 Preparation of Polyaniline Electrode 51
3.7.2 Preparation of polyaniline nanosphere electrodes 51
3.8. Electrochemical Characterization 52
3.8.1 Cyclic Voltammetry test 52
CHAPTER FOUR 55
RESULTS AND DISCUSSION 55
4.1 UV/Vis spectroscopy result 55
4.2 Fourier Transform Infrared Spectroscopy result 58
4.3 Thermogravimetric analysis 60
4.4 Scanning Electron Microscope studies 61
4.5 X-ray Diffraction analysis 66
4.6 Electrical Conductivity 70
4.7 Electrochemical performances of the prepared electrodes 71
4.7.1 Cyclic voltammetry 71
4.7.1.1 Specific capacitance calculated from the CV curve 73
4.7.1.2 Effect of scan rate on specific capacitance of the prepared electrode materials 75
CHAPTER FIVE 79
CONCLUSION AND SUGGESTION FOR FURTHER WORK 79
5.1 Conclusion 79

5.2 Suggestion for further work 80
REFERENCES.....81

LIST OF FIGURES

Figure 1: Ragone plots for several types of energy-storage devices (Kulandaivalu, 2019). 1
Figure 2: The yearly development of novel electrode materials (J. Zhang et al., 2019). 2
Figure 3: Schematic diagram of three different materials used as supercapacitor electrodes: CPs, carbon materials, and transition metal oxides/hydroxides (Kulandaivalu, 2019)..... 3
Figure 4: Timeline for evolution of supercapacitor technologies (Conte, 2010)..... 10
Figure 5: Schematic diagram of a conventional capacitor (Chen et al., 2014) 11
Figure 6: Schematic of an electrochemical double-layer capacitor (Chen et al., 2014) 13
Figure 7: Schematic illustration of the charging / discharging process in a basic supercapacitor (Miller et al., 2018) 13
Figure 8: Types of a supercapacitor (Hadjipaschalis et al., 2009). 14
Figure 9: Electrochmical double-layer (EDLC) energy storage mechanism (Wayu, 2021)..... 15
Figure 10: Schematic illustration of the mechanism of a basic pseudocapacitor (Miller et al., 2018) 16
Figure 11: Different types of reversible redox mechanisms that give rise to pseudocapacitance: (a) underpotential deposition, (b) redox pseudocapacitance, (c)intercalation pseudocapacitance (Augustyn & Dunn, 2014). 17
Figure 12: Schematic of carbon family in 0 - dimensional fullerene, 1 - dimensional carbon nanotube, 2 - dimensional graphene, 3 - dimensional graphite (Tian et al., 2011)..... 22
Figure 13: Comparison of charging of (a) double-layer capacitor (carbon) and (b) pseudo- capacitor (conducting polymer) (Snook et al., 2011). 27
Figure 14: Conductivity of conductive polymers compared to those of other materials, from quartz (insulators) to copper (conductor) (Prize, 2000)..... 28
Figure 15: Chemical structure of polyaniline (Majumdar, 2019) 29
Figure 16: Three oxidation states of Polyaniline : (a) a fully reduced leucoemeraldine base (LEB) ; (b) a fully oxidized pernigraniline base (PNB) and (c) a half oxidized/half reduced emeraldine base (EB) state (Afzal et al., 2009) 30
Figure 17: Schematic drawing of a scanning electron beam incident on a solid sample showing some of the signals generated that can be used to help characterize the microstructure (Brandon, 2014.). 40
Figure 18: The schematic of X-ray diffracted from crystal lattice planes (Bernstein & Desiraju, 2018) 42

Figure 19: Schematic of (a-b) a three-electrode configuration (Moussa et al.,2016) 44
Figure 20: Flow chart of Polyaniline preparation 46
Figure 21: Flow chart of Polyaniline nanospheres preparation 48
Figure 22: Polyaniline (a) and polyaniline nanosphere films: b) N0.5,c) N0.6 and d) N0.8 50
Figure 23: chemically synthesized polyaniline as a working electrode 51
Figure 24: chemically synthesized polyaniline nanosphere as a working electrode 51
Figure 25: UV-visible absorption spectra of bulk polyaniline and polyaniline nanospheres dissolved in dimethyl sulfoxide (DMSO). (a) HCl doped Polyaniline, (b, c, d) Salicyclic acid doped polyaniline nanospheres obtained by changing the molar ratio of the dopant to monomer ([SA]/ [An]). (b) 0.1:0.2, (c) 0.12:0.2, and (d) 0.16:0.2.Other synthetic conditions: [aniline] = 0.2 M, [aniline]/ [APS] = 1:1, t = 12 h. 56
Figure 26: Plot of $(\alpha h\nu)^2$ versus of hv for the as-prepared of polyaniline (a) and polyaniline nanospheres with different molar ratio of the dopant to monomer: b) [SA]/[An] = 0.5, c) [SA]/[An] = 0.6, and [SA]/[An] = 0.8. 58
Figure 27: FT-IR spectra of the bulk polyaniline and polyaniline nanospheres: (a) bulk polyaniline, (b, c, d) polyaniline nanospheres synthesized at molar ratio of [SA]/[An] = 0.5, 0.6, and 0.8, respectively. Other synthetic conditions: [SA] = 0.1M, 0.12M, and 0.16M. [An] = 0.2M, [Aniline]/ [APS] = 1:1, t = 12 h. 59
Figure 28: Thermogravimetric analysis of PANI nanosphere synthesized at [SA]/ [An] ratio = 0.8. Other synthetic conditions: [SA] = 0.16 M and [An] = 0.2 M, [aniline]/ [APS] = 1:1, t = 12 h.. 61
Figure 29: SEM images of bulk polyaniline (a) and polyaniline nanospheres (b-d) synthesized with different molar ratio of [SA]/ [An]:0.5, 0.6, and 0.8 (with low magnification X300).Other synthetic conditions: [SA] = 0.1M, 0.12M, and 0.16M. [An] = 0.2M, [Aniline]/[APS] = 1:1, t = 12 62
Figure 30: SEM images of bulk polyaniline (a) and polyaniline nanospheres (b-d) synthesized with different molar ratio of [SA]/ [An]:0.5, 0.6, and 0.8 (with medium magnification X1000).Other synthetic conditions: [SA] = 0.1M, 0.12M, and 0.16M. [An] = 0.2M, [Aniline]/ [APS] = 1:1, t = 12 64
Figure 31: SEM images of PANI nanospheres synthesized with different molar ratio of salicylic acid to aniline ([SA]/ [An]).With higher magnification of X2000: a) 0.5 (0.1:0.2); b) 0.6 (0.12:0.2); c) 0.8 (0.16:0.2). Other reaction conditions [An] = 0.2 M, [An]/ [APS] = 1:1, t = 12 h. 65
Figure 32: XRD patterns of conventional (bulk) polyaniline and polyaniline nanospheres prepared in molar ratio of the dopant to monomer (a) ([SA]/[An] = 0.5),(c) [SA]/[An] = 0.6 and (d)

[SA]/[An] = 0.8. Other synthetic conditions: [SA] = 0.1 M, 0.12 M, and 0.16 M. [An] = 0.2 M, [Aniline]/ [APS] = 1:1, t =12. 70
Figure 33: Cyclic voltammogram of the prepared material: a) B-bulk polyaniline, b) G-glassy carbon electrode, c) polyaniline nanosphere (N 0.5), d) polyaniline nanosphere(N 0.6), and e) polyaniline nanosphere (N 0.8) material as electrode..... 73
Figure 34: Area of cyclic voltammetry of the bulk polyaniline electrode material with 200 mV/s scan rate. 73
Figure 35: Area of cyclic voltammetry of N 0.6 electrode material with 300 mV/s scan rate. 74
Figure 36: Area of cyclic voltammetry N 0.8 electrode material 74
Figure 37: Effect of scan rate (100-250 mV/s) on polyaniline nanosphere (N 0.8) electrode material in 1M H_2SO_4 solution 76

LIST OF TABLES

Table 1: Detailed parametric comparison of capacitor, supercapacitor and battery (Modified from (Schneuwly & Gallay, 2000)). 10
Table 2: Advantages and disadvantages of an electrical double layer capacitor and pseudocapacitor (Adopted from (Navarro et al., 2021)). 18
Table 3: Comparison of EDLCs and pseudocapacitor (Modified from (Y. Zhang et al., 2009)). 19
Table 4: Summary of the different types of hybrid ES (Zhi et al., 2013) 21
Table 5: Preparation details of polyaniline nanosphere samples. 47
Table 6: Demonstrates electrical measurements for both bulk polyaniline and polyaniline nanospheres 50
Table 7: Crystallinity index of prepared polyaniline and polyaniline nanospheres (N 0.5, N 0.6, and N 0.8) materials. 66
Table 8: The XRD data of polyaniline 67
Table 9: The XRD data of polyaniline nanospheres (with molar ratio of [SA]/ [An] = 0.5)..... 67
Table 10: The XRD data of polyaniline nanospheres (with molar ratio of [SA]/[An] = 0.6)..... 68
Table 11: The XRD data of polyaniline nanospheres (with molar ratio of [SA]/[An] = 0.8)..... 68
Table 12: The conductivities of bulk polyaniline and polyaniline nanospheres (N 0.5, N 0.6, and N 0.8) samples. 71
Table 13: Specific Capacitance of polyaniline, polyaniline nanosphere (N 0.6), and polyaniline nanosphere (N 0.8) at different scan rates. 75
Table 14: Specific capacitance of Polyaniline nanosphere (N 0.8) (synthesized at [SA]/ [An] = 0.8 or 0.16M: 0.2M) at different scan rates. 76
Table 15: Summary of reported literatures on Polyaniline based electrode for supercapacitor performance. 78

CHAPTER ONE

1. INTRODUCTION

The development of renewable energy storage devices has attracted more and more scientific attention due to environmental pollution caused by the rapid consumption of nonrenewable fossil fuels (Wang et al., 2012) (Chu & Majumdar, 2012). Among all energy storage devices, supercapacitors are one of the most attractive with their unique properties such as high power density, fast charge rate, long cycle life and short charging time compared with conventional capacitors and batteries (Long et al., 2011). Figure1 shows the ragone plot comparison, supercapacitors (SCs), also called electrochemical capacitors (ECs), hold a significant position because of the superior energy density than traditional electrostatic capacitors and the faster power delivery than batteries.

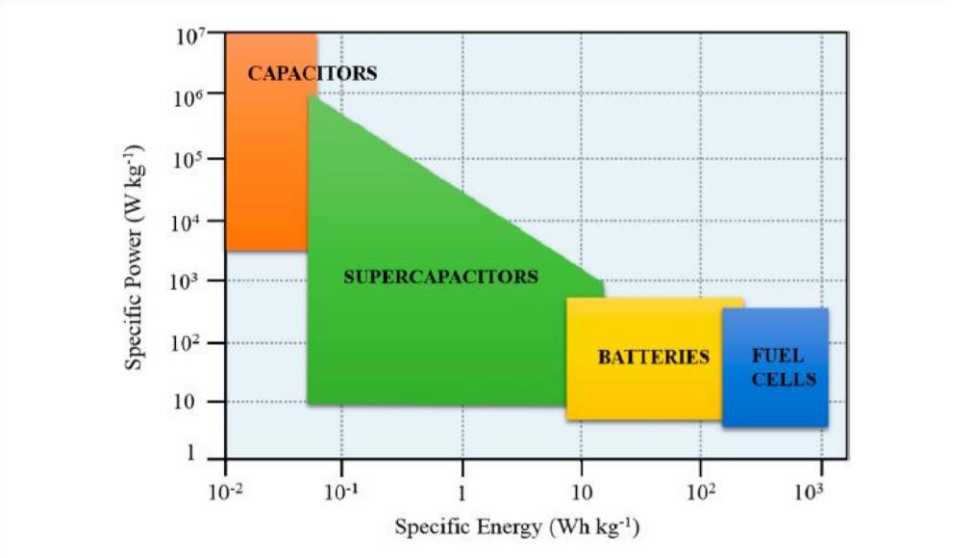

Figure 1: Ragone plots for several types of energy-storage devices (Kulandaivalu, 2019).

Supercapacitors' performance is limited due to several inherent shortcomings of the electrode materials, such as the poor intrinsic conductivity, low energy density of activated Carbon, and high cost of RuO_2 and unsatisfactory cycling performance of polyaniline (PANI) due to slow diffusion of ions, low charge transfer reaction, and densely packed with limited accessible surface area, respectively (Hussain & Yu, 2019) (Liu et al., 2020). Meaning, the electrochemical performance of supercapacitor is heavily dependent on electrode materials and electrolytes. Hence, it is necessary to design novel electrode materials to meet high specific capacitance and

good cyclic stability requirements. Figure 2 displays the yearly development of novel electrode materials for boosting the electrochemical performance of SCs.

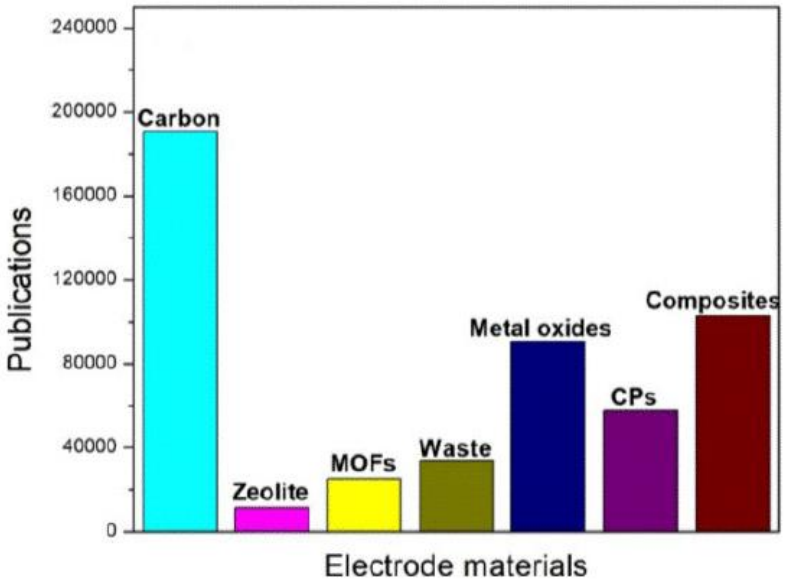

Figure 2: The yearly development of novel electrode materials (Zhang et al., 2019).

Supercapacitors are divided into two categories based on energy storage mechanism; electric double-layer capacitor (EDLC) and Faraday pseudo-capacitors (Xing et al., 2014). The electrode material of EDLCs accumulates charges through the adsorption and desorption of ions or polar molecules in the electrolyte. Carbon-based materials are typical electrode materials for the EDCLs, including activated carbon, porous carbon, carbon nanotubes (CNTs) and graphene (Zhang et al., 2010). On the other hand, the energy storage of pseudo capacitors is sourced from the rapid Faraday reaction of electrochemical energy storage substances under their characteristic potentials; and the electrode materials are mainly transitioning metal oxides, metal hydroxides and conductive polymers (Du et al., 2018). Supercapacitors' electrochemical performance depends mainly on electrode materials and electrolytes, which play a significant role as energy storage devices. These electrode materials can be classified into three main types as Carbon species, metal compounds and conducting polymers (Lokhande et al., 2011). Due to their low cost, lightweight, high theoretical specific capacitance, high mechanical stability, and easy production, conducting polymers (CPs) has become an excellent pseudocapacitive electrode material than other electrode materials SCs (Zhang et al., 2018). Figure 3 illustrates different materials used as supercapacitor electrodes.

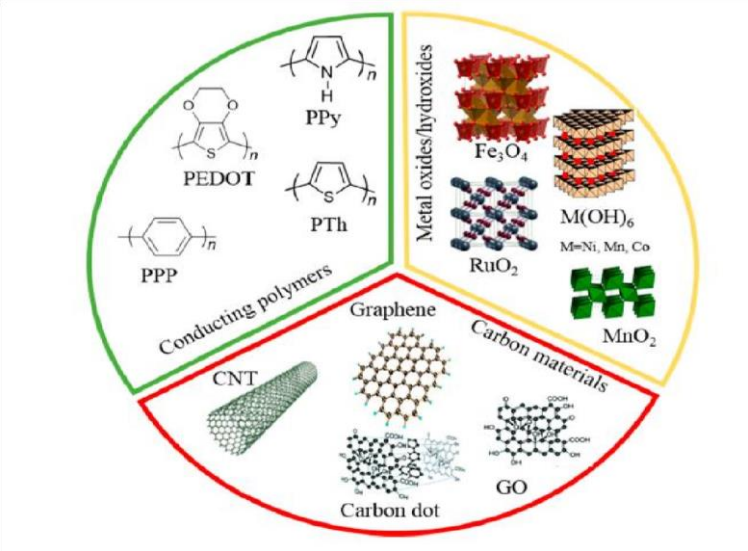

Figure 3: Schematic diagram of three different materials used as supercapacitor electrodes:CPs, carbon materials, and transition metal oxides/hydroxides (Kulandaivalu, 2019).

Conducting polymers including polyaniline, polypyrrole, polythiophene, phenylenevinylene and their derivatives have been widely used for the development of supercapacitor electrode materials (Haiqiang Zhang et al., 2014). Among the various conducting polymers, polyaniline materials are considered attractive electrode materials for pseudo capacitance electrodes. This is due to their advantages of low cost, high conductivity in a partially oxidized state, large theoretical capacitance due to its multiple redox states, good environmental stability, and fast and reversible doping/dedoping kinetics (Fu et al., 2016**)** and good electronic properties due to protonation (Wang et al., 2016). It also shows good thermal stability and can be easily prepared by chemical or electrochemical methods, resulting in powder or thin films (Gao & Chen, 2016). However, the specific capacitance is still unsatisfactory because PANI materials become densely packed with limited accessible surface area in bulk dimensions, resulting in a comparatively low coefficient of utilization. Moreover, the practical applications of polyaniline electrode is limited by two aspects. Firstly, the polyaniline electrodes' cyclic stability had a fatal deficiency due to the mechanical degradation and break of the PANI chains caused by the swelling, breaking or shrinking in the skeleton of PANI during the repeated charge-discharge processes (Frackowiak et al**.,** 2006). Secondly, the redox reactions usually do not diffuse into the bulk material, which results in the inner layer of the electrodes cannot be fully used. Furthermore leading experimental specific capacitance is much lower than the theoretical value (Kang et al., 2002).This further means that, when bulk polyaniline powders are used as electrodes, they mostly show poor cycle stability and

low specific capacitance value due to the slow charge transfer reaction and mechanical degradation. To overcome these limitations, nanostructure design, an effective approach for the micro/nanostructure materials involved interface reaction, can demonstrate a large surface area, shorten the diffusion paths of electrolyte ions and electrons, and supply abundant excess interspace for buffering the big volume expansion of active materials during charge/discharge processes. This indicates that, design and construction of nanostructured PANI electrodes is an important method to improve the electrochemical performance of PANI electrodes.

In the present work, polyaniline nanospheres were successfully synthesized by simply changing the molar ratio of the dopant to monomer through chemical oxidative polymerization method (via a self-assembly process). In addition to this, polyaniline was also synthesized by chemical oxidation of aniline with ammonium persulfate at lower temperatures (0-5^{o}C). We studied polyaniline nanosphere as electrode materials for supercapacitor applications. Furthermore, conventional polyaniline electrode was also studied to compare with that of polyaniline nanosphere electrodes.

1.1 Statement of the problem

Nowadays, the energy crisis and environmental pollution challenges have become dominant in modern society's rapid development. Therefore, it is necessary to explore new renewable energy sources to address these issues. From energy storage devices, supercapacitors have been widely applicable in hybrid vehicles, portable electronic devices, telecommunications, railways and other fields because of their unique power property, fast charge-discharge capability and superior cycling stability (Chen et al., 2017). As the most critical part of supercapacitors, electrode materials affect their electrochemical performances (Zhang et al). Among conducting polymers, PANI is the most widely used electrode for pseudo supercapacitor. However, polyaniline suffers from volumetric shrinkage during dedoping (discharge) process which lead to problems concerning the specific capacitance, electrical conductivity, mechanical properties, cyclic stability, ions/charge movement, surface area, thermal stability and resistance to electrochemical oxidation/reduction. Therefore, we will design an efficient PANI nanosphere as electrode material. In so doing, by moving from bulk PANI to nanostructured PANI, the potential advantages of nanostructured-based PANI electrodes include: fully use the inner layer of the active materials, new reactions not possible with bulk materials, large contact surface area, accessible internal surface, short ion/electron diffusion distance and better accommodation of the strains.

1.2 Objectives of the study

1.2.1 General objective

The main objectives of this study is to design polyaniline nanosphere based electrode material for supercapacitor applications.

1.2.2 Specific objectives

The specific objectives are to:

- ✓ Synthesize polyaniline and polyaniline nanosphere materials/electrodes.
- ✓ Test the capacitance performance of polyaniline and polyaniline nanosphere based electrodes.
- ✓ Evaluate the electrochemical behavior of polyaniline and polyaniline nanosphere electrode materials using cyclic voltammetry technique.
- ✓ Study the thermal stability, chemical structure, and morphology and crystal size of the prepared samples.
- ✓ Determine the electrical conductivity of the prepared materials.

1.3 Scope of thesis

The main scope of this thesis is to address the main objective which is to develop polyaniline nanospheres as electrode material for supercapacitor applications. Besides, having high specific surface area and high electrical conductivity, the PANI nanosphere materials will have various outstanding properties such as, high temperature stability, long term stability, and high specific capacitance value.

1.4 Significance of the Study

Nowadays, our modern society huge challenges are energy savings as well as energy management. This is partly, to improve and extend the standard of living to a grown population, and do it with sustainable technologies becomes our main survival role play. Therefore, there is great need to find efficient energy storage materials. So, conducting study on improving the efficiency of electrode materials for energy storage devices may play a fundamental role for the globe. The present work gives background related to energy storage on supercapacitors. It attempts to place the supercapacitors device in context of available and future technologies for alternative energy systems management. In addition to this, our study encourages sustainable development goals (SDGs) such as ensure access to affordable, reliable, sustainable, and modern energy storage devices for all community. In this regard, conducting polymers can be used as electrode materials without facing low electrical conductivity, low cyclic stability low redox reaction, high cost of production and harmfulness for the environment as opposed to unlock as many applications of supercapacitors which are highly demanded almost in every energy sector. That is why in the present work, the electrochemical performances of polyaniline nanosphere electrodes were investigated. All in all, the findings of this study will have significant input for beginner investigators on the field of polyanilines nanosphere materials in supercapacitor application. And it will give contribution through information provision about the electrochemical performances of the prepared electrode materials in brief. In particular, electrochemical performance of PANI nanospheres based electrodes and synthesis techniques.

CHAPTER TWO

LITERATURE REVIEW

2.1 Historical background

Supercapacitors, also known as electrochemical capacitors and ultracapacitors, have been studied over the past few decades (Ko & Carlen, 2000). In 1853, Helmholtz proved that the electrical charge could be stored on the surface of a conductor and at the double layer interface between an electrode and an electrolyte (Davis, 2019). However, it was not until 1957 that the first patent on double-layer capacitance structure was granted to Becker at General Electric Corporation. Porous Carbon with a high specific surface area was used as electrode material for an electrochemical capacitor for the first time. SOHIO in 1969 made the first attempt to display the electric double-layer capacitors (EDLC) with porous carbon materials consisting of tetraalkyl ammonium salt-based electrolyte in the market place (Menzel et al., 2015). In 1971, this double-layer capacitor technology was licensed to the Nippon Electric Company (NEC) by SOHIO, and NEC successfully manufactured the first commercially double-layer capacitor with the name of "supercapacitor". From that time on, the supercapacitor's industrialization period had started with the development of key technologies. These included improving the electrode materials, electrolytes and the manufacturing process. A supercapacitor named "Gold capacitor," used for memory backup applications, was developed by Panasonic in 1978. The Pinnacle Research Institute (PRI) developed the first high power double layer capacitors named "PRI Ultracapacitors" by incorporating metal-oxide in the electrode in 1982. In the late '70s and '80s, Conway et al. made a great contribution to the supercapacitor research, using RuO_2 as the electrode material, which showed a high specific capacitance and a low internal resistance (Conway, 1991). The US Department of Energy developed a study in hybrid electric vehicles, in which Maxwell Laboratories developed the Ultracapacitor Development Program in 1992. Nowadays, supercapacitors are manufactured by many companies around the world and widely used. In Japan and America, Panasonic, NEC, Epoch, ELNA, Cooper and AVX have developed various electric double-layer capacitor (EDLC) components. Also, Evans and Maxwell produce integrated modules with voltage balancing circuitry. ESMA in Russia offers different kinds of EDLC modules for applications in power quality improvement and electric vehicles. Currently, commercial supercapacitors are widely used as power sources for communication devices, digital

cameras, mobile phones, electric hybrid vehicles, electric tools, pulse laser techniques, uninterruptible power supplies for computers, stand by power for random access memory devices and storage of the energy generated by solar cells (Schneuwly & Gallay,2000). Figure 4 displays the timeline for evolution of supercapacitor technologies.

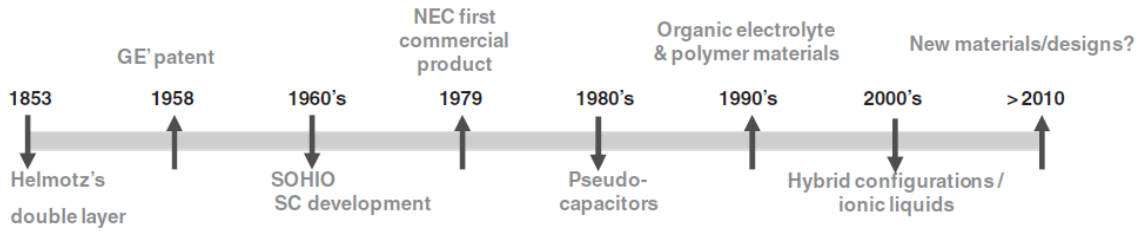

Figure 4: Timeline for evolution of supercapacitor technologies (Conte, 2010).

The unique high power characteristic of supercapacitor leads to the new concept of hybrid charge storage devices, which combines supercapacitor interfaces with the fuel cell or battery. The following table provides a detailed comparison of the supercapacitor and battery.

Table 1: Detailed parametric comparison of capacitor, supercapacitor and battery. (Modified from (Schneuwly & Gallay, 2000)).

Parameters	**Capacitor**	**Supercapacitor**	**Battery**	**Comparison**
Charge Time	10^{-6}~10^{-3} sec	1~30 sec	0.3~3hrs	Moderate charging time
Discharge Time	10^{-6}~10^{-3} sec	1~30 sec	1~4hrs	Moderate discharging time
Energy Density(W/kg)	<0.12	1~10	20~100	High energy density
Power Density(W/kg)	>10,000	1000-2000	50~200	Moderate power density
Cycle Life	>500,000	>100,000	500~2000	Reasnoable good cycle life
Charge/discharge Efficiency	~1.0	0.90-0.96	0.7-0.84	High efficiency

2.2 Energy storage principles of conventional capacitor and electrochemical supercapacitors

The electrochemical capacitor has a greater capacity than a conventional capacitor. The description of the working mechanisms for conventional capacitors and supercapacitors are as follows.

2.2.1. Principle of conventional capacitors

As indicated in Figure 5, the conventional capacitor contains two conducting electrodes, and to prevent electrical contact between them, an insulating dielectric material called a separator is interposed. Opposite charges accumulate on the surface of each electrode when a voltage is applied between the two electrodes. The charges can be kept separate by the dielectric. That is how a capacitor stores energy (Ko & Carlen, 2000). Figure 5 illustrates the working mechanism of a conventional capacitor.

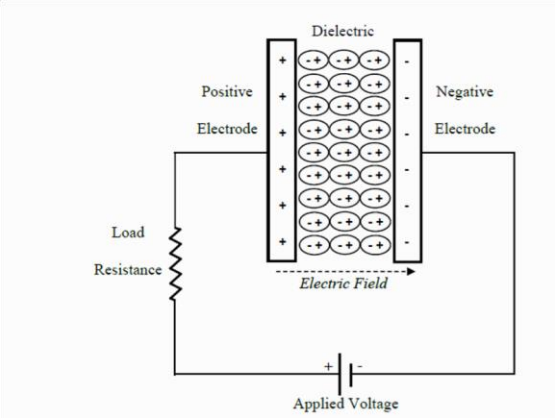

Figure 5: Schematic diagram of a conventional capacitor (Chen et al., 2014)

Capacitance *C* (F) is defined as the ratio of stored charge *Q* (C) to the applied voltage *V (V)*:

$$C = \frac{Q}{V} \qquad (1)$$

For a conventional capacitor, *C* can be calculated by the equation:

$$C = \frac{\varepsilon_{\circ}\varepsilon_{r}A}{D} \qquad (2)$$

Where A is the surface area of each electrode ($m^2\ g^{-1}$), D is the distance between the two electrodes (m), ε_o is the dielectric constant of free space ($F\ m^{-1}$), and ε_r is the dielectric constant of the insulating material between the two electrodes. Energy density and power density are two key terms for the characteristics of a capacitor. The energy *E* of a capacitor is directly calculated as follows:

$$E = \frac{1}{2} CV^2 \qquad (3)$$

The power P is the energy expended per unit time. As indicated in Figure 5, capacitors are generally described as a circuit in series with an external resistance R to determine P for a capacitor. The internal resistance, named the equivalent series resistance (ESR), is usually measured as an aggregate. So the capacitor's internal components, such as electrodes, current collectors and dielectric materials, all contribute to the ESR. These resistances determine the discharge current. When matched impedance (R=ESR) is measured, the maximum power (P_{max}) for a capacitor (A. Chu & Braatz, 2002) can be calculated by

$$P_{\max} = \frac{V^2}{4 \times ESR} \qquad (4)$$

This equation shows how the ESR can affect the maximum power of a capacitor. For a capacitor, the energy or power density can be calculated as a quantity per unit mass or per unit volume. Conventional capacitors have relatively high power densities but relatively low energy densities compared to electrochemical batteries and fuel cells, as indicated in Figure 1. In other words, a battery can store more energy than a capacitor, but it cannot deliver it very quickly, so its power density is low. On the other hand, Capacitors store relatively less energy per unit mass or volume, but electrical energy stored can be discharged rapidly to produce a large power, so their power density is usually high.

2.2.2. Principle of supercapacitors

Generally, the basic principle for conventional capacitors is also true for supercapacitors. As shown in the Figure 5 and Figure 6, schematics of supercapacitors and conventional capacitors are similar. Supercapacitors consist of two conducting electrodes separated by an insulating dielectric material. The difference between them is that electrodes for supercapacitors normally have much higher surface areas than those for conventional capacitors, and an electrolyte solution in a separator between them. Therefore, the capacitance and energy calculated from Equations (2) and (3) increase dramatically over conventional capacitors because of the much higher surface area A and smaller distance *D* between two electrodes. Figure 6 shows the working principle of electrochemical double layer (EDLC).

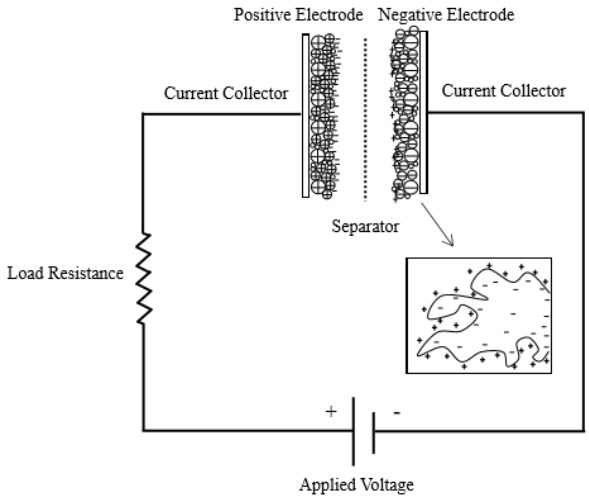

Figure 6: Schematic of an electrochemical double-layer capacitor (Chen et al., 2014)

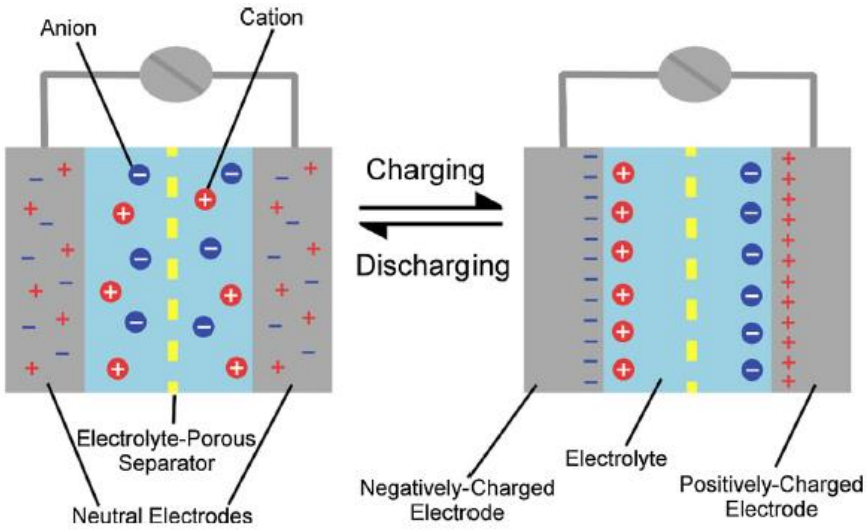

Figure 7: Schematic illustration of the charging/discharging process in a basic supercapacitor (Miller et al., 2018)

2.3. Types of supercapacitors

Depending on the energy storage mechanism, supercapacitors could be classified into three main divisions: electrochemical double-layer capacitors (EDLCs), pseudo capacitors and hybrid capacitors. All the supercapacitors can be characterized by unique mechanisms for storing charge, which are electrostatic storage, reversible Faradaic redox and a combination of the two. For pseudo capacitors, there are Faradaic processes which consist of oxidation-reduction reactions (Gómez et al., 2011). The energy is stored in pseudo capacitors by a chemical mechanism, such as in transition metal oxide-based supercapacitors. In contrast, a non-Faradaic mechanism occurs in EDLCs, in which the charges are kept separately at the electrode/electrolyte interface by physical processes that do not include the making or breaking process of chemical bonds. The third type is the hybrid capacitor. The energy storage process combines the Faradaic and non-Faradic, such as carbon and transition metal oxide materials composite supercapacitors. Figure 8 displays the classification of supercapacitors.

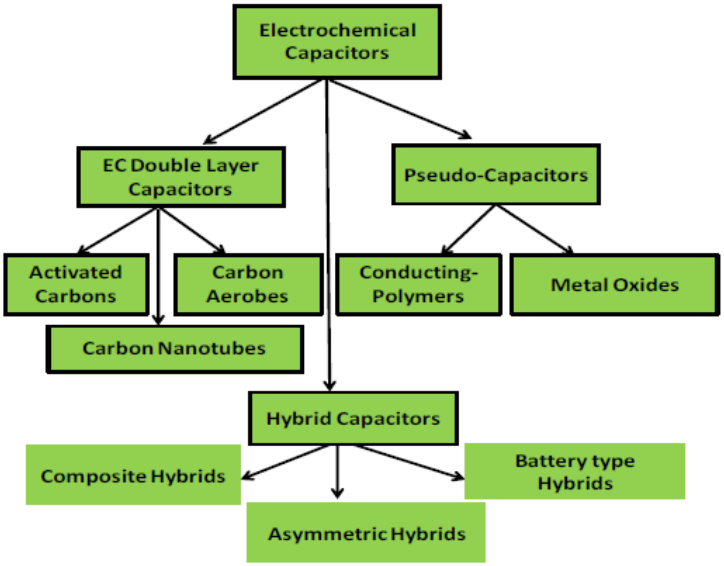

Figure 8: Types of a supercapacitor (Adopted from (Hadjipaschalis et al.,2009)).

2.3.1. Electrical double-layer capacitors (EDLC)

Helmholtz first noticed the double-layer capacitance in supercapacitor in 1879. According to the Helmholtz theory, the electrical double layer's evaluation is due to the strong interactions between the ions/molecules at electrode and electrolyte interface, and reversible ion adsorption onto carbon electrode is responsible for the energy storage in electrochemical capacitors (Valleau & Torrie, 1982). A schematic of a typical charged EDLCs is illustrated in Figure 9. EDLCs consists of two electrodes, an electrolyte, and a separator. For EDLCs, charging and discharging storage is highly reversible. This results in very high cycling stabilities. Figure 9 illustrates the energy storage mechanism of electrochemical double layer capacitors.

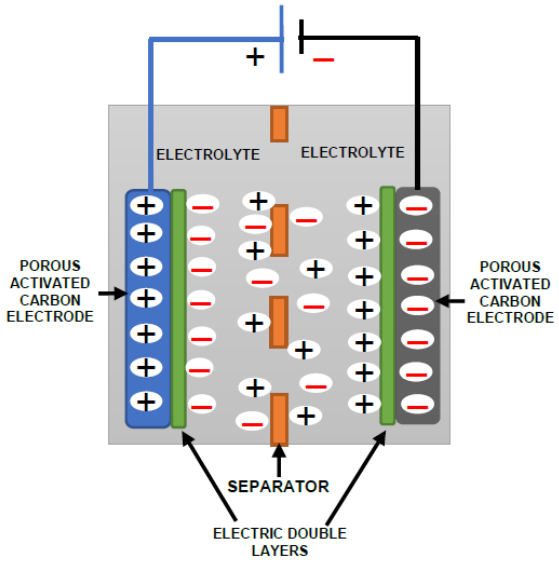

Figure 9: Electrochemical double-layer (EDLC) energy storage mechanism (Wayu, 2021).

EDLCs store energy by using an electrochemical double-layer of charge. Charges on the electrode surfaces accumulate when a voltage, which is less than that to cause a chemical reaction, is applied. Ions of the electrolyte solution diffuse across the separator and enter the pores of the electrode. Opposite charges accumulate at the interface between the electrode and the electrolyte because of the applied potential. Nevertheless, the recombination of the ions is prevented by careful engineering of the electrodes. Therefore, the two electrodes produce a double-layer of charge. Porous Carbon with high surface area, low cost and high stability have been utilized as electrode material ever since the electrochemical capacitor's development began. Different kinds

of carbon materials are recently widely used to store charge in EDLC electrodes, including activated carbons (ACs), carbon aerogels, carbon nanotubes, and graphene.

2.3.2. Pseudocapacitors

In addition to electrostatic charge separation, supercapacitors can perform electrochemical processes contributing to the energy storage capacity. Supercapacitors that store energy electrochemically is called pseudocapacitors. It is also named a redox-based electrochemical capacitor. Redox-based capacitance arises at electrode surfaces where a completely different charge storage mechanism applies. It is not just an accumulation (or deficiency) of electrostatic charge at the two electrodes' interfaces, as the double-layer type of capacitor. When an external potential is applied to a pseudocapacitor, a fast and reversible redox reaction occurs on the electrode. Pseudocapacitor, a fast and reversible redox reaction on the electrode. It involves the passage of charge between electrode and electrolyte. EDLCs store charges electrostatically, while pseudocapacitors store charge by the reversible redox reactions at active materials' surface. Metal oxides and conducting polymers have mainly been used as electrode materials to store charges in pseudocapacitors (Rudge et al., 1994). A higher specific capacitance and energy density can be achieved in pseudocapacitors due to these Faradaic processes in redox-active materials compared with EDLCs. Figure 10 illustrates the energy storage mechanism of pseudocapacitors.

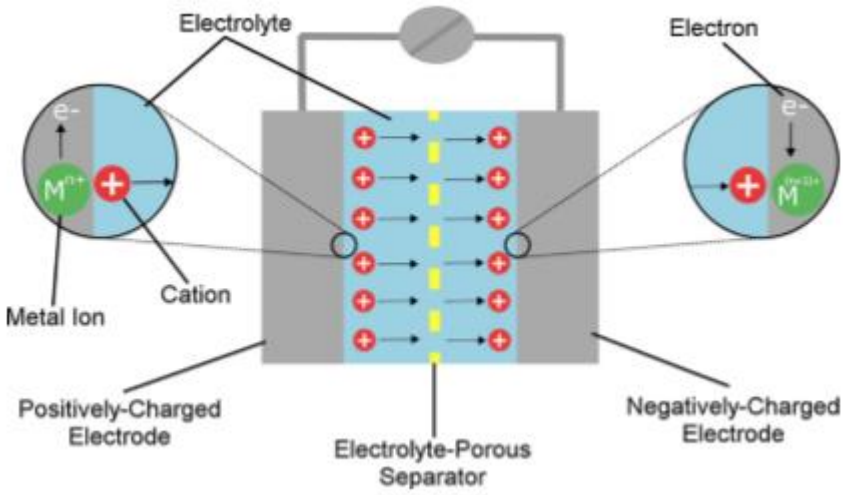

Figure 10: Schematic illustration of the mechanism of a basic pseudocapacitor (Miller et al., 2018)

In the 1970s, B.E.Conway indicated that several mechanisms could result in pseudocapacitive electrochemical features: such as under potential deposition, redox pseudo capacitance and

intercalation pseudo capacitance (Augustyn & Dunn, 2014).These processes are illustrated in Figure 11. Under potential deposition occurs when metal ions form an adsorbed monolayer at a different metal's surface well above their redox potential. The typical example of under potential deposition is the Langmuir-type electro sorption of H on the noble metal substrate such as Pt, Rh, Ru. Redox pseudocapacitive behavior occurs when ions are electrochemically adsorbed onto the surface or near-surface of a material with a concomitant faradaic charge-transfer. Metal oxides, such as RuO_2 (Hu et al., 2006), NiO (Lang et al., 2008), Co_3O_4 (Zhu et al., 2010) and MnO_2 (Hao Zhang et al., 2008), as well as conducting polymers (polypyrrole (Chem,2012) and polyaniline (Girija & Sangaranarayanan, 2006), are classic examples of redox pseudocapacitive materials, which are currently under extensive research. Intercalation pseudo capacitance results from ion intercalation into tunnels or layers of a redox-active material, accompanied by a faradaic charge transfer process but with no crystallographic phase change. Figure 11 shows the types of reversible redox mechanisms in pseudocapacitance.

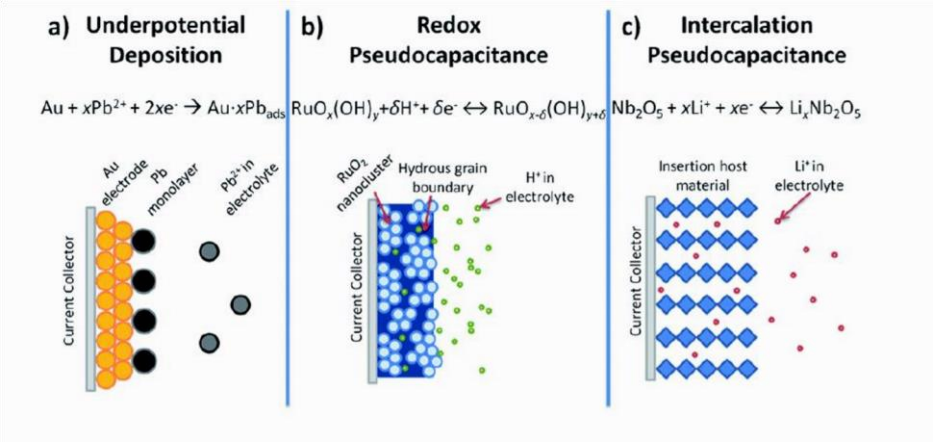

Figure 11: Different types of reversible redox mechanisms that give rise to pseudocapacitance:(a) underpotential deposition, (b) redox pseudocapacitance, (c) intercalation pseudocapacitance (Augustyn & Dunn, 2014).

For all three types of pseudocapacitive behavior, the pseudocapacitance is proportional to differentiated Y concerning potential (V) ($C \propto dY/dV$), in which Y is the property of capacitive materials. In the case of underpotential deposition, Y is the extent of fractional coverage of an electrode surface. Y could be the extent of converting an oxidized species to a reduced species and fractional absorption for redox pseudocapacitance and intercalation pseudocapacitance,

respectively. Table 2 and Table 3 displays the advantages, disadvantages and comparison of both electrical double layer and pseudocapacitor.

Table 2:Advantages and disadvantages of an electrical double layer capacitor and pseudocapacitor (Adopted from (Navarro et al., 2021)).

Electric Double Layer Capacitor	**Pseudocapacitor**	**Difference (pseudocapacitor)**
Phase angle 90^0	Phase angle 45^0	More transmission like behavior
Low specific energy density	High specific energy density	Good capacity of charge storage
High reversibility	Moderate reversibility	Reasonably good cyclic life
Capacitance remains constant with voltage	Capacitance changes with voltage	Small leakage effect
Narrow potential window (13V)	Large potential window (1-5V)	A broad range of applications
High Power due to good diffusion	Low Power due to Kinetic limitations	High diffusion resistance

Table 3: Comparison of EDLCs and pseudocapacitor (Modified from (Y. Zhang et al., 2009)).

Electrical double-layer capacitors (EDLC)	**Pseudocapacitors**
Non-Faradaic process	Faradaic process
20–50 μF cm^{-2}	2000 μF cm^{-2} for single-electron transferred process; 200–500 mF cm^{-2} for multi-electron transferred process
Capacitance is fairly constant with potential, except for a point of zero charge (PZC)	Some single-state materials exhibit marked maximum capacitance
Highly reversible charging/discharging	Quite reversible but has intrinsic electrode kinetic rate limitation
High power compared to pseudocapacitor	High energy compared to EDLCs

In conclusion, the high values of specific capacitance attainable through ESs technology arise from double-layer capacitance and often pseudocapacitance. Double-layer capacitance could offer good charge storage capabilities due to electrodes' highly active area and charge separation at the atomic dimension. Pseudocapacitance that arises from redox or ion sorption reactions further improves the achievable capacitance.

2.3.3. Hybrid supercapacitors

Hybrid supercapacitors, also known as asymmetric supercapacitors, are electrochemical devices that combine pseudocapacitances with double-layer capacitances using asymmetric electrodes. This means that one electrode contains a material that conducts a pseudocapacitive process. At the second electrode, charge separation occurs due to double-layer formation only. Hybrid electrochemical capacitors (hybrid supercapacitors), which consist of double-layer carbon material and a pseudocapacitance material, have attracted significant attention. The capacitance of hybrid supercapacitors consists of double-layer capacitance stored by porous carbon materials and the pseudocapacitance stored by the metal oxide or conducting polymer. Hybrid supercapacitors are designed to combine the advantage of the EDLCs and the pseudocapacitors (Laforgue et al., 2003), meanwhile overcoming most of their disadvantages. Hybrid

supercapacitors are classified into three different electrode configuration types: asymmetric hybrids, composite hybrids and battery type hybrids. Asymmetric hybrids consist of an EDLC electrode and a pseudocapacitor electrode (Laforgue et al., 2003). For example, in 2001, Arbizzani and co-workers developed a new hybrid supercapacitor using a p-doped polymer as the positive electrode and AC as the negative electrode. This hybrid supercapacitor showed good specific power and significantly higher specific energy by utilizing both faradaic and non-faradaic processes to store energy. Asymmetric hybrid supercapacitors have better cycling stability than comparable pseudocapacitors. They can achieve higher energy and power densities than comparable EDLCs. Composite hybrid supercapacitors are different from the asymmetric hybrids and use the composite materials to integrate carbon materials with either metal oxides or to conducting polymer materials as electrode materials (Peng et al., 2008). Porous carbon materials can provide a high surface area backbone to enhance the contact between the metal oxides or conducting polymer materials and the electrolyte. The metal oxides or conducting polymer materials can further increase the capacitance by faradaic reactions. The third type is battery-type hybrids, which have two different electrodes: one is a supercapacitor electrode; the other one is a battery electrode (Pell & Conway, 2004). As shown in Figure 1, the batteries showed higher energy densities than supercapacitors, while the power densities of supercapacitors were higher than those of batteries. The battery-type hybrids have a big potential to fill the gap between the normal supercapacitors and batteries if they can combine the higher energy density of batteries and specific power, short charge time, cycle life as well as the reversibility of supercapacitors. Different types of hybrid electrochemical supercapacitors are shown in table 4.

Table 4:Summary of the different types of hybrid ES (Zhi et al., 2013) .

Type of ES	Electrode material	Charge storage mechanism	Advantage and disadvantage
Symmetric hybrid ES	Anode: Metal oxide or conductive polymer	pseudocapacitance	High energy density, moderate cost and cycle stability
Asymmetric hybrid ES	Anode: Metal oxide or conductive polymer	pseudocapacitance	High energy density and power density, good cycle stability
	Cathode: Carbon Material	Double-layer capacitance	
Battery-like hybrid ES	Anode: Li-ion intercalation material	Vitiation/delithiation	High energy density,
	Cathode: Carbon Material	Double-layer capacitance	

2.4 Electrode Materials for Supercapacitors

Supercapacitor electrodes can be fabricated by utilizing its inherent capacitance properties of various materials in different types of supercapacitors, as illustrated in Figure 3.The first group of materials, which is most frequently used in commercial supercapacitor electrodes, is Carbon. Carbon has gained considerable interest due to its various properties, including different allotropies, accessibility, low cost, high surface area, high conductivity, superior corrosion inhibition property, and high-temperature stability environmental friendliness and easy processibility. It exists in various micro-textures (powder, fibers, foams, fabrics, nanocomposites) and different dimensionality from 0 to 3D (Tian et al., 2011). The unique, adaptable porosity of Carbon with various surface functionality is, preferred to use as conductive additives inactive materials of supercapacitor substrates for current leads. So far, the forms of Carbon, which are well recognized in the use of the supercapacitor electrodes, are activated Carbon, carbon aerogels, carbon nanotubes (CNTs), carbon fibers and graphene (Tian et al., 2011). The different forms of Carbon are depictes in Figure 12.

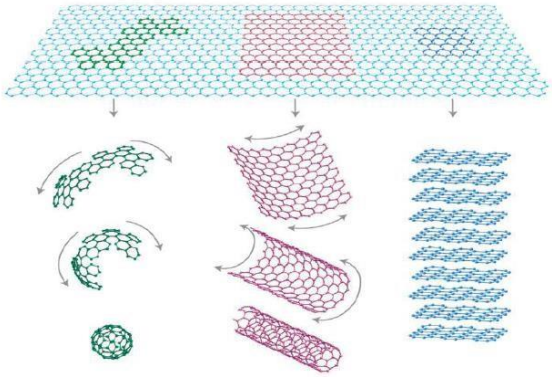

Figure 12:Schematic of carbon family in 0-dimensional fullerene, 1-dimensional carbon nanotube, 2-dimensional graphene, 3-dimensional graphite (Tian et al., 2011).

2.4.1 Activated Carbon

Activated Carbon is a widely known material used for supercapacitor electrodes due to its highly economical processing method and large surface area (BET), which has been reported in the range of 500 to 3000 m^2g^{-1} (Tian et al., 2011). It has shown a good capacitive trend for electrochemical applications. In the electrochemical capacitor (EC), the specific capacitance (SC) obtained by activated Carbon is in the range of 25 to 150 F/gm in both aqueous and organic electrolytes. It has shown the higher capacity tendency due to the existence of three different pore types in activated Carbon, example, micropores (diameter <2 nm), mesopores (diameter from 2-50 nm), or macropores (diameter >50 nm) (Qu & Shi, 1998). However, to have all pores accessible electrochemically, the size of the pores should be essentially bigger than the size of electrolyte ions. Besides the material's porosity, the charge rate is another key factor in the overall enhancement of the specific capacitance of the activated Carbon-based electrode. Other than activated Carbon, another attractive material for supercapacitor electrodes is Carbon black, which is more conducting than activated Carbon and has a high surface area to volume ratio. The conductivity range in Carbon black is from 0.1 to 100, which is mainly due to the graphitic conduction mechanism in Carbon black (Elzbieta Frackowiak, 2001).It is suitable for supercapacitor electrode material, but it can also be used as a conducting additive to improve the overall conductivity and performance of the material.

2.4.2 Carbon Aerogels

Carbon aerogels are considered one of the promising materials for supercapacitor electrodes, and so far, the maximum reported specific capacitance (SC) value for carbon aerogel is 180 F/g (Saliger et al., 1998). Carbon aerogels are highly porous solid materials composed of interlinked colloidal like carbon particles or polymeric chains. So far, the large surface area for carbon aerogels have been reported approximately (400-1000 m^2g^{-1}) with uniform pore size (3-60 m), high packing density, and possess good electrically conductivity (Saliger et al., 1998). Carbon aerogels are available in different forms, for example, monoliths, composites, thin films, powders or microspheres. Furthermore, the surface area of aerogels can be substantially increased by surface activation.

2.4.3 Carbon Nanotubes (CNTs)

Carbon nanotubes (CNTs) are important forms of Carbon, which were first observed by Iijima in carbon soot in 1991. CNTs are classifieds into two types, known as single-wall carbon nanotubes (SWCNTs) and multiwall carbon nanotubes (MWCNTs). Due to their amazing electronic and mechanical properties, CNTs have captured the attention of researchers worldwide. It has an elastic modulus greater than a diamond, which is one of the hardest materials. It has also shown a capacity to carry and generates an electric current 1000 times greater than copper wire (Emmenegger et al., 2003). The most notable characteristic of CNTs is the diameter of a tube, which is usually in the range of 1-3 nm in length in the order of tens of microns. CNTs naturally show capacitive behavior in their pure form. CNTs have supercapacitor electrodes due to mesopore structures and allow easy diffusion of ions within, and provides lower ESR (equivalent series resistance) than activated Carbon and shows the enhancement in power density and energy density of the supercapacitor. However, the high cost in the production of CNTs limits uses in different applications. The maximum specific capacitance reported for SWCNTs electrodes is 160 F/g and the achieved power density was 20 KW/kg for the supercapacitor device (Emmenegger et al., 2003). Moreover, CNTs show high resiliency due to the nanotubular structure, which could be useful in forming composite materials with either conducting polymers or transition metals, e.g., MnO_2, $Ni(OH)_2$ to improve overall capacitance and stability of supercapacitor electrodes (Engineers, 2009). In addition to CNTs, another attractive material for supercapacitor electrodes is carbon fiber. Carbon fiber has superior charge transportation property due to one-dimensionality. It provides high adsorption capacities to ions due to the existence of many pores

at the surface of the fiber and proves to be the best candidate for EDLC electrodes (Mcdonough et al., 2013). Recently, graphene is expected as one of the most promising new materials used in an electrochemical double-layer capacitor. The intrinsic properties, such as high flexibility, high conductivity, large surface area, large porosity, and excellent thermal and mechanical properties, make graphene the best candidate. Graphene is recognized mostly as a single sheet of graphitic Carbon. However, it shows lower Columbic efficiency in the beginning due to the large surface area to volume ratio, but beyond a number of cycles, it renders constant capacity (Mcdonough et al., 2013).

2.4.4 Metal oxides

Metal oxide has a large energy density for application as an electrode due to the electrochemical reactions happening between the electrodes and ions in the electrolyte. To satisfy the application's requirement, the metal oxide usually should have characteristics: good conductive material, more than one oxidation state, and easily intercalated with ions (Y. Liu et al., 2020). According to this, several materials are investigated like ruthenium oxide, manganese oxide, cobalt oxide, nickel oxide and vanadium oxide etc. Ruthenium oxide (RuO_2) is extensively attractive for its wide potential window, good conductivity, high specific area, long cycle life and high rate capacity (Yong-gang & Xiao-gang, 2004). The material's specific area truly influences the device performance by providing more capable metal centers for redox reactions. The amorphous structure also facilitates the redox reaction both on the surface and the bulk of the powder, which gives it superior device performance to the crystalline structure. Therefore, the synthesis parameter plays an important role, like temperature etc. As the redox reaction for the material happens through the hopping of alkaline ions and H+ ions in H_2O and OH-sites, the combination of water with RuO_2 will significantly enhances the cation diffusion the electrode layer (Hu & Wang, 2002). It is reported that the hydrous RuO_2 ($RuO_2.0.5H_2O$) can reach capacitance as 970 F/g. However, ruthenium oxide's drawbacks are mainly its high cost and harmfulness to the environment, which restricts its widely commercial application. Compared with RuO_2, manganese oxide is a lower cost, less toxicity, high capacitance (ranging from 1100 F/g to 1300 F/g). The capacitance of manganese oxide mainly attributes to the oxidation state transition between Mn (III)/Mn (II), Mn (IV)/Mn (III), and Mn (VI)/Mn (IV) (E Frackowiak et al., 2006). Similar to the RuO2, the crystallinity also influences the capacitance performance. The trade-off of conductivity and ions transport exists for the crystallinity issue. Moreover, the specific area and low

conductivity are a concern for the good performance of this material. To solve this problem, different dopants can be used to address it. Metals like cobalt nickel, molybdenum are helpful to improve the performance. Additionally, carbon materials such as activated carbon, carbon nanotube and graphite and conducting polymer can also promote the conductivity.

2.4.5 Conducting polymer

Conducting polymers (CPs) is considered a good second electrochemically active phase for enhancing the capacitance since the faradaic reactions occur on both the surface and the bulk of electrodes, which promote the energy density (Snook et al., 2011). As there are no structural alternations for polymer during the charge-discharge process, the reversibility of conducting polymer is high and the capacitance comes not only from the surface of the material but also from the entire bulk (Snook et al., 2011). The three most commonly investigated CPs in supercapacitor applications are polyaniline (PANI), polypyrrole (PPy), poly (3, 4 ethylene dioxythiophene) (PEDOT), and their corresponding derivatives (Sivakkumar & Saraswathi, 2004), (K. Wang et al., 2013). The main reason is they are stable, good conductivity, cheap and high theoretical capacitance and environmentally friendly. In addition to this, Conducting polymers are different from carbon and metal oxides. They have their unique properties. It is mainly a low cost, large scale, easy to process, fast redox reactions, substrate independent, and high conductivity. The charging-discharging mechanism in conducting polymers, either n-type or p-type, is different from carbon material: it is solely associated with the faradic reaction process of ions, cations, and electrons electrodes/electrolyte interface (E Frackowiak et al., 2006). Unlike the cyclic voltammogram (CV) of Carbon, conducting polymers is not rectangular. Instead, current peaks at the particular redox potential of polymers are observed (Manuscript, 2016).The only main drawback of the conducting polymers in poor mechanical stability. Since cycling polymers undergo a series of physical changes, e.g., swelling, shrinkage, doping and undoping, which degrades the performance of material over time, enhancing the mechanical property of the conducting polymer synthesis of the nanostructured materials can be a good choice.The conductivity of conducting polymers is rendered by a conjugated bond system along the polymer backbone (Snook et al., 2011). As shown in Figure 13, the energy storage mechanism of conducting-polymer-based supercapacitors is different from that of the EDLCs. In general, the EDLCs store energy by an electrostatic method. The ions' fast sorption and desorption on the inter surface between the porous carbon materials and electrolyte result in high power capabilities but

low specific energy (Pasquier et al., 2002). Conducting polymers store charge by a redox reaction and thereby can increase the energy stored and reduce self-discharge. However, these materials' power capabilities are relatively low because of the slow diffusion of ions within the electrode. Particularly, the conducting polymers can be *p*-doped with anions during oxidation and n-doped with cations when being reduced. These two charging processes can be demonstrated by the simplified equations as follows:

$$Cp \rightarrow Cp^{n+}\left(A^{-}\right)_{n} + ne^{-} \quad (5)$$

$$Cp + ne^{-} \rightarrow \left(C^{+}\right)_{n} Cpn^{-} \quad (6)$$

Where Cp is conducting polymers, $Cp^{n+}\left(A^{-}\right)_{n}$ is an anion - polaron, and $\left(C^{+}\right)_{n} Cpn^{-}$ is a cation – polaron. In the discharging processes, the reverse reactions will occur following the reverse of the above equations. Complications can occur given that on oxidation a certain degree of cation inclusion (mixed doping) is possible under certain circumstances.

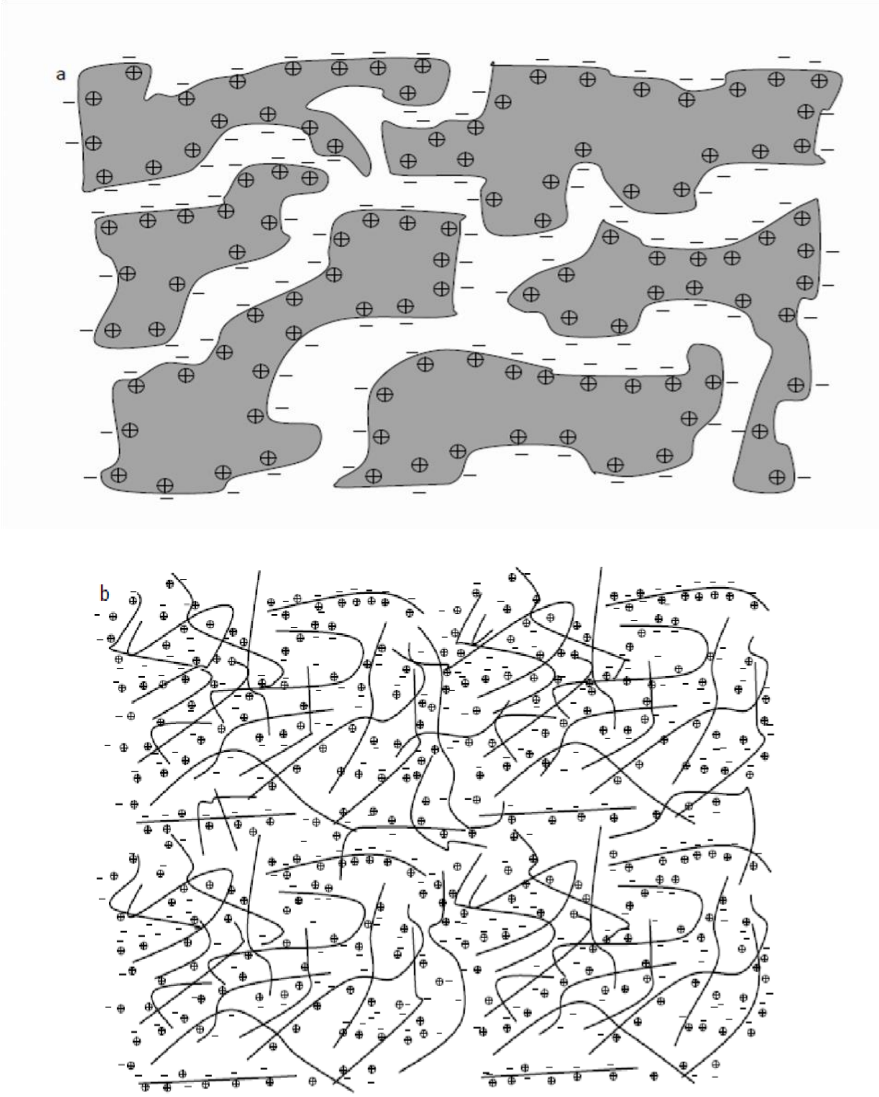

Figure 13: Comparison of charging of (a) double-layer capacitor (carbon) and (b) pseudo-capacitor (conducting polymer) (Snook et al., 2011).

- ✓ Conductivity of conductive polymers compared to other materials

What is electrical conductivity?

Conductivity is explained by Ohm's law:

$$V = RI \qquad (7)$$

Where I is the current (A) through a resistor and V is the drop in potential (v) a cross it. The proportion R is the called the resistance (Ω) measured in ohms. Resistance is measured by applying a known voltage across the resistor and measured the current through it. Ohms law is an empirical law, related to irreversible thermodynamic (Ilya Prigogine, Nobel Prize in Chemistry 1977), the

flow current (I) as a result of a gradient in potential leads to energy being dissipated. In ohmic material the resistance is proportional to the length (L) of the sample and inversely proportional to the sample cross-section area (A)

$$R = \frac{\rho l}{A} \qquad (8)$$

Where ρ is the resistivity measured in Ω cm (in SI units Ω m). Its inverse $\sigma = \rho^{-1}$ is the conductivity. The unit of conductance is the Siemens ($S = \Omega^{-1}$).The unit of conductivity is S m^{-1}.

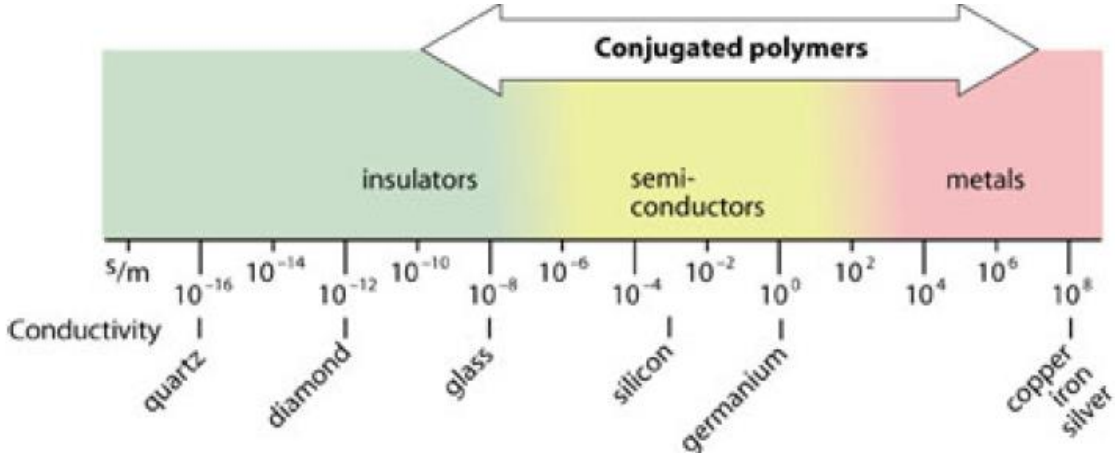

Figure 14: Conductivity of conductive polymers compared to those other materials, from quartz (insulators) to copper (conductor) (Prize, 2000).

Conductivity depends on the number density of charge carriers (number of electrons n) and how fast they can move in the material (mobility μ):

$$\sigma = n\mu e \qquad (9)$$

Where σ is conductivity $(\Omega.cm)^{-1}$, e^- is charge per carrier (electron charge), n is the number of charge carriers (in cm^{-3}) and μ is the mobility of charge carrier. In the case of semiconductors and electrolyte solutions, one should also add in equation (9) an extra term owing to positive charge carriers (holes or cations).The other an interesting point is conductivity depends on temperature: it totally rises with diminishing temperature for metallic materials (some of which becomes superconductive below a certain critical temperature Tc), while it totally decreases with lowered temperature for semiconductors and insulators. For example, among conducting polymer

polyaniline can have a high doping level and high electroactivity and show a high specific capacitance of 400-500 F/g in an acidic medium (P. Liu et al., 2019).Polyaniline requires a proton to be exchanged during charge or discharge; therefore, an acidic solution or a protic ionic liquid is used in the pseudocapacitors using polyaniline materials. PANI is the most popular conducting polymer that owns the largest theoretical pseudocapacitance (approximately 2000 F g-1 in H_2SO_4) (Mooss et al., 2020) owing to its multiple redox states. PPy is another attractive conducting polymer because it can be prepared by a simple method and good conductivity and thermal stability. Generally speaking, PEDOT owns the highest conductivity (up to 550 S cm^{-1}) (Yavuz et al., 2020), but its specific capacitance is normally the worst of the largest molecular mass. PPy ranks the worst regarding the cycling performance since the larger particles formed in the PPy film make it less porous than PANI or PEDOT.

- **Polyaniline (PANI):** Among these conducting polymers, PANI is expected to be a good candidate for electrodes because of its high capacitance, cheap fabrication cost, and environmental stability (Fusalba et al., 2001). However, due to the shortcoming of mechanical stability in the charge-discharge process, it is difficult to get high cycle stability of devices with only PANI utilization. The application of composite material must enhance electrochemical performance. The composite electrode material with graphene and PANI gives a synergistic effect of both graphene and PANI. Jangling Xu et al fabricated hierarchical nano-composite with PANI and graphene oxide sheet and got the enhanced capacitance 555 F g^{-1}. Qiong Wu et al. reported the PANI nano-fiber and graphene composite with filtration method and enhanced the performance of devices exhibiting high cycle stability and specific capacitance of 210 F g^{-1}.

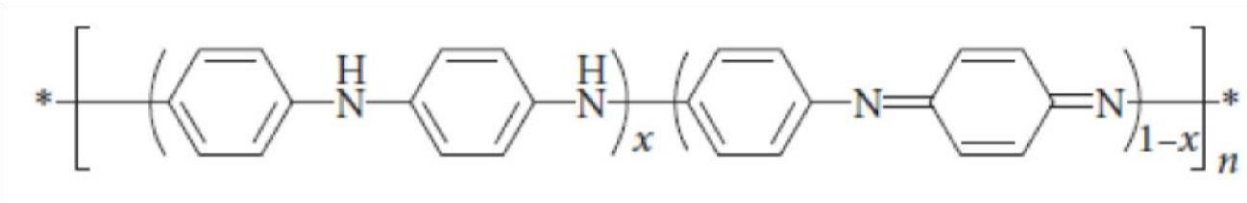

Figure 15: Chemical structure of polyaniline (Majumdar, 2019)

Totally, Polyaniline exists in three forms based on its oxidation rates, such as leucoemeraldine (fully reduced), emeraldine (half oxidised), and pernigraniline (fully oxidised). Leucoemeraldine is the completely reduced form of polyaniline. Pernigraniline is the completely oxidized state with imine connects rather than amine joins. The emeraldine type of polyaniline, frequently alluded to as emeraldine base (EB) is unbiased, whenever doped it is called emeraldine salt (ES), with the

imine nitrogen's protonated by acid. Emeraldine base is showed as the most useful type of polyaniline because of its high stability at room temperature and the way that , after doping with acid, the subsequent emeraldine salt type of polyaniline is electrically conducting .Leucoemeraldine and pernigraniline are poor conductors, notwithstanding when doped with acid. The conductive form of emeraldine is called emeraldine salt (ES). Moreover, Emeraldine salt form is obtained upon protonation of Emeraldine Base with protonic acids i.e., oxidative doping. In this study, the conductive form (emeraldine salt) will be used. The structure of PANI in different forms is shown below.

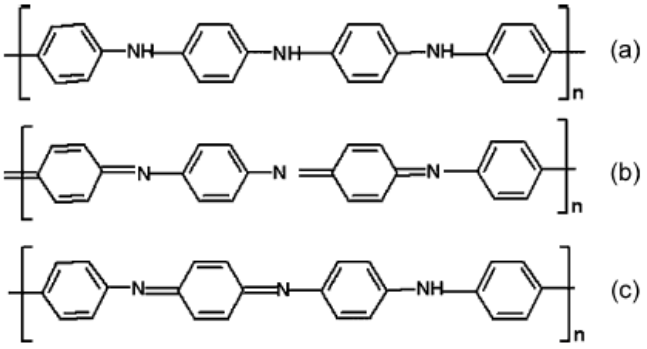

Figure 16: Three oxidation states of Polyaniline: (a) a fully reduced leucoemeraldine base (LEB) ; (b) a fully oxidized pernigraniline base (PNB) and (c) a half oxidized/half reduced emeraldine base (EB) state (Afzal et al., 2009).

2.5 Literature Survey

In recent years, the design and fabrication of polyaniline (PANI) micro/nanostructures has been increasing because of their unique properties compared to the bulk materials. Many researchers are involved in the investigations of polyaniline nanostructured materials since they have attracted intensive interest in the areas of nanoscience and nanotechnology due to their unique properties and potential applications in transistors, sensors, actuators, batteries, microcapacitors, electronic devices, polymeric conducting molecular wires, separation membranes and antistatic coatings. Due to this fact, a lot of work has been done on polyaniline (PANI) micro/nanostructure based electrodes for supercapacitor application. Some of them are discussed as follows.

Athira et al. have reported nanotubular Polyaniline as electrode materials for supercapacitor application. Which were successfully synthesized at room temperature by the chemical oxidative polymerization of aniline with Ammonium persulphate (APS) in aqueous acetic acid. Chemically synthesized PANI nanotubes were studied using Field emission scanning electron microscopy (FESEM), Brunauer -Emmett-Teller (BET) analysis, X-ray diffraction analysis (XRD) and Fourier transform infrared spectroscopy (FTIR). The electrochemical or supercapacitive performance of the synthesized PANI nanotubes was tested using cyclic voltammetry (CV) technique in H_2SO_4 electrolyte with in potential range of -0.2 to 0.8V.They identified that Polyaniline nanotube exhibits better structural, physical, and electrochemical properties than that of bulk Polyaniline materials. The effect of scan rates on specific capacitance of PANI electrode was also studied. They obtained the highest specific capacitance of 232.2 Fg^{-1} at the scan rate of 5 mVs^{-1}.

Dhawale et al.have prepared stable nanostructured polyaniline electrode for supercapacitor application. Which were successfully synthesized by chemical oxidative polymerization using ammonium persulfate as oxidizing agent and sulfuric acid as a dopant. Brunauer -Emmett-Teller (BET) analysis confirmed that the textural characteristics such as surface area (32.7 m^2g^{-1}), pore volume (0.05 cm^3g^{-1}) and pore diameter (2.96 nm) of the nanostructured Polyaniline on a stainless substrate. Field emission scanning electron microscopy (FESEM) have proved the surface morphology of nanostructured polyaniline. This further mean that, the nanograins of polyaniline are homogeneous, uniformly distributed and provide good covered on the substrate without any voids, pinholes or cracks. The crystallinity and orientation of conducting polymers were studied by X-ray diffraction (XRD). The supercapacitve studies of nanostructured polyaniline was examained using cyclic voltammetry (CV) at different scan rates. They observed that, the specific capacitance of reaches a maximum value of 503 Fg^{-1} with a specific energy and a specific power of 96.23 Wh kg^{-1} and 8.88 KW kg^{-1}.

Guan et al. studied Polyaniline nanofibers obtained by interfacial polymerization for high-rate supercapacitors. Which were fabricated by interfacial polymerization in the presence of para-phenylenediamine (PPD).The morphological, chemical, and electrochemical properties of the synthesized materials were characterized via field emission scanning electron microscopy (FESEM) and Fourier transformer infrared spectroscopy techniques, Cyclic Voltammetry (CV),

Galvanostatic charge–discharge method (GCD), and electrochemical Impedence spectroscopy (EIS), respectively. The observed a high specific capacitance value of 548 Fg^{-1}, a specific power value of 127 Wkg^{-1} and a specific energy value of 36 Wkg^{-1}.

Subramania & Devi.have reported Polyaniline nanofibers as electrode materials for supercapacitor applications. Which were successfully prepared by surfactant-assisted dilute polymerization technique. The synthesized materials were characterized by conductivity (four-pore method), Fourier transformer infrared spectroscopy (FT-IR), and X-ray diffraction (XRD) studies. The specific capacitance behavior of the Polyaniline nanofibers was studied using cyclic voltammetry which exhibits highest specific capacitance value of 298 Fg^{-1}.

Radhakrishnan et al. reported the performance of phosphoric acid doped Polyaniline as electrode for aqueous redox supercapacitor. Which were successfully synthesized chemically and electrochemically method and tested for its specific capacitance properties by constructing a supercapacitor using stainless steel electrodes. The optical, structural, and supercapacitance properties were characterized by Ultra-violet Visible spectroscopy, Fourier transformer infrared spectroscopy, X-ray diffraction, and Cyclic voltammetry, respectively. The electrochemical analytic result indicates that the sample exhibits higher specific capacitance values in the range of 244-305 Fg^{-1}. Chemically synthesized samples show lower capacitance values due to over-oxidation of the polymer and presence of impurities.

Fan et al. have also studied Polyaniline nanotube synthesized from natural tubular halloysite template as high performance pseudocapacitive electrode. Nanotubular-structure Polyaniline was successfully synthesized using natural tubular halloysite as hard template. FT-IR was carried out to investigate the structural characterization of the as-prepared samples. X-ray photoelectron spectroscopy (XPS) was used to confirm the surface composition and oxidation state of PANI. TEM was performed to further confirm whether the as-prepared PANI (HNTs) possesses a tubular structure. The electrochemical performance of the synthesized samples were characterized by cyclic voltammetry (CV). For supercapacitors, due to the PANI (HNTs) with hollow structure and higher specific surface area the Polyaniline hollow nanotubes electrode exhibits excellent rate performance, and the values of specific capacitance achieve 504 F g^{-1} and 442 F g^{-1} at current densities of 1 A g^{-1} and 20 A g^{-1}, respectively. This indicates that, the obtained tubular polyaniline

presents high specific capacitance at various current density as electrode material for supercapacitors.

Patil et al. synthesized a Mn Doped Polyaniline Electrode for Electrochemical Supercapacitor thin films were deposited on stainless steel substrates by sonochemical method. Films deposition was done using dip coating technique. To study the Mn doping effect on the specific capacitance of PANI, concentration of Mn was varied from 0.4 to 1.6 wt %. The Fourier Transform-Infrared (FT-IR) and Raman spectroscopy techniques were used for the phase identification and determination of the Mn in the PANI films. Surface morphology of prepared samples were examined by using Field Emission Scanning Electron Microscopy (FESEM) which showed nanofiber aggregate structure of undoped PANI and porous and well distributed nanofibers for the doped PANI. The supercapacitive behavior of the electrodes was tested in three electrode system with 1.0 M H_2SO_4 electrolyte by using cyclic voltammetry. They observed that the specific capacitance value increases from 285 to 474 Fg^{-1} as the Mn concentration was increased. This work demonstrates a simple strategy of improving specific capacitance of the polymer and hence may be adopted easily for other dopants also.

In 2002 Ryu, Kim, Park, & Chang et al.have also studied symmetric redox supercapacitor with conducting polyaniline electrodes. Which were successfully synthesized by electrochemical polymerization aniline with hydrochloric acid (HCl) and Lithium salt ($LiPF_6$) as a dopant. The electrochemical characteristics' of the prepared samples were also investigated by cyclic voltammetry), Galvanostatic charge and discharge method (GCD), and Electrochemical Impedence Spectroscopy (EIS), respectively. This work demonstrates that the specific capacitance of PANI-HCl decreases ~400 cycles and then becomes constant at ~40 Fg^{-1}.On the other hand, the polyaniline electrode doped with lithium salt like $LiPF_6$ shows a specific discharge capacitance of ~107 Fg^{-1} Initially and ~84 Fg^{-1} at 900 cycles.

Shaikh et al.have reported nano-nest polyaniline electrodes for supercapacitor applications. Nano-nest polyaniline electrodes were synthesized by using electrodepostion method at room temperature (27^{o}C) without the use of templating. The fabrication of supercapacitors are carried out by direct electrodeposition on stainless steel and indium tin oxide (ITO) substrates. The formation of elemental bonds and the degree of crystallinity were confirmed by FTIR and XRD studies, respectively. The surface morphology of nano-nest polyaniline is confirmed by SEM studies. This unexpected rise in capacitance is discussed in terms of the electroactive

material/electrolyte interface area. The electrochemical performance of the PANI nano-nest electrode was investigated from cyclic voltammetry in 1 M H_2SO_4 electrolyte solution at a scan rate from 5 to 100 mVs^{-1}. When the scan rate is 5 mVs^{-1}, pseudocapacitance is 412, 757, 676 F g^{-1} were respectively obtained for PANI 35, PANI 47, and PANI 59. The galvanostatic and potentiostatic experiments have conducted on stainless steel substrate shown that the polyaniline material has very good stability and with maximum capacitance 757 Fg^{-1} and minimum capacitance 412 F g^{-1} in 1 M H_2SO_4 electrolyte within the potential windows of -200 to 800 mV vs SCE at 5 mVs^{-1} scan rate.

2.6. Research gaps and literature review summary

Previous studies of the working principle, electrode materials and types of supercapacitors were summarized in this chapter. The future developments of supercapacitors are moving towards flexible and efficient supercapacitors. The conducting polymer based supercapacitor research has become a relatively new field of scientific interest. Current works in this field were also reviewed. Most of the work in this field focused on improving the performance by developing new electrode materials of supercapacitors.

The gaps identified to be investigated through this thesis are as follows:

1. Among conducting polymers, eventhough bulk Polyaniline materials have been considered desirable electrode material for pseudocapacitance supercapacitors, it offers good electrical conductivity, specific capacitance, and reversible redox, fast doping/dedoping rate, low cost, flexibility, controllable morphologies, and high environmental stability. However, achieving high specific capacitance with long-term cyclic stability is still a challenge. In addition to this, it mostly shows poor cycle stability and low rate capability owing to the slow charge transfer reaction, mechanical degradation and swelling/shrinkage changes.
2. Even if carbonaceous materials (Activated Carbon, carbon aerogels, and carbon nanotubes), Transition metal oxides/hydrides, and Conducting polymers have been used as electrode materials for supercapacitors. But, each of those still has some challenges in developing advanced energy storage devices due to having a porosity of the material, high cost of production, harmfulness for the environment, and swelling/shrinkage changes, respectively.

To overcome these problems, the following will be solutions.

1. Surface modification of PANI morphology could enhance the electrical properties and electrochemical performance of nanostructured polyaniline materials. This further means that, by simply changing the molar ratio of the dopant to monomer, the morphology of salicylic acid (SA)-doped PANI nanosphere can be obtained, and the resulting structures will provide unique optical, electronic, thermal, and electrochemical properties.
2. It is believed that the progress in this study of polyaniline nanosphere as electrode materials for supercapacitor applications will contribute to some unfilled gaps in knowledge of this new field, and enable the further development of highly stable and efficient energy storage devices.

CHAPTER THREE

EXPERIMENTAL: MATERIALS AND METHODS

In this chapter, the general materials, experimental techniques and instrument details used in this thesis are described.

3.1. Reagents and apparatus

3.1.1. Chemicals and reagents

All the reagents used in the experiments like Aniline ($C_6H_5NH_2$), Ammonium persulfate ($(NH_4)_2S_2O_8$), Salicylic acid ($C_7H_6O_3$), Hydrochloric acid (HCl), Sulfuric acid (H_2SO_4), Methanol (CH_3OH), Potassium Bromide (KBr), Dimethyl sulfoxide **(**C_2H_6OS) Acetone(C_3H_6O),were of analytical grade and taken from Laboratories of Material Science and Engineering (JIT,Jimma, Ethiopia) except for Salicyclic acid. Double distilled water was used throughout the work. All the materials above were used without further purification.

3.1.2. Instruments and Apparatus

The general equipment for materials preparation, physical and chemical characterization, and electrochemical performance measurement is as follows: Magnetic stirrer with hot plate (HSC-19T, Bibby Scientific Limited), Laboratory Furnaces (Nabertherm Company, Germany), Ultrosonicator (DAWE) (DAWE 43 Instruments Limited) were employed during the experiments. The Spin Coater machine (model, CY-SP4) and Multimetre (model, keithley 2400) were also used. Postlip filter papers (d=127 mm, the thickness is 130 ± 1 μm) were manufactured by Evans Adlard & Company limited. Copper wires (50 μm and 100 μm in diameter) were obtained from the market. Ultraviolet Visible Spectroscopy (UV-Vis) spectra were recorded with a model of PerkinElmer Lambda 25. The Fourier Transform Infrared spectroscopy signals were recorded with a model of PerkinElmer Spectrum Two. Thermogravimetric analysis was performed on a model of PerkinElmer TGA 4000. Powder X-ray diffraction (XRD) pattern was tested on a Philips PW7000 instrument (Cu Kα radiation, 1.5418 Å). Scanning electron microscope (SEM) images were recorded JCM-600 Ius instrument operated at 15 KV. Cyclic Voltammetry (CV) was monitored with an electrochemical workstation (BASi Epsilon- EC-Ver.2.13.77 XP electrochemical analyzer system). This experiment was performed with a conventional three-electrode system, in which the

prepared samples (Polyaniline and polyaniline nanosphere) was the working electrode, a platinum wire was the counter electrode and an Ag/AgCl was the reference electrode.

3.2 Characterization of the material

3.2.1 Physical and Structural characterization

The main characterization techniques and instrumentation employed are shown in this section. The samples' physical, chemical, and electrochemical characterizations where studied by TGA, SEM, XRD, FT-IR, UV-VIS, and CV, respectively.

3.2.1.1 Ultraviolet-Visible Spectroscopy (UV-VIS)

Ultraviolet–Visible Spectroscopy is a relevant physical tool which exploits light in ultraviolet , visible and near infrared range of electromagnetic spectrum. Beert-Lambert law tells a linear relationship between absorbance, concentration of absorbers in the solution and the path length. The beer-Lambert law equation is as shown in the following relation as:

$$A = \varepsilon l c \qquad (10)$$

Therefore, UV-Vis spectroscopy can be conducted for determining the concentration of the absorbing species, for a fixed path length (Navarro et al., 2021). In addition to this, UV/Vis absorption spectrum is related to molecular structure, bonding/conjugation, therefore, it can provide qualitative information about the material of interest from ε and λ. The absorption or reflectance in the visible range straightforwardly; affects the perceived color of the chemicals involved. In this region of the spectrum, atoms and molecules undergo electronic transitions. Absorption spectroscopy is complementary to fluorescence spectroscopy, in that fluorescence deals with transitions of electrons from the excited state to the ground state to the ground state, while absorption measures transitions from the ground state to the excited state. In this study, the UV-Vis spectra of all the synthesized samples were measured using a model of PerkinElmer Lambda 25 in the wavelength region between 200-800 nm. For this purpose, the synthesized four samples were grinded into very fine particles in agate mortar and pestle for 2 minutes. These very fine particles then were dispersed with in a Dimethyl Sulfoxide (DMSO) solvent. A 1 cm x 1 cm x 10 cm glass cuvette cell was used as the sample holder with the following method parameters: 200-800 nm scan, slit width of 0.5 mm, and medium scan speed. In this work, the optical band gap energy was also estimated from the absorption coefficient data as a function of wavelength using the Tauc relation as shown in the following relation as (Saleh et al., 2019):

$$(\alpha h\nu)^2 = A(h\nu - Eg) \qquad (11)$$

3.2.1.2 Fourier Transform Infrared Spectroscopy (FT-IR)

Fourier transform infrared spectroscopy (FTIR) is an advanced and extensively used analytical tool that investigates the structural chemistry of the sample by irradiating with IR radiations. The IR region is lying between visible and microwave end of the electromagnetic radiation spectrum. It is basically divided into three main portions: near IR (14000–4000 cm^{-1}), mid-IR (4000–400 cm^{-1}), and far IR (400–40 cm^{-1}) (Khan et al., 2018). An infrared spectroscopy measured the absorption of IR radiation made by each bond in the molecule and as a result gives spectrum which is commonly designated as percentages (%) transmittance versus wavenumber (cm^{-1}). A diverse range of materials containing the covalent bond absorbed electromagnetic radiation in the IR region. The IR region is at lower energy and higher wavelength than the UV-visible light and has higher energy or shorter wavelength than the microwave radiations. For the determination of functional groups in a molecule, it must be IR active. An IR active molecule is the one which has dipole moment. When the IR radiation interacts with the covalent bond of the materials having an electric dipole, the molecule absorbed energy, and the bond starts back and forth oscillation. Therefore, the oscillation which caused the change in the net dipole moment of the molecule should absorbed IR radiations.

In this work, the FT-IR spectra of all the prepared samples were measured using a model of PerkinElmer Spectrum Two spectrometer in the wavenumber region between 4000 cm^{-1} and 500 cm^{-1}. For this purpose, the prepared four samples were grinded into very fine particles in agate mortar and pestle for 2 minutes. These fine particles then were mixed with a IR transparent KBr powder. The resulting powder mixture was transferred into 10 mm stainless steel disk for a die set and 5 tons of pressure were applied using a hydraulic press for 4-5 minute to form a very fine thin pellet.

3.2.1.3 Thermogravimetric Analyzer (TGA)

Thermogravimetric or Thermogravimetric Analysis (TGA) is a well proven Thermal Analysis method. TGA measures the absolute amount and rate of change in weight of a sample as either functions of time or temperature in a controlled environment. TGA has a wide range of properties

that can be measured such as thermal stability, oxidative stability, effects of different atmospheres, moisture and volatile content, and sometimes the composition of multi-component systems (Edition et al., n.d.). Furthermore, a thermogravimetric analyzer consists of a sample pan that is supported by a precision balance. That pan resides in a furnace and is heated or cooled during the experiment mass of the sample is monitored during the experiment. A sample purge gas controls the sample environment. This gas may be inert or a reactive gas that flows over the sample and exists through an exhaust. In this work, In order to see the effect temperature on the thermal behavior of the polymer thermogravimetric analysis of polyaniline nanosphere has been carried out from 20 ^{o}C and 800 ^{o}C.

3.2.1.4 Scanning Electron Microscopy (SEM)

Scanning electron microscopy (SEM) is a versatile tool to reveal the microstructures inside objects.The scanning electron microscopy uses a focused beam of high-energy electrons to generate a variety of signals at the surface of solid specimens. The signals that derive from electron-sample interactions reveal information about the sample including external morphology, chemical composition, and crystalline structure and orientation of materials making up the sample. The electron source generates electrons at the top of the column and accelerated down and passes through different lenses and apertures to generate a focused beam of an electron that hits the sample surface. SEM uses a highly energetic electron beam up to 30 keV to scan the surface of the specimen. The secondary and backscattered electrons, carrying information about the specimen morphology and composition, are used as the principal signals for sample imaging. Secondary electrons are the excited inner shell electrons that have been ejected from the sample during the inelastic scattering of the incident beam electrons. Figure 17 illustrates a scanning electron beam incident on a solid sample

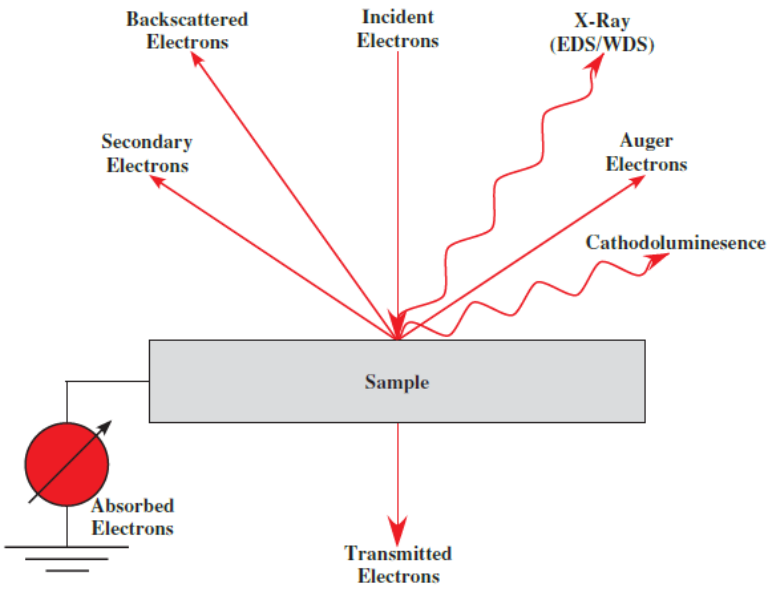

Figure 17: Schematic drawing of a scanning electron beam incident on a solid sample showing some of the signals generated that can be used to help characterize the microstructure (Brandon, 2014.).

The interaction of electrons with a sample can generate different signals including secondary and backscattered electron, x-ray, absorbed current, and transmitted electrons. Most widely SEM uses backscattered (BSE) and secondary electron (SE) for imaging (Niedrig & Niedrig, 1982). BSE is reflected back after elastic interactions between the beam and the sample and SE is a result of inelastic interactions between the electron beam and sample, while secondary electron originates from surface regions, therefore, they carry different types of information. Backscattered image shows high sensitivity to differences in atomic numbers. The higher the atomic numbers the brighter the material appears in the image. Secondary electrons are used to give the morphology (texture) and topology of sample and backscatter electrons illustrate the contrast in composition in multi-phase samples.

In this study, SEM characterization was conducted using JCM-6000 instrument for microstructural analysis and operated at 15 KV. All the prepared samples were coated with gold before the characterization was conducted.

3.2.1.5 X-ray Diffraction (XRD)

X-ray diffraction is a most widely used technique that determine a sample's composition or crystalline structure. For larger crystals such as macromolecules and inorganic compounds, it can be used to determine the structure of atoms within the sample. If the crystal size is too small, it can determine sample composition, crystallinity, and phase purity. This technique sends x-ray beams through it. X-ray beams are chosen because their wavelength is similar to the spacing between atoms in the sample, so the angle of diffraction will be affected by the spacing of the atoms in the molecule, as opposed to using much larger wavelengths, which would be unaltered by the spacing of the atoms. The X-rays then pass through the sample, bouncing of the atoms in the structure, and, changing the direction of the beam at some different angle, theta, from the original beam. This is the angle of diffraction. Some of these diffracted beams cancel each other out, but if the beams have similar wavelengths, then constructive interference occurs. X-ray is electromagnetic radiation that has a wavelength in the range from 0.01 to 10 nm. XRD takes advantage of the coherent scattering of x-rays by polycrystalline materials to obtain a wide range of structural information of phases. Therefore XRD is an important structural technique for structural characterization of the prepared samples. Apart from providing the nanocrystals' structural phase, this technique also provides an estimate of the size of the nanocrystals. The crystal is formed by long range ordering of atoms and the distance between these regularly arranged atoms (bond length) is of the same order of magnitude as the X-ray wavelength (CuKα = 1.54 Å). When a beam of monochromatic X-ray diffracts in the crystal, the atomic lattice of the sample acts as a three-dimensional diffraction grating, causing the X-ray beam to be diffracted at specific angles. Figure 18 illustrates X-ray diffracted from crystal lattice planes.

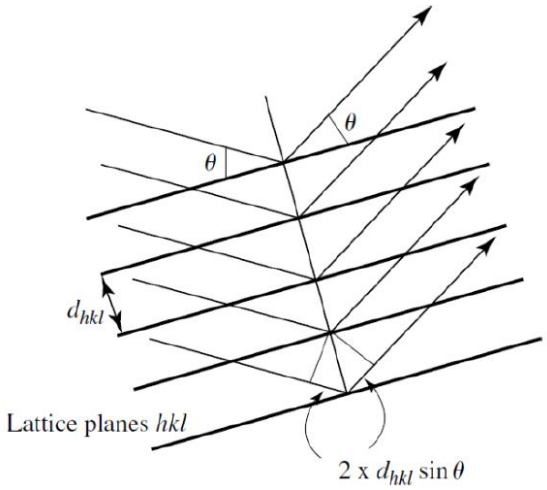

Figure 18: The schematic of X-ray diffracted from crystal lattice planes (Bernstein & Desiraju, 2018.)

The diffraction pattern, including the peak positions (angles), provides the specific information of the crystal according to Bragg's Law (Equation 11) from the Figure 18 written as follow:

$$2d_{hkl}\sin\theta = n\lambda \qquad (12)$$

The angles are used to calculate the inter-planar atomic spacing d_{hkl}. That means when the inter-planar atomic spacing increase the peak shift to low angle and vice versa. The width of the diffraction peaks is used to determine crystallite size and micro-strain in the sample. The d-spacing is important as it is directly related to the unit cell parameter of the specimen.

In the present work, the structure of all prepared samples were detected by using characterized using a Philips PW7000 instrument (Cu Kα radiation, 1.5418 Å) over a 2θ range from 10^o up to 80^o.The average crystallite size of the prepared samples will be calculated by Debye Scherer equation (Devi et al., 2014);

$$D = \frac{k\lambda}{\beta\cos\theta} \qquad (13)$$

Where, k is the shape factor (0.89); D is the average crystallite size; λ is the X-ray wavelength, θ is the Bragg diffraction angle; β is the full width at half maximum (FWHM).

3.3 Conductivity Measurements

The conductivity of the synthesized materials is an important experimental parameter for specifying their use as electrodes in supercapacitor applications. For this matter, electrical resistances were performed by multimeter.The electrical conductity can be determined by knowing the resistivity of synthesized materials. Considering that conductivity is the inverse of resistivity, in this study the conductivity was obtained by utilizing the two-prope method to measure the electrical resistivity of Polyaniline and Polyaniline nanospheres, using Eq. 8 (Alice et al., 2017). The resistivity (ρ) of the films is calculated by using the following equation.

$$\rho = \frac{RA}{L} \qquad (14)$$

Where R is the sample resistance, A is the cross section area of the film and L is the distance between the electrodes. The conductivity of the films was determined from the relation:

$$\sigma = \frac{1}{\rho} \qquad (15)$$

Where: σ is conductivity and ρ is the resistivity of the film**.**

3.4 Electrochemical method

3.4.1 Cyclic Voltammetry

Cyclic voltammetry (CV) is an electrochemical technique, where the electrode is ramped linearly and is inverted when a specific potential is reached. The cyclic voltammetry is a function of time. CV can be used to study a various range of electrochemical reactions. The electrochemical cell, where the voltammetric experiment is carried out, consists of a working (indicator) electrode (WE), a reference electrode (RE), and usually a counter (auxiliary) electrode (CE). The current flow through the working electrode was measured, and the potential is acquired by computing the current against the reference electrode. On the other hand, the counter electrode is used to finalize the electrical circuit for the current flow (Obeidat & Rastogi, 2018). In general, an electrode provides the interface across which a charge can be transferred or its effects felt. Since the working electrode is where the reaction or transfer of electrons taking place, whenever we refer to the

electrode, we always mean the working electrode. The reduction or oxidation of a substance at the surface of a working electrode, at the appropriate applied potential, results in the mass transport of new materials to the electrode, surface and generation of current. Even though the various types of voltammetric techniques may appear to be very different at first glance, their fundamental principles and applications derive from the same electrochemical theory. Figure 19 illustrated a three-electrode configuration in electrochemical set up.

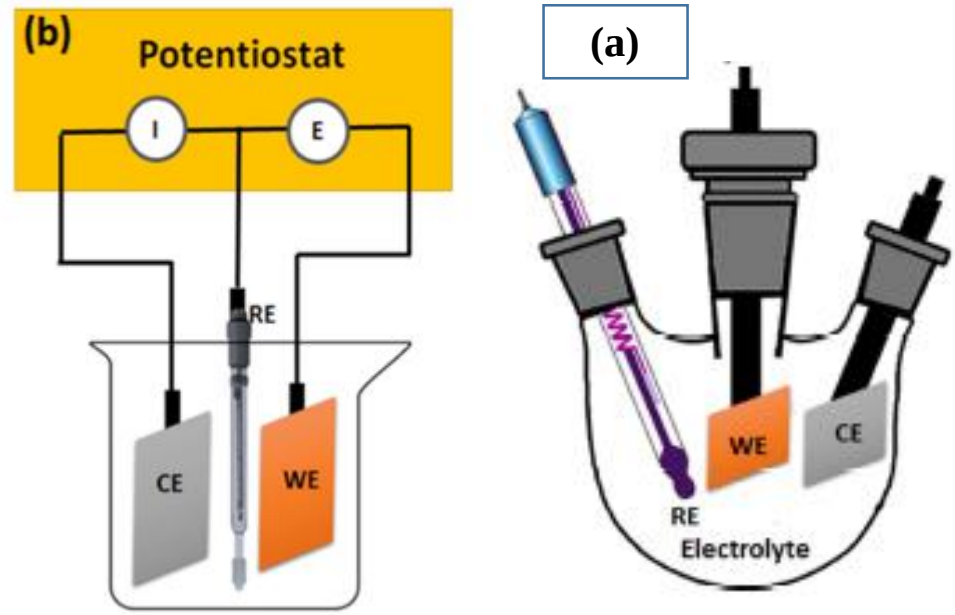

Figure 19: Schematic of (a-b) a three-electrode configuration (Moussa et al., 2016)

In this work, cyclic voltammetry, an electrochemical technique, was performed to evaluate the electrochemical performance of the prepared samples when used as electrode material.

3.5 Experimental procedures

3.5.1 Synthesis of Polyaniline

The synthesis of Polyaniline was carried out by chemical oxidative polymerization of aniline with ammonium persulfate at lower temperatures (0-5^{o}C) (Qaiser et al., 2017). The procedures are described as follows: 5 g of APS (APS is oxidizing agent) and 2 ml of aniline were dissolved separately in 1mol L^{-1} aqueous solution of HCl in the volume of 50 ml. This solution was kept in ice bath maintaining the temperature between 0-5^{o}C. Then 5 g of ammonium persulfate solution was added drop by drop in to aniline solution by using a dropper and continuously stirred using a magnetic stirrer for 4 h. As the ammonium persulfate mixed with the aniline solution, it turned to greenish black color, indicating that the organic polymerization reaction has begun. After 4 h of reaction, the products were collected by filtration and washed successively using 1 mol L^{-1} HCl followed by double distilled water and acetone for several times until the washings become colorless. Finally, the residue (paste) was dried under a vacuum oven at 60 ^{o}C for 24 h.

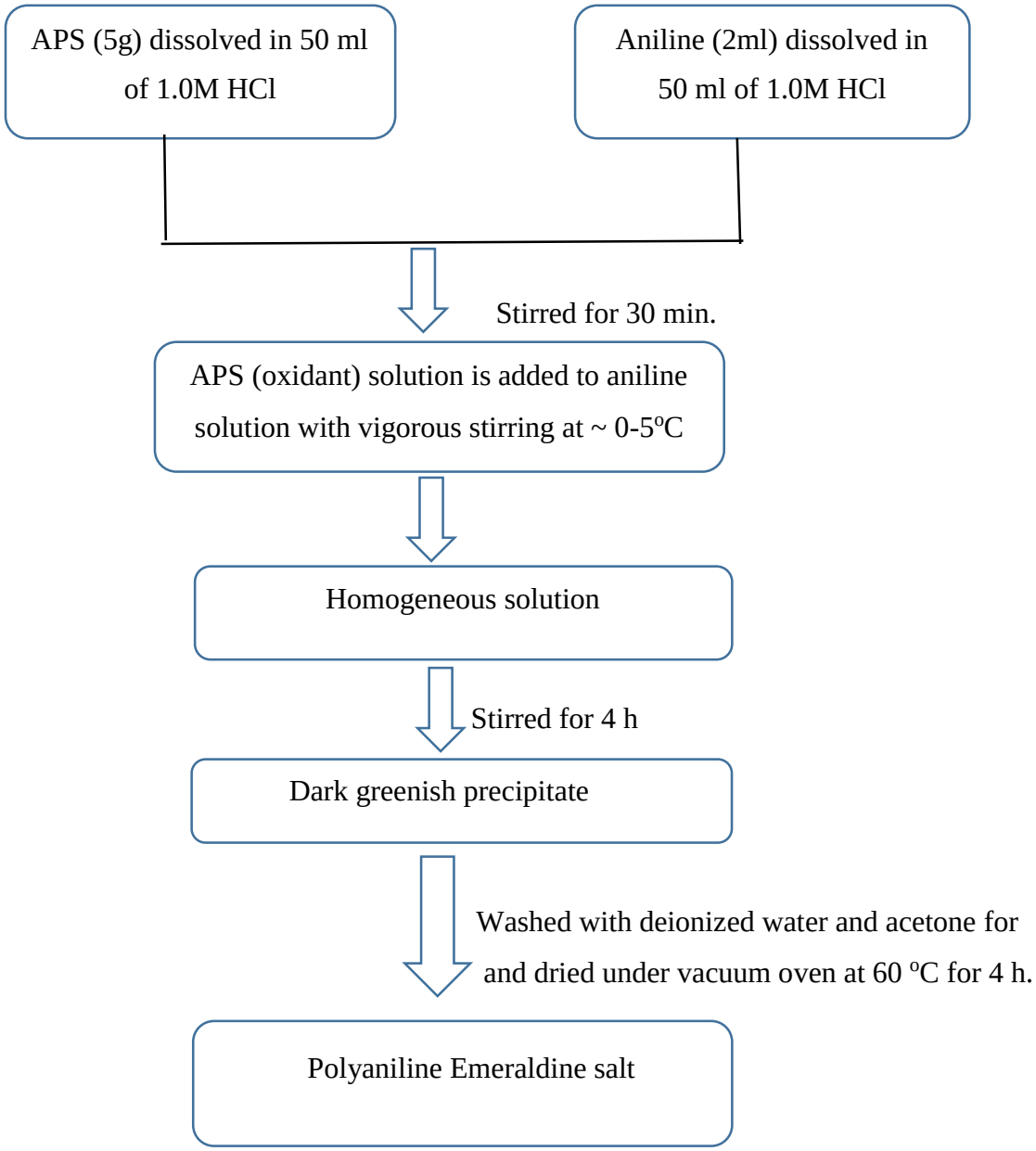

Figure 20: Flow chart of Polyaniline preparation

3.5.2 Synthesis of polyaniline nanospheres

PANI nanospheres were prepared by oxidative polymerization (Via. Self-assembly process) of Aniline at room temperature using Ammonium persulfate as the oxidant in the presence of Salicylic Acid (as a dopant) (Zhang & Wan, 2003). A typical polymerization process of polyaniline nanosphere is as follows: 2×10^{-3} mol Aniline and 1×10^{-3} mol salicylic acid were dissolved in 10 ml of de-ionized water with magnetic stirring at room temperature for 30 minutes. The stirring was then stopped, 5 ml of aqueous solution of APS (0.456 g, 2×10^{-3} mole in 5 ml of distilled water) was added, and the reaction was left for 12 hours. The resulting PANI precipitate was filtered and washed with distilled water and methanol several times. Finally, the product was dried in vacuum at room temperature for 24 hours. In the reactions, the salicylic acid was varied from 0.1 M, 0.12 M and 0.16 M, i.e., mole ratio of dopant to monomer mole ratio is varied from 0.1:0.2, 0.12:0.2 and 0.16:0.2 by keeping monomer-initiator ratio constant([An]/[APS] as 1:1. This further means that, a different molar ratio of Salicylic acid to Aniline monomer ([SA]/[An] =0.5, 0.6, and 0.8) was used under the same concentration of Aniline monomer (0.2 M). Table.5 shows experimental parameters in the synthesis of polyaniline nanosphere materials.

Table 5: Preparation details of polyaniline nanosphere samples.

S.N	[SA]/[An] ratio	[SA]	[An]	Volume of aniline	Mass of salicylic acid (SA)	Mass of Ammonium persulfate(APS)
1	0.5	0.1M	0.2 M	0.18 ml	0.138 g	0.456 g
2	0.6	0.12M	0.2 M	0.18 ml	0.165 g	0.456 g
3	0.8	0.16M	0.2 M	0.18 ml	0.221 g	0.456 g

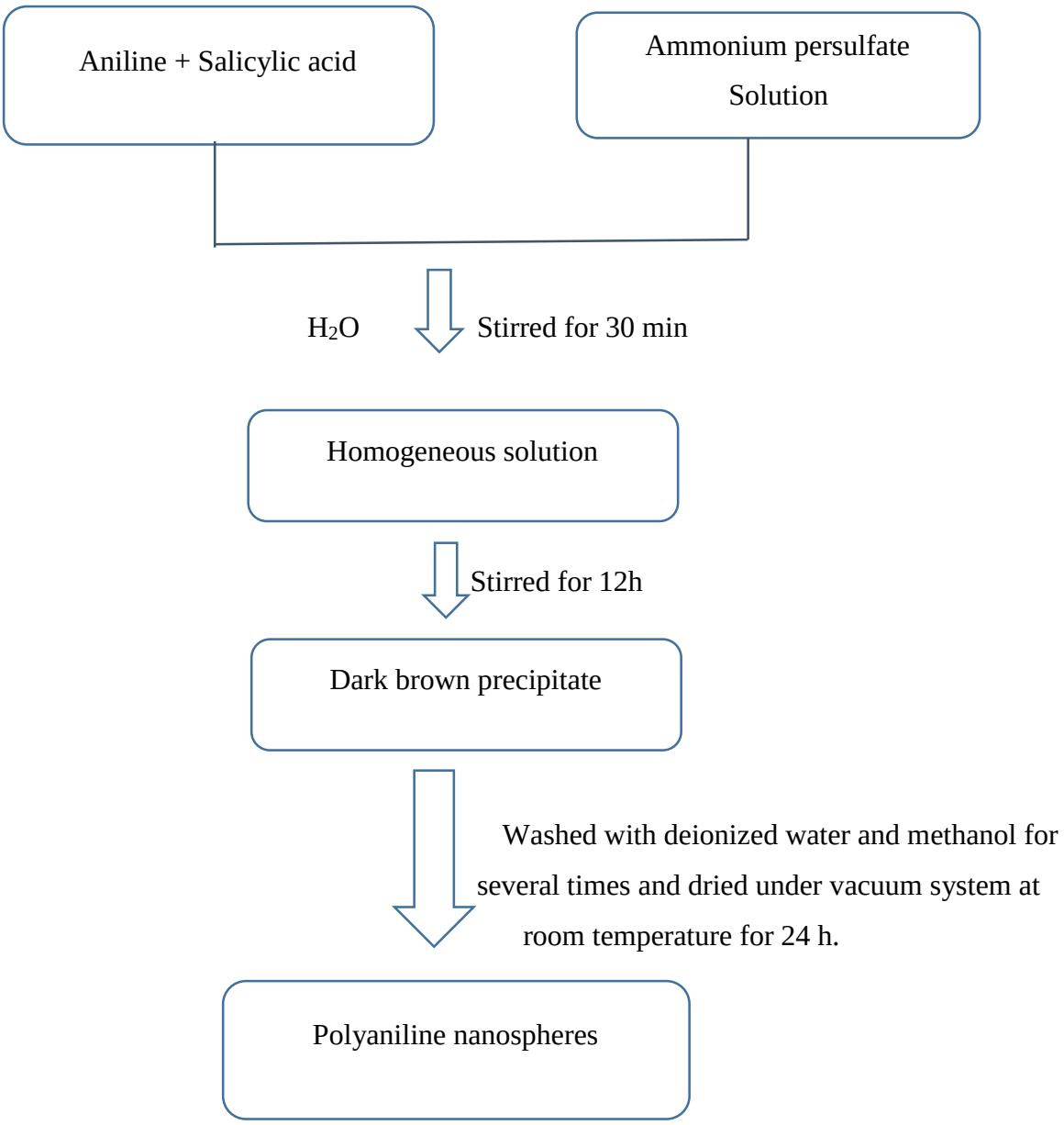

Figure 21: Flow chart of Polyaniline nanospheres preparation

3.5.3 Synthesis of polyaniline solution

To prepare a polyaniline solution, polyaniline (PANI) powder must be synthesized first. The synthesis of PANI uses the chemical oxidation method as has been done in earlier studies (Qaiser et al.,2017). The oxidized Polyaniline powder was then dried and crushed with mortar until a fine powder was obtained with granules that could escape in the 325-mesh filter. 0.2 g of Polyaniline (emeraldine salt) powder was dissolved in 15 ml of Dimethyl Sulfoxide solvent, and vigorously stirred using a magnetic stirrer with a speed of 1500 rpm for 2 hours, then continued with ultra-sonication for 2-hours to obtain a homogeneous solution (Series et al, 2019).

3.5.4 Synthesis of polyaniline nanosphere solution

To make a polyaniline nanosphere solution, polyaniline nanosphere powder must be synthesized first. The synthesis of PANI nanosphere uses the oxidation method (via Self-assembly process) as has been done in previous studies (Zhang &Wan, 2003).The methods for making PANI nanosphere solution is the same as polyaniline solution.

3.5.5 Synthesis of thick films

Figure 22: Schematically shows that the formation of polyaniline and polyaniline nanosphere films on the glass substrate. A clean, flat glass (2 cm x 1 cm) was used as the substrate in this experiment. The polyaniline and polyaniline nanosphere homogenized solutions (5-6 ml) were dropped over the surface of the glass substrate by the spin coating method and rotated with a variety of rotational speed 1000- 3000 rpm for 60 seconds. The coated glass then dried in a vacuum oven at temperature 100˚C for 10 minutes. To get a thicker film, a second layer of polyaniline and polyaniline nanosphere solutions (5-6 ml) were cast overlaying the first layer using the same procedure.

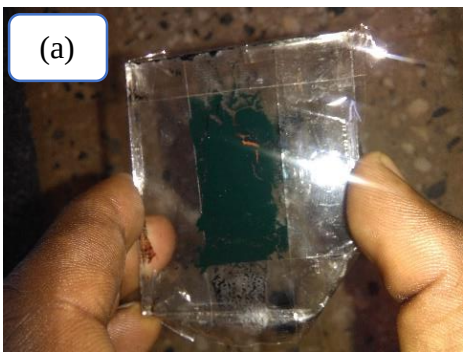

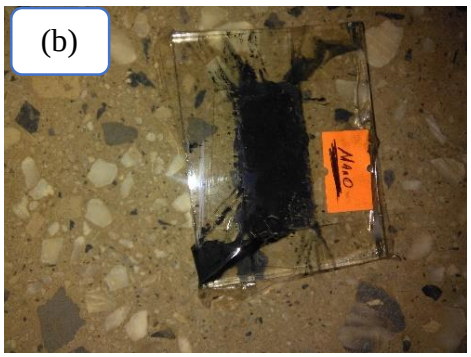

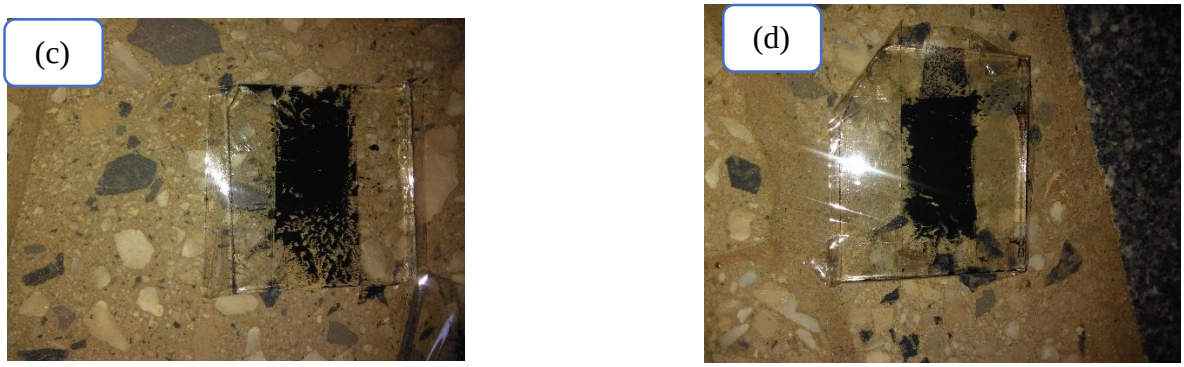

Figure 22: Polyaniline (a) and polyaniline nanosphere films: b) N 0.5, c) N 0.6 and d) N 0.8

3.6 Electrical Conductivity Measurement

Electrical measurements were performed with a two-electrode scheme using multimetre. For the two-electrode scheme, a pair of silver electrodes where used. The spin coating method was used to deposite the prepared samples on the glass substrate (Neelgund & Oki, 2011). A 5 wt% dispersion of PANI & PANI nanospheres in DMSO was cast on top of the glass substrate and dried well before initiating the measurements.

Table 6: Demonstrates electrical measurements for both bulk polyaniline and polyaniline nanospheres.

Sample code	Sample Resistance (R)	Cross-sectional area of the film (cm^2)	The distance between electrodes
PANI	$0.08x10^6\,\Omega$	(2x1) cm^2	2 cm
N0.5	$0.008x10^6\,\Omega$	(2x1) cm^2	2 cm
N0.6	$0.009x10^6\,\Omega$	(2x1) cm^2	2 cm
N0.8	$0.007x10^6\,\Omega$	(2x1) cm^2	2 cm

3.7 Electrode Preparation

3.7.1 Preparation of Polyaniline Electrode

To prepare electrode materials from polyaniline, 70% (w/w) of polyaniline powder and 30% (w/w) of Dimethyl sulfoxide (DMSO) solvent were mixed homogeneously for 20 min. with a mortar and pestle. The homogenized mixture was kept in the refrigerator for 24 h and then the paste was housed in a tip of an insulin syringe by introducing a conducting copper wire that extends between the tip and the back of the syringe as demonstrated in Figure 23.

Figure 23: Chemically synthesized polyaniline as a working electrode

3.7.2 Preparation of polyaniline nanosphere electrodes

To make electrode from polyaniline nanosphere, 70% of polyaniline nanosphere powder and 30% (w/w) of Dimethyl sulfoxide (DMSO) solvent were mixed homogeneousely for 20 min.with a mortar and pestle. The homogenized mixture was kept in the refrigerator for 24 h , and then the paste was housed in a tip of an insulin syringe by introducing a conducting copper wire that extends between the tip and the back of the syringe as demonstrated in Figure 24.

Figure 24: Chemically synthesized polyaniline nanosphere as a working electrode

3.8. Electrochemical Characterization

3.8.1 Cyclic Voltammetry test

In order to evaluate the electrochemical performance of the PANI & PANI nanosphere based electrodes, cyclic voltammetry (CV) test was performed. In this study, electrochemical performances were determined mainly by the cyclic voltammetry (CV) using a BASi Epsilon-EC-Ver.2.13.77 XP electrochemical analyzer system in 1.0 M H_2SO_4 electrolyte. The three electrode system was equipped with PANI and PANI nanosphere as working electrode, platinum wire as counter electrode and Ag/AgCl as reference electrodes.The paste (1mg) housed in a tip of an insulin syringe by introducing a conducting copper wire that extends between the tip and the back of the syringe were used as the working electrodes.The PANI and PANI nanosphere working electrode for electrochemical measurement was fabricated by mixing 70% of polyaniline nanosphere powder and 30% (w/w) of Dimethyl sulfoxide (DMSO) solvent. The specific capacitance value can be obtained from the cyclic voltammetry curve according to the equation (Athira et al., 2018)

$$Cp = \frac{\int_{V_{min}}^{V_{max}} I(V)dv}{mv(V_{max} - V_{min})} \qquad (16)$$

Where, I (v) is average current for unit area dipped in electrolyte, m is mass of material deposited, v is scan rate and V_{max}- V_{min} is potential window. The simplification of the above equation for specific capacitance is shown below by,

$$Cp = \frac{Q}{mV} \qquad (17)$$

Where Q is the charge stored in Coulombs, m is the mass of active material in grams, V is the potential and Cp is the specific capacitance. As we know that,

$$I = \frac{Q}{t} \quad \text{Or} \quad Q = I \times t \qquad (18)$$

By putting equation (18) in equation (17) we get,

$$Cp = \frac{(I \times t)}{mV}$$

Dividing nominator and denominator by t,

$$Cp = \frac{\frac{(I \times t)}{t}}{\frac{mV}{t}}$$

$$Cp = \frac{I}{m\left(\frac{V}{t}\right)}$$

In above equation, $\frac{V}{t}$ is the scan rate of Cyclic Voltammetry and it would be represented by K

$$Cp = \frac{I}{m \times \mathrm{K}} \qquad \text{Or} \qquad I = Cp \times m \times \mathrm{K} \tag{19}$$

In CV curve, the current changes by changing the potential from V_1 to V_2. Therefore, equation (19) can be written in its integral from as.

$$I(v)\,dv = \int_{V_1}^{V_2} (Cp \times m \times K)\,dv \tag{20}$$

If we look carefully to above equation, the integral on left hand side $\left[\int_{V_1}^{V_2} I(v)\,dv = Area\right]$ represent the area of the CV curve. $(I(v) \times dv) = yx = Area)$.Therefore, equation (20) can be written as,

$$Area = \int_{V_1}^{V_2} (Cp \times m \times \mathrm{K})\,dv \tag{21}$$

For a specific material, the value of Cp, m, and K is constant. Therefore, the integral in equation (21) can be solved as,

$$Area = (V_2 - V_1)\,Cp \times m \times \mathrm{K} \tag{22}$$

In CV, we have three areas,

When capacitor is charging, then Area= A_1 and equation (22) can be written as,

$$A_1 = (V_2 - V_1)\,Cp \times m \times K \tag{23}$$

Similarly, when capacitor is discharging, then Area= A_2 and equation (22) can be written as,

$$A_2 = (V_1 - V_2)\,Cp \times m \times \mathrm{K} \tag{24}$$

For the calculation of area (A) inside the CV curve, we have to subtracts equation (23) from equation (24)

$$A = A_1 - A_2 = \left[(V_2 - V_1)Cp \times m \times \mathrm{K}\right] - \left[(V_1 - V_2)Cp \times m \times K\right]$$

$$A = \left[(V_2 - V_1)Cp \times m \times \mathrm{K}\right] + \left[(V_2 - V_1)Cp \times m \times K\right]$$

$$A = 2\left[(V_2 - V_1)Cp \times m \times K\right] \tag{25}$$

$$\frac{A}{2} = (V_2 - V_1)Cp \times m \times K$$

$$Cp = \frac{A}{2(V_2 - V_1) \times m \times K} \quad \text{Or} \quad Cp = \frac{A}{2mK(V_2 - V_1)} \tag{26}$$

CHAPTER FOUR

RESULTS AND DISCUSSION

4.1 UV/Vis spectroscopy result

For both polyaniline nanospheres, the absorption bands are seen with maxima at 630 nm, which is essentially the same with that for bulk polyaniline. The band at 630 nm is associated with the transition of benzenoid rings (π–π* transtions) into quinoid rings (polaron-π* transitions) (Neelgund & Oki, 2011). In addition to this, the absorption band located at 605–635 nm is attributed to the quinoid ring transition (charge transfer from HOMO of the benzenoid ring to LUMO of the quinoid ring). The results are in agreement with earlier report (Bilal et al., 2019). So, it is reasonable that the PANI nanosphere have the highest absorbance ratio of benzenoid to quinoid due to the low oxidant (APS) concentration. The absorption peaks for all four samples are indicating that the samples are in doped state, and the peak nearly about 630 nm for all four samples assigns the polaron band (Sironi et al., 2015). There was also clear increase in red shifting of the peak. The difference in the band shifting might be the reason of the molecular interaction of dopants with imine nitrogen of PANI. The increasing intensity of the peak around 470 nm with increased concentration SA indicates that the environments of the quinoid and benzenoid rings are apparently charged and it is reasonable that the higher SA concentration increases the chance for aniline to dope with SA.Thus, it could improve the doping degree of PANI. The decrease of the peak intensity at 760 nm with increasing the concentration of SA implies the simultaneous shortening of the conjugation length, corresponding to the increase of the branched and crosslinked chain structures in the polymer. Figure 25 illustrates UV-Vis spectra of polyaniline and polyaniline nanosphere materials.

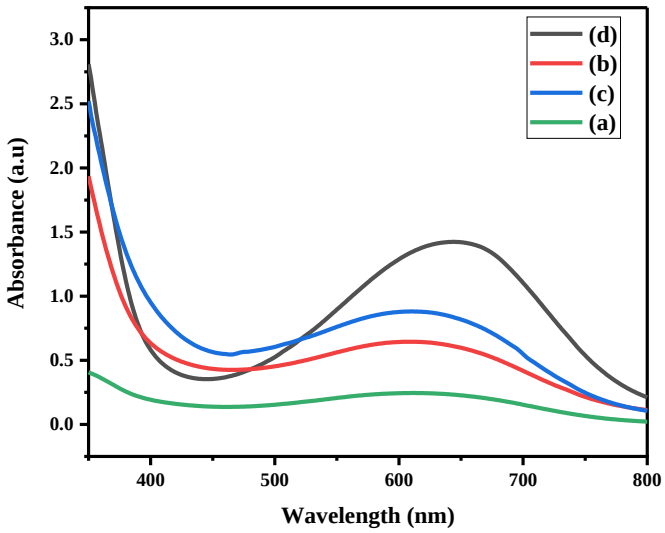

Figure 25: UV-visible absorption spectra of bulk polyaniline and polyaniline nanospheres dissolved in dimethyl sulfoxide (DMSO). (a) HCl doped Polyaniline, (b, c, d) Salicyclic acid doped polyaniline nanospheres obtained by changing the molar ratio of the dopant to monomer ([SA]/ [An]). (b) 0.1:0.2, (c) 0.12:0.2, and (d) 0.16:0.2 other synthetic conditions: [aniline] =0.2 M, [aniline]/ [APS] =1:1, t = 12 h.

In this work, the optical band gap energy was estimated from the absorption coefficient data as a function of wavelength using the Tauc relation as shown in the following relation as (Saleh et al., 2019):

$$(\alpha h\nu)^2 = A(h\nu - Eg) \qquad (27)$$

Where α is the absorption coefficient, hv is the photon energy (eV), A is an energy independent constant (the band tailing parameter), Eg is the optical band gap energy of the nanoparticles

The above equation can be simplified as:

$$(\alpha h\nu)^2 = \alpha \times Eg \text{ , but } \quad Eg = \frac{1240}{\lambda}$$

$$(\alpha h\nu)^2 = \alpha \times \frac{1240}{\lambda} \qquad (28)$$

The absorption coefficient (α) ,at the corresponding wavelengths (λ) is calculated using the Beer-Lamberts relation (Saleh et al., 2019)

$$\alpha = \frac{2.303A}{L} \tag{29}$$

Where L is the path length of the quartz cuvette (cm) and A is the absorbance (arbitrary unit).

$$(\alpha h\nu)^2 = \frac{2.303A}{L} \times \frac{1240}{\lambda} \quad \text{But,} \quad (\alpha h\nu)^2 = (\alpha h\nu) \times (\alpha h\nu)$$

So,
$$(\alpha h\nu)^2 = \left(\frac{2.303A}{L} \times \frac{1240}{\lambda}\right) \times \left(\frac{2.303A}{L} \times \frac{1240}{\lambda}\right) \tag{30}$$

The energy band gap values were calculated by plotting the graph between $(\alpha h\nu)^2$ vs hv as depicted in the Fig.27. Furthermore, the direct energy gap values were found by extrapolating the straight-line portion of the curve to intercept of the energy axis (Devi et al., 2018). At different molar ratio of the dopant (salicylic acid) to aniline (An). The energy band gap values of hydrochloric acid doped polyaniline is 3.2 eV. And organic acid (salicylic acid) doped polyaniline nanotubes found in the value of 3.0 eV ([SA]/[An] = 0.5), 2.89 eV ([SA]/ [An] = 0.6) and 2.75 eV ([SA]/[An] = 0.8), respectively. The observed energy band gap values clearly show that the band gap values decreases with increasing molar ratio of dopant to aniline. This further means that, the energy band gap values of prepared samples diminishes when the concentration of salicylic acid (dopant) increases while the concentration of monomer (aniline) remaining constant. Fig.26 displays a plot of $(\alpha h\nu)^2$ versus hv for the prepared polyaniline and polyaniline nanosphere materials.

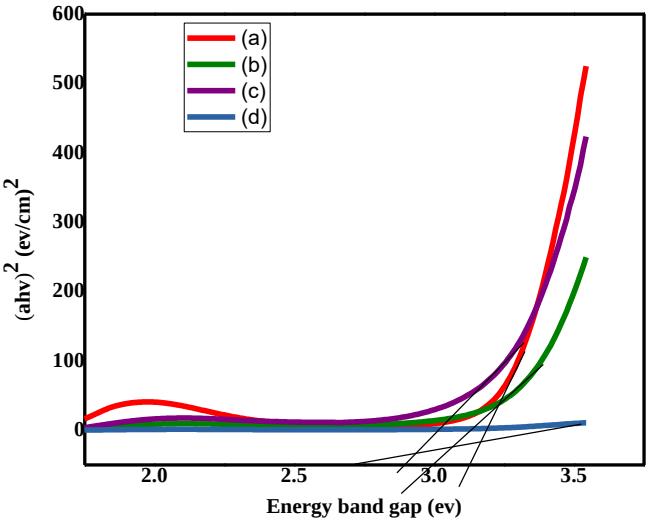

Figure 26: Plot of $(\alpha h\nu)^2$ versus hv for the as-prepared of polyaniline (a) and polyaniline nanospheres with different molar ratio of the dopant to monomer: b) [SA]/ [An] = 0.5, c) [SA]/ [An] = 0.6, and [SA]/ [An] = 0.8.

4.2 Fourier Transform Infrared Spectroscopy result

FTIR spectroscopy was employed to characterize the chemical structure of the polyaniline and polyaniline nanospheres. In the spectrum, the band observed 3465cm^{-1} is due to O-H stretching vibrations. The polymer shows the absorption bands at 2827.7 cm^{-1} is due to asymmetric C-H stretching vibrations. The PANI nanosphere also exhibit characteristics of PANI peaks at 15785.27 and 1503.87 cm^{-1},which are assigned to the C-C stretching of the quinoid ring and benzenoid rings, respectively (Lyu et al., 2019).The absorption peak observed at 1353.85 cm^{-1} could be assigned to C-N stretching of primary aromatic amines. The characteristic peak at 1007.52 cm^{-1} is due to –SO_3H mode. As the concentration of acid continued to increase to 0.1 M, 0.12M, and 0.16 M, the peak of 1374.61 cm^{-1} proceeded moving to the low frequency region and the peak intensity decreased slowly. The position shift of peak was also reflected in other peaks, such as the peaks at 1150.36, 1347.56, and 1523.82 cm^{-1}.The absorption peak observed at 1333.9 cm^{-1} was assigned to C-N stretching of primary aromatic amines. Also, the peak at 1374 cm^{-1} decreased in intensity, and the bands at 1109 and 1001 cm^{-1} disappeared during the polymerization. These changes indicate increased delocalization of the electrons along the polymer chains due to a para-coupling,

elongation of the polymer, and an increase in doping level. Which means that, the aniline oxidation products change from an insulator state, the oligomeric flakelike structures to conducting forms of PANI nanospheres. FT-IR results suggest that the hydrogen bond of OH group of salicylic acid with the amine group of PANI might be a driving force for self-assembling nanospheres, while the hydrogen bond through hydrogen and oxygen of the adjacent SA doped on the polymer chains in short-range order of the counter-ions on the polymer chain in the nanospheres. All in all, FTIR spectroscopy strongly support this study that a hydrogen bond between the OH groups of PANI exist in the nanospheres.

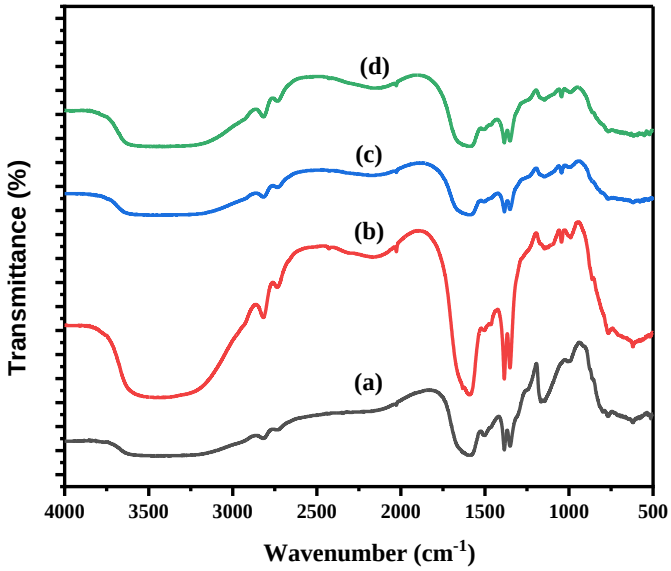

Figure 27: FT-IR spectra of the bulk polyaniline and polyaniline nanospheres: (a) bulk polyaniline, (b, c, and d) polyaniline nanospheres synthesized at molar ratio of [SA]/ [An] = 0.5, 0.6, and 0.8, respectively. Other synthetic conditions: [SA] = 0.1 M, 0.12 M, and 0.16 M. [An] = 0.2 M, [Aniline]/ [APS] = 1:1, t = 12 h.

4.3 Thermogravimetric analysis

Knowing the knowledge of polyaniline nanosphere thermal stability is important for its use in many practical applications. Due to this fact, the thermal degradation of PANI nanosphere is shown by thermogravimetry (Ding et al., 1999). The TGA was performed under a nitrogen atmosphere to minimize mass increase due to oxidation, and let PANI nanosphere thermally decompose almost fully. In the TGA curve of the PANI nanospheres (Fig 29.) two major weight loss steps are observed. The first weight loss (10 %) occurs at 100 ^{o}C and is related OH evaporation, and outflow of unknown small molecules. Generally, the weight losses observed below 90◦C for the samples correspond to the loss of water molecules/moisture, which is due to the hygroscopic nature of the polymer. And, the sample is stable up to 330^{o}C due to the Interfacial polymerization of aniline gives Polyaniline salt containing salicylic acid group in excellent yield with nanospheres morphology and semicrystalline nature and then undergoes degradation of the polymer chain (Raghava et al., 2009). The second weight loss (38%), starting at 320 ^{o}C and finishing at 620 ^{o}C is predicated to complex and irreversible processes of decomposition of the polymeric chain. Furthermore, the improved thermal stability of the polyaniline nanosphere can be attributed to the reduced mobility of the polymer chains that in turn suppresses the free radical transfer via interchain reactions. As result, the process of degradation will be slowed and decomposition will take place at higher temperature. So, the significance of thermal stability of polyaniline nanosphere in supercapacitor is to improve polyaniline electrodes cyclic stability which had a fatal deficiency due to the mechanical degradation and break of the PANI chains caused by the swelling breaking or shrinking in the skeleton of PANI during the repeated charge-discharge processes. Figure 28 illustrates TGA curves of prepared polyaniline nanosphere materials.

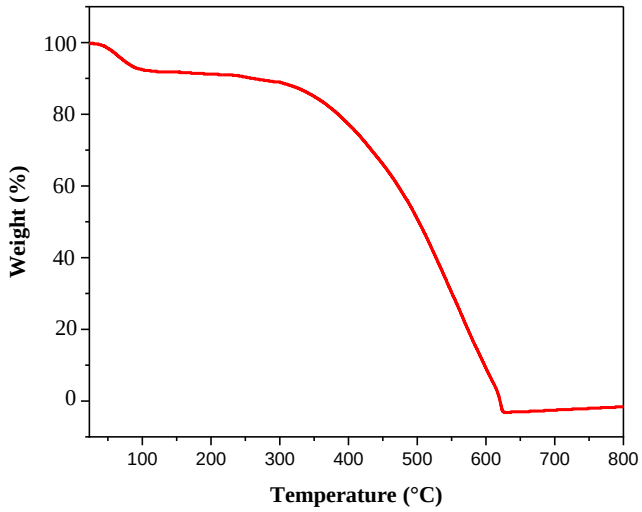

Figure 28: Thermogravimetric analysis of PANI nanosphere synthesized at [SA]/ [An] ratio = 0.8. Other synthetic conditions: [SA] = 0.16 M and [An] = 0.2 M, [aniline]/ [APS] = 1:1, t= 12 h.

4.4 Scanning Electron Microscope studies

As shown in low magnification in Figure 29, it is found that the bulk polyaniline sample only shows aggregates of precipitated PANI, while polyaniline nanosphere (N0.5, N0.6, and N0.8) shows mixture of nanoparticle and aggregates. The higher aggregation state of the prepared Polyaniline material (Figure 29 a) was owing to the physical and chemical properties of the solution and rate of polymerization. As the initial pH of the reaction medium drop fall, the temperature rises noticeably. This is related to the exothermic nature of the polymerization reaction, particularly at the stage of initiation which means that in the case of oxidation reaction and further proton liberation. For a highly acidic medium (pH-initial<2) such as the 1.0M solution of HCl, the initial oxidation rate was high with a shorter oxidation induction period viewed at the beginning of the process. In the studied cases, the temperature of the reaction medium was keep up at below 5^{o}C. The higher concentration of acid evoked a more profound increase in temperature leading to a shorter an induction period and a sensibly higher rate of oxidation. As a result, more chains were formed and aggregated in a more dense, compact structure visible in the SEM image (Figure 29 a). In the low magnification SEM images (Figure 29 b-d), it can be noted that the semi-ordered micro/nanostructures of PANI have been successfully self-assembled via the simple chemical oxidative polymerization method. Furthermore, in the case of 0.16M (molar ratio of 0.8),

synthesis of a more smoothly packed structure was presented (Figure 30 d). A high acid concentration seems to favor nucleation site formation, which further enhances three-dimensional (3D) nanoparticle agglomeration at the initial and secondary growth stages (Xiong et al., 2019). Hence, a more loosely structure was found in this case. It was also shown that the presence of dopant ions imparted both hydrophilicity and solubility to PANI. The SEM images of both polyaniline nanospheres (Figure 29 b–d) show that the grains were packed but still recognizable, owing to their hydrophobic nature. In all the images it is clear that each nanosphere is well separated with small aggregation. Interstingly, it is evident from low magnification (Figure 29 (d)) that the surface of the nanospheres is slightly smooth. Figure 29 showed SEM images of prepared polyaniline and polyaniline nanosphere materials (with low magnification X300).

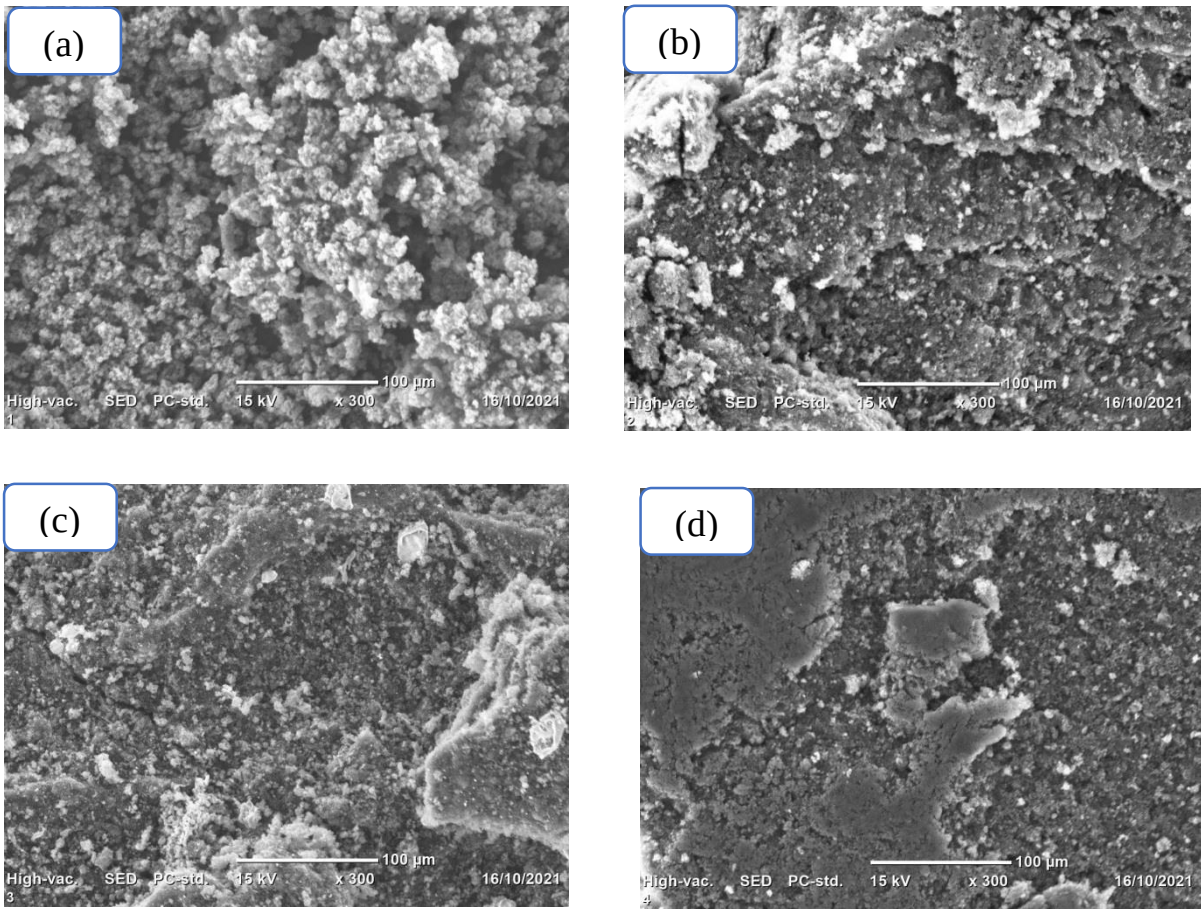

Figure 29: SEM images of bulk polyaniline (a) and polyaniline nanospheres (b-d) synthesized with different molar ratio of [SA]/ [An]: 0.5, 0.6, and 0.8 (with low magnification X300). Other synthetic conditions: [SA] = 0.1 M, 0.12 M, and 0.16 M. [An] = 0.2M, [Aniline]/ [APS] = 1:1, t = 12

The SEM images (Figure 30 a) clearly show that the conventional/bulk polyaniline sample contains aggregates of precipitated PANI. In brief, upon the formation of interface between organic and aqueous phase, aniline monomers migrated into aqueous phase to form anilinium ions. These ions then served as nucleation centers to make the polymer grow further. The average diameter of bulk polyaniline prepared in acid reaction medium was 4 µm. Figure 30 (c-d) shows morphological structure of PANI shows nanospheres with diameter ranging from 2.5 µm to 2.95 µm size. The morphology of the samples is clearly evident in that the hydroxyl substitutions at the aniline monomer drastically change the morphology of the resultant nanomaterials from bulk to nanospheres. The difference in the nanosphere morphology is a result of the difference in the monomer interactions at the molecular level during the polymerization process. The differences on the diameter and size distribution of the PANI nanospheres are related to the nature of salicylic acids that can affect significantly the assembly of aniline oligomers. Therefore, the incomplete aniline oligomers serve as precursor for the formation of PANI nanospheres, and salicylic acid plays a significant role in controlling the self–assembly behavior of aniline oligomers, as a result, promoting the orientation growth of the nanospheres (Dhand et al., 2010). This highly interconnected and porous morphology is highly desirable for fast ion diffusion and migration in the electrodes. Fig.30 showed SEM images of prepared polyaniline and polyaniline nanosphere materials (with medium magnification X1000)

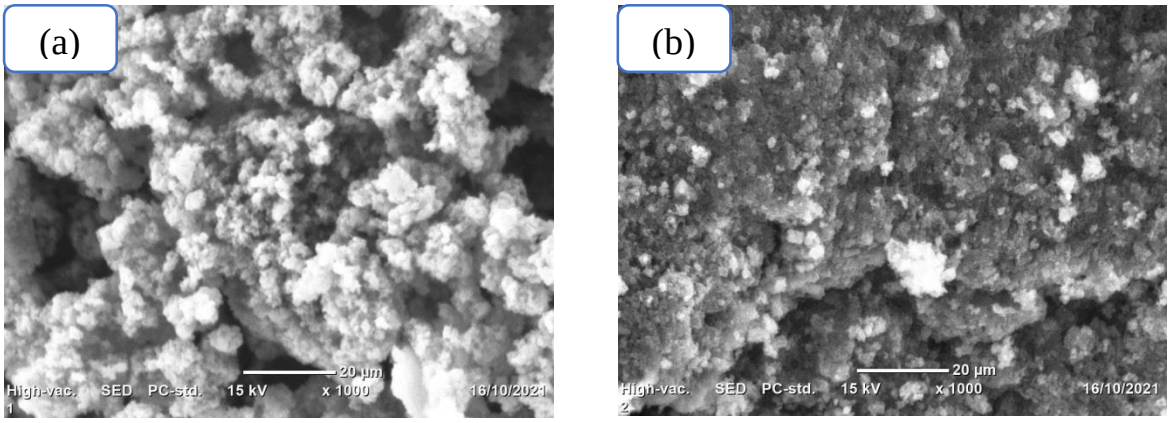

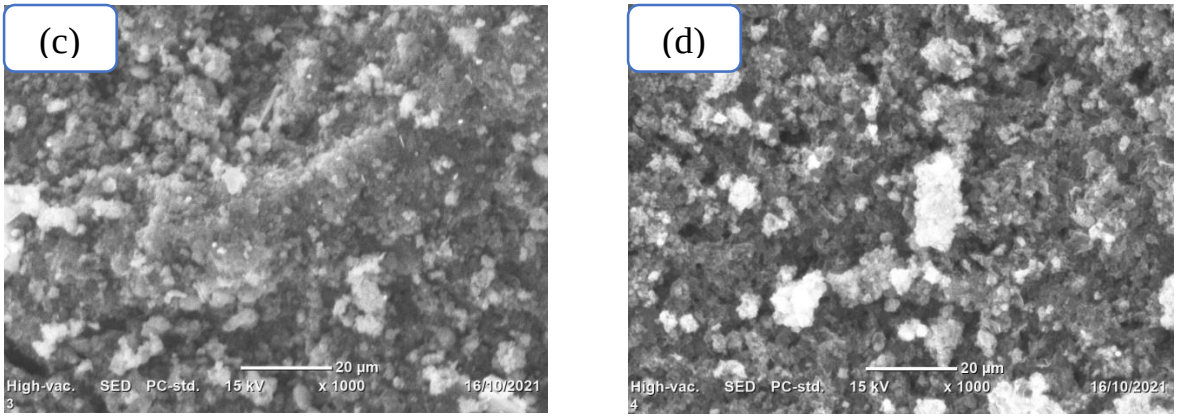

Figure 30: SEM images of bulk polyaniline (a) and polyaniline nanospheres (b-d) synthesized with different molar ratio of [SA]/ [An]: 0.5, 0.6, and 0.8 (with medium magnification X1000). Other synthetic conditions: [SA] = 0.1 M, 0.12 M, and 0.16 M. [An] = 0.2 M, [Aniline]/ [APS] = 1:1, t = 12.

The higher-magnification SEM images shown in Figure 31 (a-c) demonstrated that the chemically synthesized polyaniline sample, the image illustrate that the obtained nanostructure appears in the form of nanospheres. The solid PANI nanospheres are obtained in medium acidic media (pH-initial = 2-4) the estimated histogram of the polyaniline nanospheres illustrate that the average diameter in the range of 2.5, 2.75, and 2.95 µm, respectively with less widely distribution. Furthermore, the average outer diameter of nanospheres increases with increases of [SA]/[An] ratio. For instance, the diameter of the nanospheres increases from 2.5 µm to 2.95 µm when the [SA]/ [An] ratio changes from 0.5 to 0.8. The concentration of salicylic acid also has an impact on the size of resulting polyaniline nanospheres. Moreover, the morphology and size of the polyaniline nanosphere was influenced by the acid concentration, with smaller diameter presenting 2.5 µm showed in the less concentrated solution and larger diameter with a 3 µm showed in the more concentrated solution. This indicates that the diameter of polyaniline nanospheres can be easily controlled by adjusting the molar ratio of the dopant to aniline. The mechanism for the formation is that micelles composed of aniline/SA might be formed in the reaction solution. Owing to the hydrophobic and hydrophilic groups of aniline and salicylic acid. It is recognized that the formed micelles might have a spherical morphology in shape due to the lowest of the surface energies. The synthesis of PANI nanosphere is in agreement with the previous report (Zhang & Wan, 2003). It has been demonstrated that the micelles formed by salicylic acid and aniline serve as soft templates and the hydrogen bonds between salicylic acid

and aniline act as the driving force for the formation of self-assemble PANI nanospheres (Zhang & Wan, 2003). Figure 31 showed SEM images of prepared polyaniline and polyaniline nanosphere materials (with higher magnification X2000).

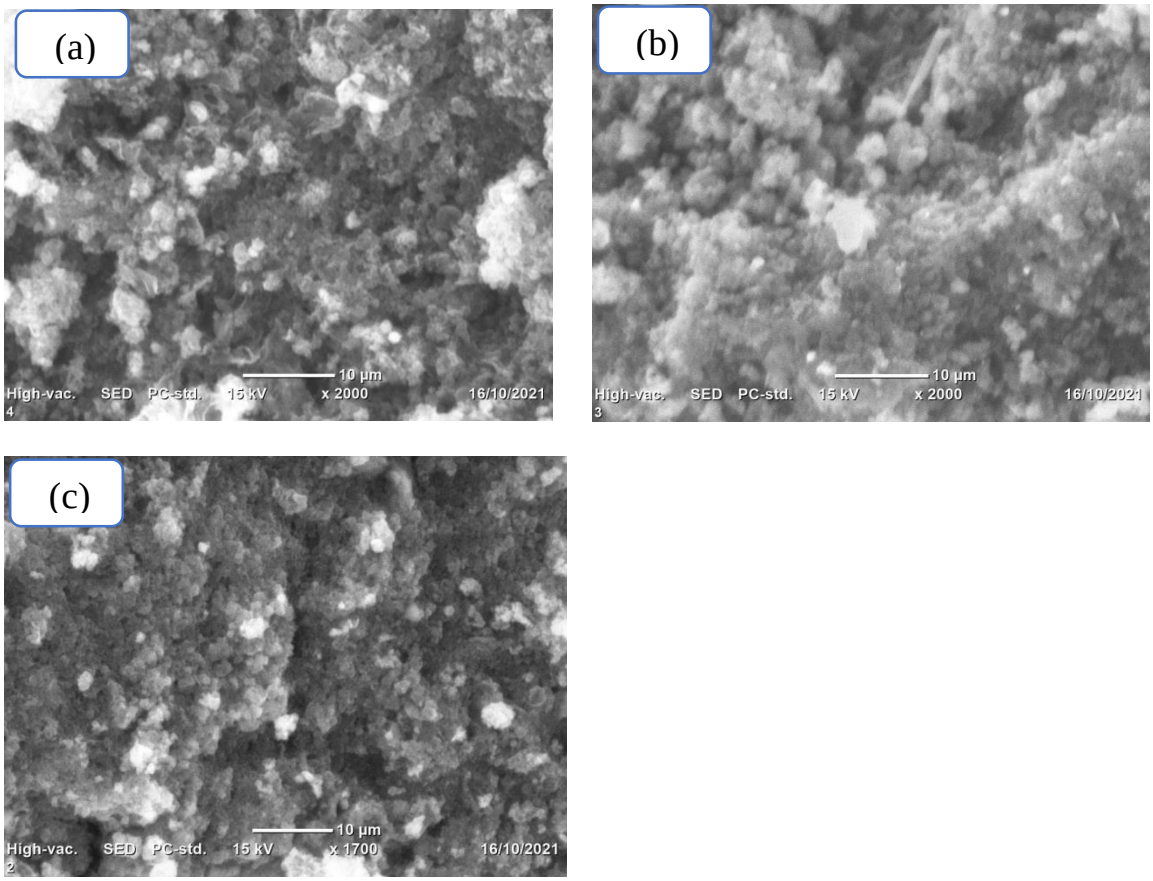

Figure 31: SEM images of PANI nanospheres synthesized with different molar ratio of salicylic acid to aniline ([SA]/ [An]).With higher magnification of X2000: a) 0.5 (0.1:0.2); b) 0.6 (0.12:0.2); c) 0.8 (0.16:0.2) other reaction conditions [An] = 0.2M, [An]/[APS] = 1:1, t = 12 h.

4.5 X-ray Diffraction analysis

XRD analysis was performed to investigate the crystallite size of the samples. The X-ray diffraction pattern of Polyaniline (Figure 32 a.) shows a peak at 2 θ = 19º, and 25º. The interplanar distance value obtained were, 4.67, and 3.55 Angstrom, respectively. The average crystalline size is calculated by Debye Scherer equation (Devi et al., 2014).

$$D = \frac{k\lambda}{\beta \cos\theta} \qquad (31)$$

Where, k is the shape factor (0.89); D is the average crystallite size; λ is the X-ray wavelength; β is the full width at half maximum (FWHM); θ is the diffraction angle.

The average crystal size of prepared polyaniline material is 4.11 Angstrom.

The crystallinity index can be calculated by the following equation:

$$\text{Crystallinity index} = \frac{Area\ of\ all\ the\ crystalline\ peaks}{Area\ of\ all\ the\ crystalline\ and\ amorphous\ peaks} \qquad (32)$$

Table 7: Crystallinity index of prepared polyaniline and polyaniline nanospheres (N0.5, N0.6, and N0.8) materials.

Sample code	Total area of the crystalline peaks	Total area of the crystalline and amorphous peaks	Crystallinity index in %
PANI	3000	8482	35.3
N0.5	3200	8482	37.7
N0.6	3330	8482	39.3
N0.8	3500	8482	41.5

Table 8: The XRD data of polyaniline

Sample code	**Parameters**		**Calculations**						
	k	$\lambda(A^{\circ})$	Peak position $2\theta(^{\circ})$		FWHM β $(^{\circ})$	Crystalline size D(nm)	Average crystalline size D (nm)	d-spacing (A°)	Average d-spacing (A°)
PANI	0.89	1.54	Peak 1	19	4.58	1.74	3.19	4.67	4.11
	0.89	1.54	Peak 2	25	1.74	4.64		3.55	

Table 9: The XRD data of polyaniline nanospheres (with molar ratio of [SA]/ [An] = 0.5

Sample code	**Parameters**		**Calculations**						
	k	$\lambda(A^{\circ})$	Peak position 2 $\theta(^{\circ})$		FWHM β $(^{\circ})$	Crystalline size D(nm)	Average crystalline size D (nm)	d-spacing (A°)	Average d-spacing (A°)
N0.5	0.89	1.54	Peak 1	25	1.74	4.64	3.035	3.55	3.99
	0.89	1.54	Peak 2	20	5.58	1.43		4.43	

Table 10: The XRD data of polyaniline nanospheres (with molar ratio of [SA]/[An] = 0.6).

Sample code	**Parameters**		**Calculations**						
	k	$\lambda(A^{\circ})$	Peak position $2\theta(^{\circ})$		FWHM $\beta\ (^{\circ})$	Crystalline size D(nm)	Average crystalline size D (nm)	d-spacing (A°)	Average d-spacing (A°)
N0.6	0.89	1.54	Peak 1	25	2.71	2.96	1.845	3.55	3.485
	0.89	1.54	Peak 2	26	11.23	0.73		3.42	

Table 11: The XRD data of polyaniline nanospheres (with molar ratio of [SA]/[An] = 0.8).

Sample code	**Parameters**		**Calculations**						
	k	$\lambda(A^{\circ})$	Peak position $2\theta(^{\circ})$		FWHM $\beta\ (^{\circ})$	Crystalline size D(nm)	Average crystalline size D (nm)	d-spacing (A°)	Average d-spacing (A°)
N0.8	0.89	1.54	Peak 1	19	5.07	1.75	1.24	0.12	2.035
	0.89	1.54	Peak 2	25	2.96	0.73		3.95	

The crystallite size value obtained for polyaniline nanospheres (N0.5, N0.6 and N0.8) are 3.04, 1.845 and 1.24 nm, respectively. The interplaner distance value obtained for polyaniline nanospheres (N0.5, N0.6 and N0.8) are also 3.99, 3.485, and 2.03 Angstrom, respectively. The

XRD data are given in Table 7 indicate that polyanilines are 35% crystalline which is considered to be amorphous in nature, but here the synthesized polyaniline nanosphere particularly (N0.8) is 41.5 % crystalline. So, it is under the category of semi-crystalline structure slightly due to its fiber nature and planar nature of benzenoid and quinoid functional groups. The crystallinity index results show that the polyaniline nanospheres have more or less ordered arrangement and better semi-crystallinity than conventional polyaniline. The X-ray diffraction pattern of polyaniline is shown in Figure 32 (a). The strong diffraction peak associated with the chain to chain stacking distance of about $2\theta = 25^{o}$ is due to scattering with momentum transfer approximately perpendicular to the polyaniline chain (Xu et al., 2012). The strong broad peak around 25^{o} indicates its amorphous nature and which is a characteristics peak of PANI corresponding to (002) crystal planes (Ali et al., 2017). Which is corresponds to the vertical periodic intervals of PANI chains /backbones. As shown in Figure 32 (b-d) all the PANI nanospheres (N0.5, N0.6 and N0.8) mainly exhibited a characteristic peaks at $2\theta = 22^{o}$, 20^{o} and 19^{o}, which could be ascribed to the (110), (100), and (100) plane of PANI, and to periodicity parallel and periodicity perpendicular to the polymer chain, respectively (Raghava et al., 2009) . Meanwhile, the presence of the peak at about $2\theta = 19^{o}$ revealed the short range ordering between the chiral counter anion and the polymer chains, and the enhancement in intensity indicated the ordered nanostructures (Zeng et al., 2015). The crystallite size value obtained for polyaniline nanospheres (N0.5, N0.6 and N0.8) were found to be about 3.04, 1.845, and 1.24 nm, respectively as estimated using Scherer's formula. As comparison of crystallite size value of PANI, N0.5, and N0.6; polyaniline nanosphere (N0.8) have smaller crystallite value. This indicates that as the crystallite size decreases surface area of the prepared material increases and which is responsible for capacitive propertits of the prepared materials.The appearance of the lower angle peak with a low value of the crystallite size in hydroxyl-substituted polyaniline nanospheres confirmed the occurrence of enhanced ordering of polymer chains in the nanospheres compared to the conventional polyaniline. The peaks related to the Polyaniline nanosphere decreased as the concentration of Salicylic acid (SA) increased. The semi-crystalline structure of the polyaniline nanosphere chains was influenced by the salicylic acid molecules, which formed micelles and resulted in the decrease of the diffraction peaks corresponding to PANI. The large amounts of salicylic acid present in the Polyaniline nanosphere could decrease PANI peak intensities. Figure 32 illustrates XRD pattern of prepared polyaniline and polyaniline nanosphere materials.

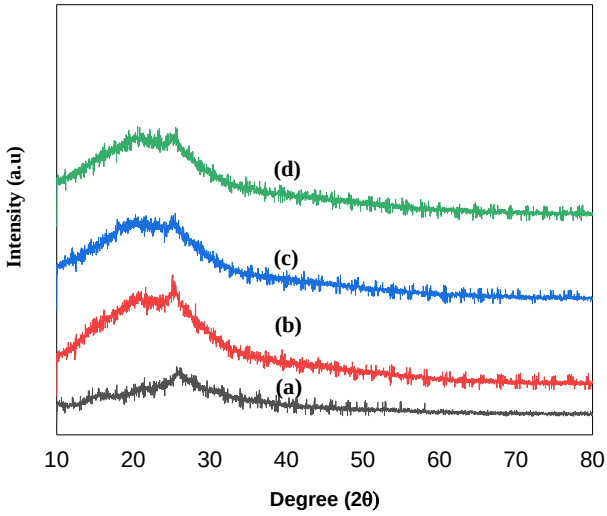

Figure 32: XRD patterns of conventional (bulk) polyaniline (a) and polyaniline nanospheres prepared in molar ratio of the dopant to monomer (b) ([SA]/[An] = 0.5), (c) [SA]/[An] = 0.6 and (d) [SA]/[An] = 0.8.Other synthetic conditions: [SA] = 0.1 M, 0.12 M, and 0.16 M. [An] = 0.2 M, [Aniline]/ [APS] = 1:1, t =12 h.

4.6 Electrical Conductivity

The electrical (DC) conductivity of a bulk polyaniline film doped with hydrochloric acid and polyaniline nanospheres (N0.5, N0.6, N0.8) film doped with salicylic acid were determined with a two-electrode scheme using a multimeter.The measured conductivity value of bulk polyaniline and polyaniline nanospheres (N0.5,N0.6,and N0.8) were $1.25x10^{-5}$ $(\Omega\,cm)^{-1}$ $1.25\ x10^{-4}$ $(\Omega.cm)^{-1}$ $1.11\ x10^{-4}$ $(\Omega.cm)^{-1}$ and $1.43\ x10^{-4}$ $(\Omega.cm)^{-1}$, respectively. Among those, polyaniline nanosphere (N0.8) sample indicates high value due to good electron delocalization in the conjugated polymer, which is extended by the formation of a nanosphere after using salicylic acid as a dopant. This further means that, on introduction of salicylic acid (SA) nanospheres were developed directly increasing conductivity from 10^{-5} to 10^{-4} and increase in sphere diameter had increase in conductivity. Furthermore, the polyaniline nanosphere structure with a large surface area and pore volume as well as highly assimilated dopant content significantly increases the conductivity of polyaniline nanospheres (Yan et al., 2011). The interaction between the PANI backbone and the dopant is also beneficial to the conductivity. Due to this high conductivity value, PANI nanospheres doped with salicylic acid is a potential candidate for use as an electroactive

electrode material in supercapacitors. Table 12 displays the conductivity value of prepared polyaniline and polyaniline nanosphere materials.

Table 12: The conductivities of bulk polyaniline and polyaniline nanospheres (N0.5, N0.6, and N0.8) samples.

Sample code	Area (A)	Length (L)	Electrical resistance (R)	Resistivity **(ρ)**	Electrical Conductivity (σ)
PANI	$(2x1)cm^2$	2 cm	$0.08x10^6\,\Omega$	$0.08x10^6\,\Omega$ .cm	$1.25x10^{-5}$ $(\Omega\,cm)^{-1}$
N0.5	$(2x1)cm^2$	2 cm	$0.008x10^6\,\Omega$	$0.008x10^6\,\Omega$ .cm	1.25 x10-4 $(\Omega$ .cm$)^{-1}$
N0.6	$(2x1)cm^2$	2 cm	$0.009x10^6\,\Omega$	$0.009x10^6\,\Omega$ .cm	1.11 x10-4 $(\Omega$ .cm$)^{-1}$
N0.8	$(2x1)cm^2$	2 cm	$0.007x10^6\,\Omega$	$0.007x10^6\,\Omega$ .cm	1.43 x10-4 $(\Omega$ .cm$)^{-1}$

From the measured conductivity value Polyaniline nanospheres (N0.5, N0.6, and N0.8) have large value compared to that of bulk Polyaniline. Indicating that the increased conductivity of polyaniline nanospheres compared with the bulk Polyaniline is due to the differences in their morphology. Furthermore, table 12. Shows a high conductivity for polyaniline nanospheres, whilst the conductivities of bulk polyaniline was relatively low due to increase in the energy gap between the conduction band and valence band; as a result, electrons cannot travel into the conduction band, and hence a decrease conductivity is observed.

4.7 Electrochemical performances of the prepared electrodes

4.7.1 Cyclic voltammetry

The electrochemical capacitive performance of prepared electrodes were tested by cyclic voltammetry (CV) in 1 M H_2SO_4 aqueous solution with in potential window of -1.2 to 1.0 V. In this study, a commercial glassy carbon electrode and polyaniline have been studied under the same experimental conditions for comparison purposes on the supercapacitor applications. The CV curves of polyaniline, glass carbon electrode, polyaniline nanosphere (N0.5), polyaniline

nanosphere (N0.6), and polyaniline nanosphere (N0.8) electrodes at optimal scan rates of 250 mV/s are shown in Figure 33, respectively. For polyaniline nanospheres (N0.6 and N0.8), the pair of redox peaks can be observed, indicating pseudocapacitive characteristic of polyaniline nanosphere (N0.6) and polyaniline nanosphere (N0.8) electrode (Jing & Chen, 2014). In comparison with the CV curves of glass carbon electrode, polyaniline, and polyaniline nanospheres (N0.6 and N0.8), the CV curves of polyaniline nanosphere (N0.8) electrode showed obvious differences. Although the shape and area of the CV curves for both electrodes were different at various scan rates. But, the area of the Polyaniline nanosphere (N0.8) electrode significantly exceeded that of the bulk polyaniline, glass carbon electrode, and polyaniline nanosphere (N0.5 and N0.6) electrodes. This could be due to the advantages of the additional surface formed by the PANI nanosphere formation are more effective at higher scan rates. In addition to this, the results suggest that the formation of porous structures within the PANI nanosphere increases the electrode surface area, which results in faster redox reactions between the PANI nanosphere electrode and electrolyte. Furthermore, the current response of the polyaniline nanosphere (N0.8) is the larger than that of the other four materials, implying that it has the highest specific capacitance value. Whereas, in CV curves, bulk polyaniline shows very low current response due to the low conductivity. Figure 33 illustrates Cyclic Voltammogram of the prepared polyaniline and polyaniline nanosphere materials.

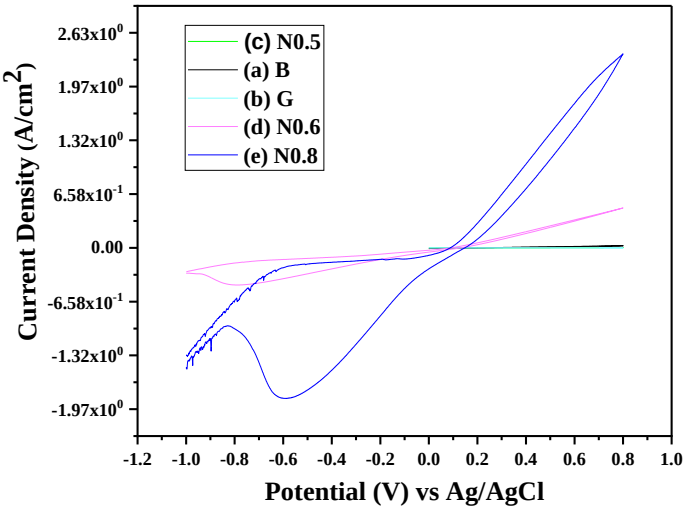

Figure 33: Cyclic voltammogram of the prepared material: a) B-bulk polyaniline, b) G-glassy carbon electrode, c) polyaniline hollow nanosphere (N 0.5), d) polyaniline nanosphere (N 0.6), and e) polyaniline nanosphere (N 0.8) material as electrode.

4.7.1.1 Specific capacitance calculated from the CV curve

In this study, the electrodes were cut into circular shapes with a diameter of 2 mm and an active material loading density of about 2 mg/cm^{-2}. However, in the calculation part we used the mass on the surface of the active substance which is 0.05 mg not the whole mass modifier used (1 mg).This further means that, we used the mass only covers the monolayer surface, not the whole mass to be responsible for the reaction.CV curve was recorded at 200, 250 and 300 mVs^{-1} scan rate from -1.2 to 1.0 V. Area of cyclic voltammetry of the prepared electrode materials were given as below:

The following plots shows the CV data and the area (A) enclosed by Cyclic voltammetry curve,

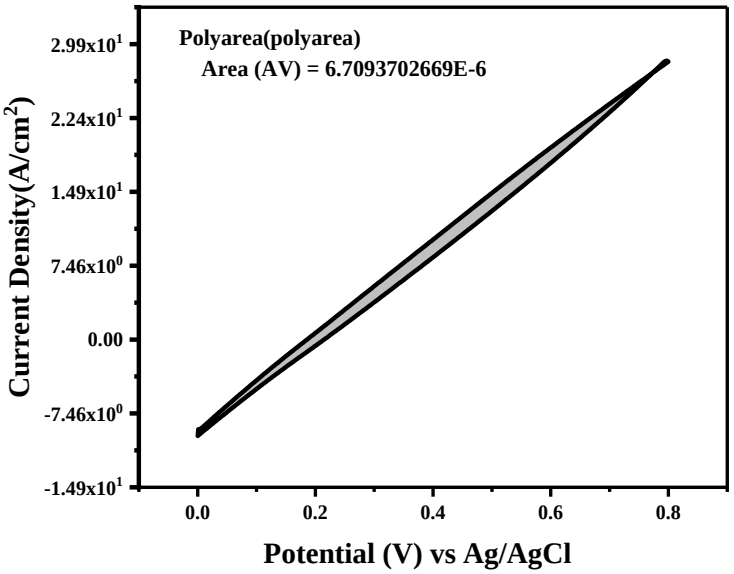

Figure 34: Area of cyclic voltammetry of the bulk polyaniline electrode material with 200 mV/s scan rate.

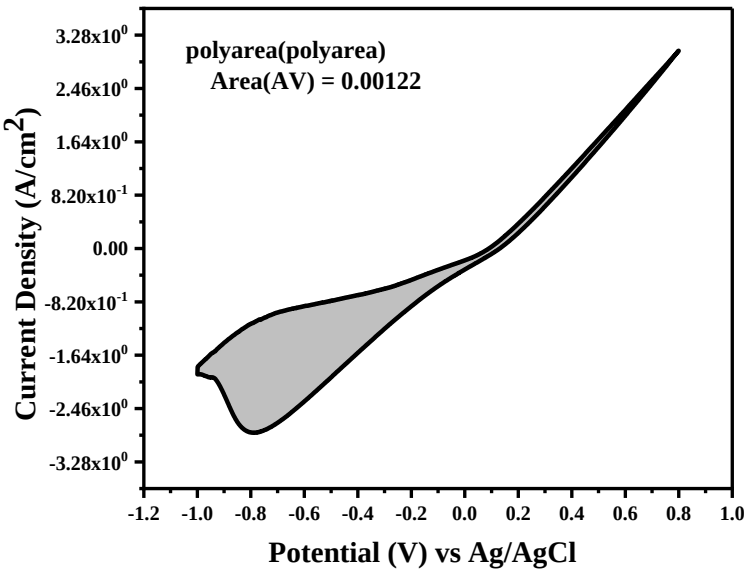

Figure 35: Area of cyclic voltammetry of N 0.6 electrode material with 300 mV/s scan rate.

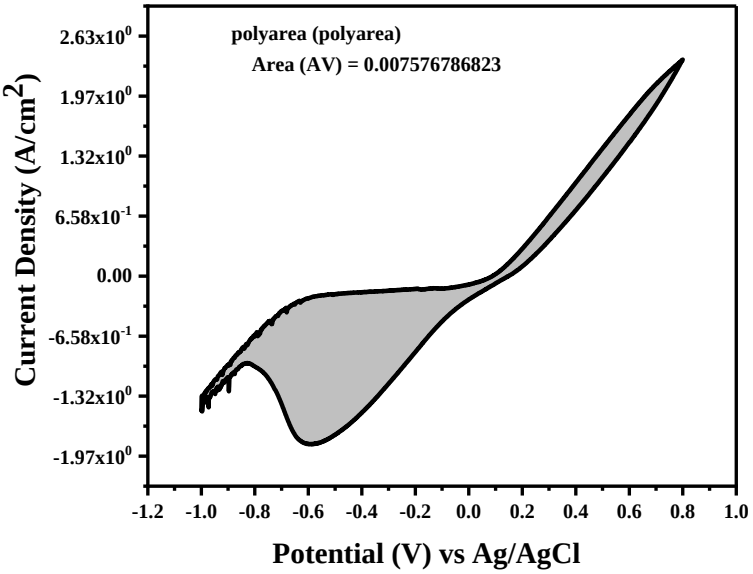

Figure 36: Area of cyclic voltammetry N 0.8 electrode material at scan rate of 250 mV/s

The calculated specific capacitance for all three electrode samples at a scan rate of (200,300 and 250 mV/s) is given in table 10.

Table 13: Specific Capacitance of polyaniline, polyaniline nanosphere (N 0.6), and polyaniline nanosphere (N 0.8) at different scan rates.

Sample code	Scan rate (mVs^{-1})	Specific capacitance (F/g)
PANI	200	0.152
N0.6	300	18.5
N0.8	250	137.7

The specific capacitance values of polyaniline, polyaniline nanosphere (N0.6) and polyaniline nanosphere (N0.8) at the different scan rates are shown in table 10. Polyaniline (PANI), polyaniline nanosphere (N0.6) and polyaniline nanosphere (N0.8) materials exhibited specific capacitance of 0.152, 18.5 and 137.7 Fg^{-1}, respectively. The higher specific capacitance of polyaniline nanosphere (N0.8) materials can be explained by its greater electro active surface area accessible to the electrolyte. Besides, the redox peaks can be observed on the CV of the prepared materials, which originates from the redox transition of PANI nanosphere between a semiconducting state (Leucoemeraldine form) and a conducting state (polaronic emeraldine form). This implies conducting polyaniline nanosphere components makes partial contribution to the overall capacitance of the prepared material. It is also found that the specific capacitance of polyaniline nanospheres is highly affected by the concentration of salicylic acid dopant. The specific capacitance of polyaniline nanospheres increases with the molar ratio of dopant to monomer 0.5, 0.6 and 0.8, until reaches the maximum value (137.7 Fg^{-1}) at 0.8. The capacitances were increased with Salicylic acid concentrations until 0.16M. This indicates that, the specific capacitance of polyaniline nanosphere is enhanced to different degrees as the concentration of salicylic acid changes.

4.7.1.2 Effect of scan rate on specific capacitance of the prepared electrode materials

Figure 37 shows the CV curves of polyaniline nanosphere (N0.8) at different scan rates.The ranges for CV tests was -1.2 to 1.0 V, and the scant rate was 100, 150, 200, and 250 mVs^{-1}. It can be noted that with an increase of scan rate, the cathodic peaks shift positively and the anodic peaks

shift negatively, which is mainly due to the resistance of the electrode (Xu et al., 2012).With the increase in scan rate response of current also increases is a signal of ideal capacitive behavior. We believe that the relative high specific capacitance of PANI nanosphere (N0.8) electrode is due to PANI nanoparticles with smaller size facilitate better utilization of polyaniline nanosphere as electrode materials and nanosized polyaniline shorten the charge diffusion distance during the charging /discharging process. Furthermore, the high surface area of polyaniline nanoparticle play also an important role in enhancing electrochemical performance of polyaniline nanosphere. Figure 37 showed the CV curves of PANI nanospheres (N0.8) at different scan rates. Fig.33 illustrated the effect of scan rates on the prepared polyaniline nanosphere materials.

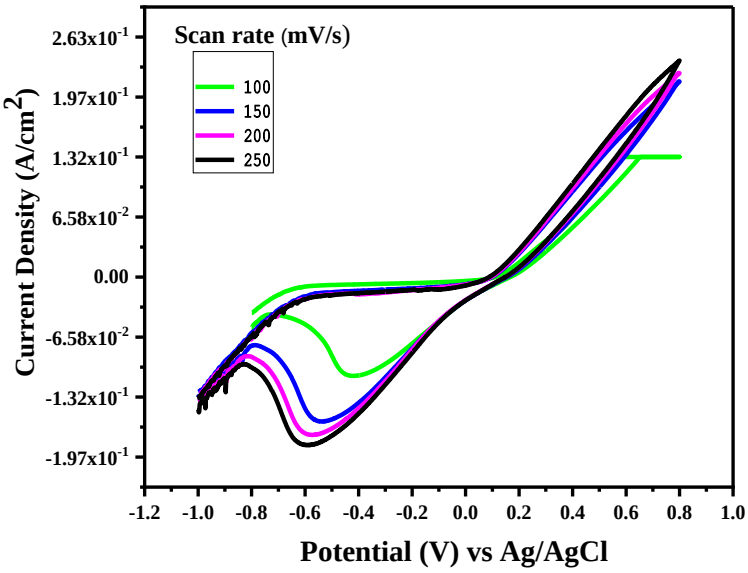

Figure 37: Effect of scan rate (100-250 mV/s) on polyaniline nanosphere (N 0.8) electrode material in 1M H_2SO_4 solution.

Table 14: Specific capacitance of Polyaniline nanosphere (N0.8) (synthesized at [SA]/ [An] = 0.8 or 0.16 M: 0.2 M) at different scan rates.

S.No.	Scan rate (mVs^{-1})	Specific Capacitance (Fg^{-1})
1	100	344.4
2	150	229.6
3	200	172.2
4	250	137.7

The variation of specific capacitance with potential scan rate is shown in Table 11. The above table result indicates that, the value of the specific capacitance decreased, when the scan rate was increased up to 250 mVs^{-1}. The calculated values of specific capacitance for PANI nanosphere (N0.8) electrode at a scan rate of 100-250 mVs^{-1} are 344.4, 229.6, 172.2 and 137.7 Fg^{-1}. The value of specific capacitance decreases with increases in the scan rates shows the presence of internal active sites that cannot totally maintain redox transitions at higher scan rates. This further means that, the presence of inner active sites which cannot sustain the redox reactions and also some parts of the surface of the electrode are inaccessible at a high charge-discharge rate (Soudagar, 2017).This is probably owing to diffusion limitation of the acidic electrolyte with in the electrode nanosphere, so that the parts of the surface electrode are not accessible at high discharge rates. All in all, the specific capacitance decreases as scan rate increases because a low scan rate electrolyte ions are completely diffused into the inner active sites of the material which undergo the redox transitions completely. However, at higher scan electrolyte ions cannot diffuse completely into the inner active sites of material. Hence, there is decrease in the specific capacitance at high potential scar rate. It can be noted that for very low scan rates, the specific capacitance values are higher since the ions have a much longer time to penetrate and reside in all the available electrode pores and form electric double layers, which are needed to generate higher capacitance. It is therefore

believed that the specific capacitance obtained at the slowest scanning rate is closest to the full utilization of the electrode material.

Table 15: Summary of reported literatures on Polyaniline based electrode for supercapacitor performance.

Electrode material	Dopant acid	Electrolyte	Potential window	Scan rates	Electrode Configuration	Specific Capacitance (F/g)	Reference
Polyaniline nanofiber	$C_6H_8O_7$	1M H_2SO_4	-1.0 to 1.0V (Ag/Angel)	20 mV/s	Three electrode	298	(Subramaniet al,2008)
Polyaniline nanotubes	CH_3COOH	1M H_2SO_4	-0.2 to 0.8V (Ag/AgCl)	5 mV/s	Three electrode	232.2	(Athira et al,2018)
Polyaniline	H_3PO_4	1M PA	-0.2 to 1.0V (E(v) vs SCE	5 mV/s	Three electrode	244	(Radhakrishnan et al,2009)
polyaniline	Mn	1M H_2SO_4	-0.2-0.9V vs SCE	20 mV/s	Three electrode	285	(Patil et al,2011)
Nano nest polyaniline	H_2SO_4	1M H_2SO_4	-200 to 800 mv/SCE	5 mV/s	Three electrode	412	(Shaikh et al,2021)
Polyaniline nanospheres	C7H6O3	1M H_2SO_4	-1.2-1.0V V(v) vs Ag/AgCl	250 mV/s	Three electrode	137.7	This work

The electrochemical performance of prepared electrode material in terms of specific capacitance is inferior than that reported in literature as shown in table 15. This mainly comes from two aspects: First, the effects of parameters during material synthesis, which means that both the molar ratio of the dopant to monomer, the concentration of salicylic acid, the reaction temperature had a significant impact on the synthesized PANI nanospheres. Second, the electrolyte used during electrode testing in cyclic voltammetry experimentation. All in all, such observable differences were commonly related to synthesis procedure, morphology (micro and nanostructures), and method of doping.

CHAPTER FIVE

CONCLUSION AND SUGGESTION FOR FURTHER WORK

5.1 Conclusion

PANI nanospheres were prepared successfully by changing the molar ratio of the dopant to monomers possess higher electrical conductivity, thermal stability, crystalline and electrochemical property. Good electrochemical performances can be achieved, and especially polyaniline nanosphere ([SA]/[An] = 0.8 or 0.16 M: 0.2 M) synthesized with a salicylic acid to aniline molar ratio of 0.8 exhibited the most outstanding performances. Polyaniline nanosphere as an electrode material for supercapacitor exhibited a maximum specific capacitance of 137.7 Fg^{-1} at a scan rate of 250 mVs^{-1}. Due to better chemical kinetics, chemical activity, shorter ionic diffusion path lengths, high specific surface area and surplus of active sites for electrochemical reactions; the polyaniline nanosphere electrode exhibits higher specific capacitance than conventional polyaniline electrode at various scan rates. Polyaniline nanosphere found interesting features that make it quite a suitable and promising electrode material for supercapacitors.

5.2 Suggestion for further work

Electrode materials are essential for realizing high electrochemical performance supercapacitors. In this thesis, bulk polyaniline and polyaniline nanosphere electrodes were designed and prepared using low-cost materials and a simple method. Polyaniline nanosphere materials as electrodes for energy storage devices will continue to obtain research attention owing to the unique properties. Recommendations for the future research work are discussed as follows.

1. Polyaniline nanosphere materials are easily suffered from agglomeration during materials processing and electrode preparation process, which often results in low actual surface area. For this matter, further surface modification of the synthesized material should be investigated to prevent the formation of agglomeration and enhance the overall electrochemical performance of the supercapacitor.
2. Even though the polyaniline nanosphere electrode has a huge surface area, most of the area has not been utilized due to pore size limitation. Future research should be directed to alter the pore size distribution and to engineer an electrode with a pre-determined or controlled pore size.
3. Other physiochemical properties of prepared materials such as, energy density, power density and cycling stability using GCD & EIS should be studied.
4. To improve the capacitance utilization; morphological and surface properties of the polyaniline nanosphere materials using SEM, TEM and BET should be studied.
5. Although significant progress has been made on improving the electrochemical performance of polyaniline materials, the specific capacitance of supercapacitors require to be further improved for the practical application.
6. The energy storage mechanism must be understood for controlling interfacial reactions the electrode and electrolyte.
7. The evaluation methods for electrochemical performance should be standard and clear for all researchers.

REFERENCES

Afzal,A.B.,Akhtar,M.J.,Nadeem,M.,Ahmad,M.,& Hassan, M. M. (2009). *Structural and electrical properties of polyaniline / silver nanocomposites*. *015411*. https://doi.org/10.1088/0022-3727/42/1/015411

Ali,N.A.,Huseen,S.I.(2017).*Struectural Thermal and Electrical properties of prepered polyaniline / Sliver Nanocomposites*. *12*(24), 14869–14873.

Alice,M.,Mazzeu,C.,Faria,L K.,Cardoso,A D.M.,Gama,M.,Baldan,M.R.&Gonçalves,E. S. (2017). *Structural and Morphological Characteristics of Polyaniline Synthesized in Pilot Scale*. *9*, 39–47. https://doi.org/10.5028/jatm.v9i1.726

Athira,A.R.,Vimuna,V.M.,Vidya, K.,& Xavier,T.S.(2018). *Nanotubular Polyaniline Electrode for Supercapacitor application*. *030141*. https://doi.org/10.1063/1.5032476

Augustyn,V.,&Dunn,B.(2014).*Environmental Science Pseudocapacitive oxide materials for high-rate electrochemical energy storage*.1597–1614. https://doi.org/10.1039/c3ee44164d

Bernstein,J.,&Desiraju,G.R.(2018) *International Union of Crystallography*.

Bilal,S.,Begum,B.,Gul, S., & Shah, A. A (2019). PANI / DBSA / H2SO4 :A promising and highly efficient electrode material for aqueous supercapacitors PANI/DBSA/ H 2 SO 4 : A promising and highly e ffi cient electrode material for aqueous supercapacitors. *Synthetic Metals*, *235*(November 2017), 1–15. https://doi.org/10.1016/j.synthmet.2017.11.004

Brandon, D. (2014). *Microstructural Characterization of Materials*.

Chem,J.M.(2012).*Porous polypyrrole clusters prepared by electropolymerization for a high performance supercapacitor †*. 3044–3052. https://doi.org/10.1039/c2jm14470k

Chen,S.,Mani,V.,& Ramiah, S. (2014). *Recent Advancements in Electrode Materials for the High-performance Electrochemical Supercapacitors :A Review*. *September*.

Chu,A.,& Braatz,P.(2002).*Comparison of commercial supercapacitors and high-power lithium-batteries for power-assist applications in hybrid electric vehicles I .Initial characterization*. *112*, 236–246.

Chu,S.,&Majumdar,A.(2012).Opportunitie and challenges for a sustainable energy future. *Nature*, *488*(7411), 294–303. https://doi.org/10.1038/nature11475

Conte,M.g.(2010).Supercapacitors Technical Requirements for New Applications.*5*,806–818. https://doi.org/10.1002/fuce.201000087

Conway,B.E.(1991).*technical papers' electrochemical science and technology Transition from "Supercapacitor" to "Battery" Behavior in Electrochemical Energy Storage*. *138*(6).

Davis, U. C. (2019). *Ultracapacitors Why How and Where Is the Technology*. *7753*(July). https://doi.org/10.1016/S0378-7753(00)00485-7

Devi,M.R.,Lawrence,Lawrence.C.B.,Prithivikumaran,N.,&Jeyakumaran,N.(2014).*Synthesis and characterization of conducting polymer Polyaniline doped with Salicylic Acid*. *6*(13), 5400–5403.

Devi,M.R.,Saranya,A.,Saranyak.Pandiarajan,J.,Dharmaraja,J.,Prithivikumaran,N.,&Jeyakumaran ,N. (2018). Journal of King Saud University – Science Fabrication , spectral characterization , XRD and SEM studies on some organic acids doped polyaniline thin films on glass substrate. *Journal of King Saud University - Science*. https://doi.org/10.1016/j.jksus.2018.02.008

Dhand,C.,Das,M.Sumana,G.,Srivastava,K.,Pandey,K.,Kim,C. G., & Dhar, B. (2010). *Preparation , characterization and application of polyaniline nanospheres to biosensing*. 747–754. https://doi.org/10.1039/b9nr00346k

Dhawale D.S.,& Lokhande,C.D.(2011).ElectrochimicaActa Stable nanostructured polyaniline electrode for supercapacitor application.*Electrochimica Acta*, *56*(25), 9482–9487. https://doi.org/10.1016/j.electacta.2011.08.042

Ding,L.,Wang,X.,&Gregory,R.V.(1999).*Thermal properties of chemically synthesized polyaniline ž EB / powder*. 73–78.

Double-layer capacitance. (2020). https://doi.org/10.1023/A

Du,P.,Wei,W.,Liu,D.,Kang,&Liu,P.(2018).Fabrication of hierarchical carbon layer encapsulated polyaniline core-shell structure nanotubes and application in supercapacitors. *Chemical Engineering Journal*, *335*(August 2017), 373–383. https://doi.org/10.1016/j.cej.2017.10.170

Edition,F.,Fifield, F.W.,& Kealey,D. (n.d.). *Principles and Practice of Analytical Chemistry*.

Emmenegger,C.,Mauron,P.,Wenger,P.,Hermann,V.,Gallay, R., & Züttel, A. (2003). *Investigation of electrochemical double-layer (ECDL) capacitors electrodes based on carbon nanotubes and activated carbon materials*.*124*,321–329.https://doi.org/10.1016/S0378-7753(03)00590-

Engineers,E.(2009).*Electrochemical Double-Layer Capacitors Using Carbon Nanotube Electrode Structures*.

Fan,P.,Wang,S.,Liu, H.,Liao G., & Mei, L (2019). Polyaniline Nanotube Synthesized from Natural Tubular Halloysite Template as Performance Pseudocapacitive Electrode. *Electrochimica Acta*, 135259. https://doi.org/10.1016/j.electacta.2019.135259

Frackowiak,E,Jurewicz,K.,&Lota, K. (2006). *Supercapacitors based on conducting polymers / nanotubes composites*. *153*, 413–418. https://doi.org/10.1016/j.jpowsour.2005.05.030

Frackowiak,Elzbieta.(2001).*Carbon materials for the electrochemical storage of energy in capacitors*. *39*, 937–950.

Fu, X., Jiang, & Sun, G. (2016). ScienceDirect Aligned polyaniline nanorods in situ grown on gas diffusion layer and their application in polymer electrolyte membrane fuel cells. *International Journal of Hydrogen Energy*, 1–9. https://doi.org/10.1016/j.ijhydene.2015.12.193

Fusalba,F.,Gouérec,P.,Villers,D.,Bélanger,Gouérec, P., & Bélanger,D.(2001). *Electrochemical Characterization of Polyaniline in Nonaqueous Electrolyte and Its Evaluation as Electrode Material for Electrochemical Supercapacitors Electrochemical Characterization of Polyaniline in Nonaqueous Electrolyte and Its Evaluation as Electrode Material for Electrochemical Supercapacitors*.*148*(1), 2–8. https://doi.org/10.1149/1.1339036

Gao,C.,& Chen,G.(2016).Conducting polymer/carbon particle thermoelectric composites : Emerging green energy materials. *Composites Science and Technology*, *124*, 52–70. https://doi.org/10.1016/j.compscitech.2016.01.014

Girija, T. C., & M. V. (2006). *Analysis of polyaniline-based nickel electrodes for electrochemical supercapacitors*. *156*, 705–711. https://doi.org/10.1016/j.jpowsour.2005.05.051

Gómez, H., Ram, M. K., Alvi, F., Villalba, P., Lee, E., & Kumar, A. (2011). *Graphene-conducting*

polymer nanocomposite as novel electrode for supercapacitors. *196*, 4102–4108. https://doi.org/10.1016/j.jpowsour.2010.11.002

Guan,H.,Fan,L., Zhang, H., & Qu, X. (2010). Electrochimica Acta Polyaniline nanofibers obtained by interfacial polymerization for high-rate supercapacitors. *Electrochimica Acta*, *56*(2), 964–968. https://doi.org/10.1016/j.electacta.2010.09.078

Hadjipaschalis,& Efthimiou (2009). *Overview of current and future energy storage technologies for electric power applications*. *13*, 1513–1522. https://doi.org/10.1016/j.rser.2008.09.028

Hu,C.,Chang,K.,Lin, M.,&Wu,Y (2006).*Design and Tailoring of the Nanotubular Arrayed Architecture of Hydrous RuO 2 for Next Generation Supercapacitors*. 2–7.

Hu,C &Wang (2002).*Improving the utilization of ruthenium oxide within thick carbon – ruthenium oxide composites by annealing and anodizing for electrochemical supercapacitors*. *4*, 554–5.

Hussain &Yu,J.S.(2019).Cobalt-doped zinc manganese oxide porous nanocubes with controlled morphology as positive electrode for hybrid supercapacitors. *Chemical Engineering Journal*, *361*(October 2018), 1030–1042. https://doi.org/10.1016/j.cej.2018.12.152

Jing,L.,& Chen,S.(2014).SC.*Elsevier Ltd*. https://doi.org/10.1016/j.electacta.2014.11.130

Khan,S.A.,Khan,S.B.,Khan,L.U.,& Farooq, A. (2018). *Fourier Transform Infrared Spectroscopy : Fundamentals and Application in Functional Groups and Nanomaterials Characterization Fourier Transform Infrared Spectroscopy : Fundamentals and Application in Functional Groups and Nanomaterials Characterization*. *July 2020*. https://doi.org/10.1007/978-3-319-

Ko, R., & Carlen, M. (2000). *Principles and applications of electrochemical capacitors*. *45*, 2483–2498.

Kulandaivalu, S. (2019). *Conducting Polymer Based Composites*.

Kwon,H.,Hong, &Yim,S. (2017). *Supercapacitive Properties of 3D-Arrayed Polyaniline Hollow Nanospheres Encaging RuO_2 Nanoparticles*. https://doi.org/10.1021/acsami.6b14331

Laforgue,A., Simon, P., Fauvarque, J. F., Mastragostino, M., & Soavi, F. (2003). *Activated Carbon Õ Conducting Polymer Hybrid Supercapacitors*. 645–651. https://doi.org/10.1149/1.1566411

Lang, J., Kong, L., Wu, W., & Kang, L.(2008).*Facile approach to prepare loose-packed NiO*

nano-flakes materials for supercapacitors w. 4213–4215. https://doi.org/10.1039/b800264a

Liu,P.,Yan J. Guang,Z.,Huang,Y.,Li,X. & Huang, W. (2019). Recent advancements of polyaniline-based nanocomposites for supercapacitors. *Journal of Power Sources*, *424*(March), 108–130. https://doi.org/10.1016/j.jpowsour.2019.03.094

Liu, Y., Zheng, Y., Xu, Q., Shi, Y., & Tian, Z. (2020). Controllable synthesis of NiSe / MoSe 2 / MoO2 3D hierarchical hollow microspheres with enhanced performance for asymmetric supercapacitors.*Chemical Engineering Journal*, *387*(December 2019), 124121. https://doi.org/10.1016/j.cej.2020.124121

Lokhande, C. D., Dubal, D. P., & Joo, O. (2011). Metal oxide thin fi lm based supercapacitors. *Current Applied Physics*, *11*(3), 255–270. https://doi.org/10.1016/j.cap.2010.12.001

Long,J.W.,Bélanger,D.,Brousse,T.,Sugimoto,W.,Sassin,M.B., & Crosnier, O. (2011). *Asymmetric electrochemical capacitors Stretching the limits of aqueous electrolytes*. *36*(July), 513–522. https://doi.org/10.1557/mrs.2011.137

Lyu,W.,Yu, M., Feng, J., & Yan, W. (2019). Facile synthesis of coral-like hierarchical polyaniline micro /nanostructures with enhanced supercapacitance and adsorption performance. *Polymer*, *162*(June 2018), 130–138. https://doi.org/10.1016/j.polymer.2018.12.037

Majumdar,D.(2019).*Polyaniline as Proficient Electrode Material for Supercapacitor Applications Innovative Energy & Research Functionalized-Graphene / Polyaniline Nanocomposites as Proficient Energy Storage Material : An Overview*. *August*. https://doi.org/10.4018/978-1-5225-7838-3.ch007

Manuscript, A. (2016). *Materials Chemistry A*. https://doi.org/10.1039/C6TA00015K

Mcdonough,J.R.,Choi J.W.,Yang,Y.,Mantia F. La, Zhang,Y.,Cui,Y.,Mcdonough, J. R., Choi, J. W. & Mantia, F. La. (2013). *Carbon nanofiber supercapacitors with large areal capacitances Carbon nanofiber supercapacitors with large areal capacitances*. *243109*(2009), 24–27. https://doi.org/10.1063/1.3273864

Menzel, J.,Fic,K.,& Frackowiak, E. (2015).Hybrid aqueous capacitors with improved energy / power performance. *Progress in Natural Science: Materials International*, *25*(6), 642–649. https://doi.org/10.1016/j.pnsc.2015.12.001

Miller,E.E.,Hua,Y.,& Tezel,F.H.(2018).Materials for energy storage :Review of electrode materials and methods of increasing capacitance for supercapacitors. *Journal of Energy Storage*, *20*(February), 30–40. https://doi.org/10.1016/j.est.2018.08.009

Mooss,V.A.,Vijayakumar,V., Kurungot, S., & Athawale, A. A. (2020). *Interconnected polyaniline nanostructures : Enhanced interface for better supercapacitance retention*. *October*.

Moussa,M., El-kady, M. F., & Zhao, Z. (n.d.). Recent progress and performance evaluation for polyaniline/ graphene nanocomposites as supercapacitor electrodes. *Nanotechnology*, *27*(44), 1–21. https://doi.org/10.1088/0957-4484/27/44/442001

Navarro,G.,Torres,J.,Blanco,M.,Jorge,N.,Santos-herran & Lafoz, M. (2021). *Present and Future of Supercapacitor Technology Applied to Powertrain ,Renewable Generation and Grid Connection Applications*.

Neelgund,G.M., & Oki, A. (2011). *A facile method for the synthesis of polyaniline nanospheres and the effect of doping on their electrical conductivity*.*November 2010*, 1291–1295. https://doi.org/10.1002/pi.3068

Niedrig, H., & Niedrig, H. (1982). *Electron backscattering from thin films Electron backscattering from thin films a). 15*. https://doi.org/10.1063/1.331005

Obeidat,A.M.,& Rastogi,A.C. (2018). Electrochemical energy storage performance of asymmetric PEDOT and graphene electrode-based supercapacitors using ionic liquid gel electrolyte. *Journal of Applied Electrochemistry*, *0*(0), 0. https://doi.org/10.1007/s10800-018-1182-6

Pasquier, A. Du, Laforgue, A.,Simon, P., Amatucci, G. G., & Fauvarque, J. (2002). *A Nonaqueous Asymmetric Hybrid Li 4 Ti 5 O 12 Õ Poly fluorophenylthiophene Energy Storage Device*. 302–306. https://doi.org/10.1149/1.1446081

Patil, D. S.,Shaikh,J. S., Dalavi, D. S., Karanjkar, M. M., Devan, R. S., & Ma, Y. R. (2011). *An Mn Doped Polyaniline Electrode for Electrochemical Supercapacitor*. *158*(6), 4–8. https://doi.org/10.1149/1.3561428

Pell, W. G., & Conway,B. E. (2004). *Peculiarities and requirements of asymmetric capacitor devices based on combination of capacitor and battery-type electrodes*.*136*, 334–345. https://doi.org/10.1016/j.jpowsour.2004.03.021

Peng, C., Zhang, S., Jewell, D., & Chen, G. Z. (2008). *Carbon nanotube and conducting polymer composites for supercapacitors*. *18*, 777–788. https://doi.org/10.1016/j.pnsc.2008.03.002

Prize, T. N. (2000). *The Nobel Prize in Chemistry , 2000 : Conductive polymers*. 1–16.

Qaiser,A.A.,Hyland,M. M.,Patterson, D. A., Istirokhatun, T., Rachmawaty, R., Yun, S., & Kim, J. (n.d.). *Synthesis of polyanilin /cellulose composite as humidity sensor Synthesis of polyaniline / cellulose composite as humidity sensor*.

Qu, D., & Shi, H. (1998). *Studies of activated carbons used in double-layer capacitors*. 99–107.

Radhakrishnan,S.,Muthukannan,R.Kamatchi,U., Rao, C. & Vijayan, M. (2011). *Performance of phosphoric acid doped polyaniline as electrode material for aqueous redox supercapacitor*. *50*(July), 970–978.

Raghava,K.,Cheol, B., Sun, K., Noh, J., & Lee, Y. (2009). *In situ self-organization of carbon black – polyaniline composites from nanospheres to nanorods : Synthesis , morphology , structure and electrical conductivity*. *159*, 1934–1939. https://doi.org/10.1016/j.synthmet.2009.06.018

Rudge,A.,Davey, J., Raistrick, I., & Ferraris, J. P. (1994). *Conducting polymers as active materials electrochemical capacitors*. *47*.

Ryu,K. S., Kim, K. M., Park, N., Park, Y. & Chang, S. H. (2002). *Symmetric redox supercapacitor with conducting polyaniline electrodes*. *103*, 305–309.

Ryu,K. S., Kim, K. M., Park, Y. J., Park, N., Kang, M. G., & Chang, S. H. (2002). *Redox supercapacitor using polyaniline doped with Li salt as electrode*. *153*, 861–866.

Saleh, H. H., Sokary, R., & Ali, Z. I. (2019). *Radiation – induced preparation of polyaniline / poly vinyl alcohol nanocomposites and their properties*.

Saliger, R., Fischer, U., Herta, C., & Fricke, J. (1998). *High surface area carbon aerogels for supercapacitors*. 81–85.

Schneuwly, A.,& Gallay, R. (2000).*Properties and applications of supercapacitors From the state-of-the-art to future trends*. 1–10.

Series, C. (2019).*Solvent Effect on Viscoelastic Behaviour and Morphology of Polyaniline Coating at QCM Sensor Solvent Effect on Viscoelastic Behaviour and Morphology of Polyaniline*

Coating at QCM Sensor. https://doi.org/10.1088/1742-6596/1417/1/012002

Shaikh, S. F., Shaikh, F. F. M., Shaikh, A. V, Ubaidullah, M., Al-enizi, A. M., & Pathan, H. M. (2021). Journal of Physics and Chemistry of Solids Electrodeposited more-hydrophilic nano-nest polyaniline electrodes for supercapacitor application. *Journal of Physics and Chemistry of Solids*, *149*(August 2020), 109774. https://doi.org/10.1016/j.jpcs.2020.109774

Sironi,A., Marinotto, D., Riccardi, C., Zanini, S. & Falletta, E. (2015). *Effect of Salicylic Acid and 5-Sulfosalicylic Acid on UV-Vis Spectroscopic Characteristics , Morphology ,and Contact Angles of Spin Coated Polyaniline and Poly (4-aminodiphenylaniline) Thin Films*. *2015*.

Sivakkumar, (2004). *Performance evaluation of poly N -methylaniline and polyisothianaphthene in charge-storage devices*. *137*, 322–328. https://doi.org/10.1016/j.jpowsour.2004.05.060

Snook, G & Best, A. S. (2011). Conducting-polymer-based supercapacitor devices and electrodes. *Journal of Power Sources*, *196*(1), 1–12. https://doi.org/10.1016/j.jpowsour.2010.06.084

Soudagar, N. M. (2017). *Chemically Synthesized Polyaniline Supercapacitor*. *10*(1), 587–594.

Subramania, A., & Devi, S. L.(2008). *Short Communication Polyaniline nanofibers by surfactant-assisted dilute polymerization for supercapacitor applications*. *March*, 725–727. https://doi.org/10.1002/pat

Tian, Y., Yan, J., Xue, R., & Yi, B. (2011). *Capacitive Properties of Activated Carbon in K 4 Fe (CN) 6*. *158*(7), 818–821. https://doi.org/10.1149/1.3591061

Valleau, J. P., & Torrie, G. M. (1982). *The electrical double layer . III . Modified Gouy − Chapman theory with unequal ion sizes The electrical double layer . III . Modified Gouy-Chapman theory with unequal ion sizes*. *4623*. https://doi.org/10.1063/1.443542

Wang, G.,& Zhang, J. (2012). A review of electrode materials for electrochemical supercapacitors. *Chemical Society Reviews*, *41*(2), 797–828. https://doi.org/10.1039/c1cs15060j

Wang, & Xiang, (2016). Journal of Science : Advanced Materials and Devices Polyaniline (PANi) based electrode materials for energy storage and conversion. *Journal of Science: Advanced Materials and Devices*, *1*(3), 225–255. https://doi.org/10.1016/j.jsamd.2016.08.001

Wang,K.,Wu,H.,&Meng, Y. (2013). *Conducting Polymer Nanowire Arrays for High Performance*

Supercapacitors. 1–18. https://doi.org/10.1002/smll.201301991

Wayu,M.(2021).*Manganese Oxide Carbon-Based Nanocomposite in Energy Storage Applications*. 232–248.

Xing, Z., Chu, Q., Ren, X., Ge, C., Qusti, A. H., Asiri, A. M., Al-youbi, A. O., & Sun, X. (2014). Ni 3 S 2 coated ZnO array for high-performance supercapacitors. *Journal of Power Sources*, *245*, 463–467. https://doi.org/10.1016/j.jpowsour.2013.07.012

Xiong, S., Zhang, Y., Wang, Y., Wu, B., Chu, J., Wang, X., Zhang, R., Gong, M., Li, Z., & Chen, Z. (2019). *Comparative study on the supercapacitive properties of PANI nanofibers , nanotubes , and nanospheres*. https://doi.org/10.1177/0954008319890644

Xu, G., Wang, N., Wei, J., Lv, L., Zhang, J., Chen, Z., & Xu, Q. (2012). *Preparation of Graphene Oxide / Polyaniline Nanocomposite with Assistance of Supercritical Carbon Dioxide for Supercapacitor Electrodes*.

Yan, Y.,Cheng,Q.,Wang, G., & Li, C. (2011). Growth of polyaniline nanowhiskers on mesoporous carbon for supercapacitor application. *Journal of Power Sources*, *196*(18), 7835–7840. https://doi.org/10.1016/j.jpowsour.2011.03.088

Yavuz,A.,Ozdemir, N., & Zengin, H. (2020). ScienceDirect Polypyrrole-coated tape electrode for flexible supercapacitor applications. *International Journal of Hydrogen Energy*, *xxxx*. https://doi.org/10.1016/j.ijhydene.2020.05.124

Yong-gang, W., & Xiao-gang, Z. (2004). *Preparation and electrochemical capacitance of RuO 2 / TiO2 nanotubes composites*. *49*, 1957–1962. https://doi.org/10.1016/j.electacta.2003.12.023

Zeng, F., Qin, Z., Liang, B., Li, T., Liu, N., & Zhu, M. (2015). Polyaniline nanostructures tuning with oxidants in interfacial polymerization system. *Progress in Natural Science: Materials International*, 1–8. https://doi.org/10.1016/j.pnsc.2015.10.002

Zhang, B. L., & Wan, M. (2003). *Self-Assembly of PolyanilineÐFrom Nanotubes to Hollow Microspheres* **. *50133010*, 815–820. https://doi.org/10.1002/adfm.200304458

Zhang, Haiqiang, Hu, Z., Li, M., & Jiao, S. (2014). polythiophene / multiwalled carbon nanotube composite by electropolymerization in an ionic liquid microemulsion. *Journal of Materials*

Chemistry A: Materials for Energy and Sustainability, *2*, 17024–17030. https://doi.org/10.1039/C4TA03369H

Zhang, Hao, Cao, G., Wang, Z., Yang, Y., Shi, Z., & Gu, Z. (2008). *Growth of Manganese Oxide Nanoflowers on Vertically-Aligned Carbon Nanotube Arrays for High-Rate Electrochemical Capacitive Energy Storage 2008*. *1*.

Zhang, J., Cui, Y., & Shan, G. (2019). *Metal oxide nanomaterials for pseudocapacitors*. http://arxiv.org/abs/1905.01766

Zhang, K., Zhang, L. L., Zhao, X. S., & Wu, J. (2010). *Graphene / Polyaniline Nanofiber Composites as Supercapacitor Electrodes*. *c*, 1392–1401. https://doi.org/10.1021/cm902876u

Zhang, L., Du, W., Nautiyal, A., Liu, Z., & Zhang, X. (2018). *Recent progress on nanostructured conducting polymers and composites : synthesis , application and*. *January*, 1–50.

Zhang, Y., Feng, H., Wu, X., Wang, L., Zhang, A., Xia, T., Dong, H., Li, X., & Zhang, L. (2009). Progress of electrochemical capacitor electrode materials : A review. *International Journal of Hydrogen Energy*, *34*(11), 4889–4899. https://doi.org/10.1016/j.ijhydene.2009.04.005

Zhi, M., Xiang, C., Li, J., Li, M.,& Wu, N. (2013). *Nanostructured carbon – metal oxide composite electrodes for supercapacitors : a review*. 72–88. https://doi.org/10.1039/c2nr32040a

Zhu, T., Chen, & Lou, X. W. (2010). *Shape-controlled synthesis of porous Co 3 O 4 nanostructures for application in supercapacitors*. 7015–7020. https://doi.org/10.1039/c0jm00867b